Reaction Chemistry & Engineering

Photocatalytic activity of undoped and Mn- and Co-doped TiO_2 nanocrystals incorporated in enamel coatings on stainless steel

Journal:	*Reaction Chemistry & Engineering*
Manuscript ID	RE-ART-07-2021-000293.R2
Article Type:	Paper
Date Submitted by the Author:	n/a
Complete List of Authors:	Diego-Rucabado, Andrea; Universidad de Cantabria Facultad de Ciencias, Física Aplicada Candela, Marina Teresa; Universidad de Cantabria, Applied Physics Department Aguado, Fernando; Universidad de Cantabria Facultad de Ciencias, CITIMAC; Universidad de Cantabria, CITIMAC Gonzalez, Jesus; Universidad de Cantabria, CITIMAC Gómez, Eugenio; VITRISPAN Valiente, Rafael; Universidad de Cantabria, Fisica Aplicada; IDIVAL-Nanomedicine Group, Cano, Israel; University of Seville Faculty of Chemistry, Crystallography, Mineralogy and Agricultural Chemistry Department; University of Cantabria Faculty of Sciences, Applied Physics Martín Rodríguez, Rosa; Universidad de Cantabria-IDIVAL,

Reaction Chemistry & Engineering

Linking fundamental chemistry and engineering to create scalable, efficient processes

ROYAL SOCIETY OF CHEMISTRY

Guidelines for Referees

Thank you very much for agreeing to review this manuscript for *Reaction Chemistry & Engineering*.

Reaction Chemistry & Engineering (*RCE*) is a community-spanning journal bridging the gap between chemistry and chemical engineering. *RCE* reports cutting edge research into all aspects of making molecules for the benefit of fundamental research, applied processes and wider society.

Reaction Chemistry & Engineering's Impact Factor is **4.239** (2020 Journal Citation Reports®)

The following manuscript has been submitted for consideration as a

PAPER

Papers in *RCE* report high quality research demonstrating a significant advance in one or more aspects of the journal scope, from laboratory based reaction discovery to plant-scale implementation. **At the core of the journal's identity is research that combines concepts from chemistry and engineering**. Known chemistry may be used to demonstrate a significant engineering development or mechanistic insight. Work covering multiple scales is encouraged, but reaction scale-up is not a requirement for publication.

When preparing your report, please:

- Focus on the **originality**, **importance**, **impact** and **reproducibility** of the science. ***RCE* publishes only the highest quality research of significant importance and interest to the journal's varied readership,** and therefore routine or incremental work – however competently performed – should **not** be recommended for publication
- Refer to the journal scope and expectations.
- **State clearly** whether you think the article should be accepted or rejected and give detailed comments (with references) both to help the Editor to make a decision on the paper and the authors to improve it. If you rate the work as routine yet recommend acceptance, please give specific reasons in your report.

Best regards,

Professor Klavs Jensen
Chair, *RCE* Editorial Board

Dr Maria Southall
Executive Editor

Contact us

Please visit our reviewer hub for further details of our processes, policies and reviewer responsibilities as well as guidance on how to review, or click the links below.

What to do when you review

Reviewer responsibilities

Process & policies

New catalysts composed of undoped and transition metal-doped TiO_2 nanocrystals incorporated in enamels on stainless steel show potential applications for pollutant photodegradation

338x190mm (96 x 96 DPI)

Photocatalytic activity of undoped and Mn- and Co-doped TiO_2 nanocrystals incorporated in enamel coatings on stainless steel†

Andrea Diego-Rucabado,[ab] Marina T. Candela,[bc] Fernando Aguado,[bc] Jesús González,[bc] Eugenio Gómez,[d] Rafael Valiente,[ab] Israel Cano*[ae] and Rosa Martín-Rodríguez*[bf]

ABSTRACT: A series of undoped and transition-metal (TM)-doped TiO_2 nanocrystals (NCs) were synthesized and calcined at different temperatures, and fully characterized. Such NCs were employed as catalyst for the photodegradation of methylene blue, which enabled to study the influence of both NCs size and anatase/brookite/rutile phases ratio on the photocatalytic activity, as well as the effect of different TM dopants, namely Mn and Co. Then, the NCs were used as active additive for the fabrication of a new photocatalytic system composed of an enamel incorporating these NCs supported onto a stainless-steel sheet. NCs both in powder form and incorporated in enamels deposited on steel were characterized by transmission electron microscopy, X-ray diffraction, and reflectance and Raman spectroscopies. We demonstrate how the calcination of TiO_2 NCs induces both a growth in the anatase ratio and formation of rutile form, which leads to a photocatalytic activity increase. Similarly, doping with Mn and Co gives rise to an enhancement of the catalytic performance attributed to a displacement of the energy bandgap. The obtained material combines the resistance of steel and the photocatalytic activity of TiO_2 deposited on enamel, which also operates as a corrosion protection layer for the former. The resulting smart photocatalytic surface presents many applications as a self-cleaning coating and potential use for NOx photodegradation.

Keywords: enamel · metal nanocrystals · methylene blue · photocatalytic surface · photocatalysis · photodegradation · TiO_2 nanocrystals · transition metal

[a] *Applied Physics Department, University of Cantabria, Avda. de Los Castros 48, 39005 Santander, Spain*
[b] *Nanomedicine Group, IDIVAL, Avda. Cardenal Herrera Oria s/n, 39011 Santander, Spain*
[c] *CITIMAC Department, University of Cantabria, Avda. de Los Castros 48, 39005 Santander, Spain*
[d] *VITRISPAN S.A., Barrio Rioseco, 39786 Guriezo, Spain*
[e] *Crystallography, Mineralogy and Agricultural Chemistry Department. Faculty of Chemistry, University of Seville, 41012 Seville, Spain. E-mail: icrico@us.es*
[f] *QUIPRE Department, University of Cantabria, Avda. de Los Castros 46, 39005 Santander, Spain. E-mail: rosa.martin@unican.es*

† Electronic supplementary information (ESI) available: XRD analyses, TEM images and photographs of supported photocatalysts.

INTRODUCTION

Nowadays, environmental pollution constitutes one of the most urgent problems[1] and thus the development of more efficient air and water decontamination treatments has become an increasingly important research area.[2] In this context, air and water treatment can be achieved through photo-oxidation processes catalysed by semiconductor catalysts.[3,4] Among them, titanium oxide (TiO_2) is the most widely employed photocatalyst to decompose organic and inorganic compounds in polluted water and air,[4,5,6] since the first report of Frank and Bard in 1977, where the reduction of CN^- in water catalysed by TiO_2 was reported.[7] This semiconductor exhibits multiple interesting properties that makes it a very suitable photocatalyst for this type of processes, including low cost, high photocatalytic activity, low toxicity, and high thermal and chemical stability.[5] Specifically, TiO_2 nanoparticles (NPs) have shown a particular ability to perform this transformation due to their high surface-to-volume ratio, which results in an increase of the number of active sites and thus leads to a higher catalytic activity.[8] Furthermore, the band gap of semiconductor nanomaterials is size-dependent, which can be employed to control the photocatalytic process through an effective tuning of redox potentials of generated electron/hole pairs.[8] However, a decrease or total loss of activity can be produced as a result of NPs aggregation. As a strategy to solve this problem, TiO_2 NPs can be dispersed and immobilised on a support, leading to more stable catalysts by preventing agglomeration. Different supports have been employed to immobilise TiO_2 NPs, such as SiO_2,[9] carbon nanotubes (CNTs),[10] multiwalled carbon nanotubes (MWCNTs),[11] graphene,[10] activated carbon,[11,12] glass,[13] zeolite,[14] clay,[15] diatomite,[16] ceramics,[13b,17] and stainless steel.[18] In this context, nanosized TiO_2 can be supported on glazed surfaces[13b,17a,19,20,21,22] or incorporated into enamels[17b,23,24] to generate smart photocatalytic materials with self-cleaning properties that may additionally serve as an interesting functionality for different applications. Particularly, a large body of literature has emerged describing the use of these functional materials as coating for high solar power receivers,[21c] electrical lines,[21b] reactors,[13b] sanity wares,[21a] building's indoor and outdoor applications,[22,23] and construction elements like floorings, glasses, roofing, and walls, tunnels and subway panels.[17,20,23]

In this work, we describe a new photocatalytic surface composed of an enamel containing 5% of TiO_2 NCs supported onto a stainless-steel substrate. This material combines the resistance of steel and the photocatalytic activity of TiO_2 deposited on enamel, which also acts as protecting layer for the former. The resulting smart photocatalytic surface holds great potential for use in a variety of applications such as self-cleaning coating used in means of transport (ships, trains), reactors to remove dye pollutants in wastewater from textile industry, water tanks, or boilers and vessels for food and water.

Firstly, the influence of both NCs size and anatase/brookite/rutile phases ratio in the photocatalytic properties has been analysed. It is generally accepted that although anatase shows better performance due to its higher Fermi level and indirect gap, the photocatalytic activity is maximized for a composition of *ca*. 70% anatase and 30% rutile.[25] However, there is still an open controversy and contradictory

results regarding this synergistic effect between anatase and rutile phases.[26,27] In addition, the brookite form is also photocatalytically active, and thus its effect in a mixture of different TiO_2 phases should not be ignored.[28] Secondly, the effect of different transition metal (TM) dopants on the catalytic performance was studied, since the modification of TiO_2 bandgap with TM may induce a shift of its spectral response towards the visible region and increase the activity of the photocatalytic material.[6b,10,29] To this end, not only undoped but also Mn- and Co-doped TiO_2 NCs were synthesized, integrated on the surface of an enamel, and supported onto stainless steel sheets. NCs both in powder form and immobilised on enamels deposited onto steel were fully characterized by different techniques, such as X-ray diffraction (XRD), transmission electron microscopy (TEM), as well as Raman and reflectance spectroscopy. The photocatalytic activity of the designed systems was evaluated using the photodegradation of methylene blue (MB) in water as a model reaction.

EXPERIMENTAL

1. Materials

Urea (99.5%, Merck), titanium (IV) isopropoxide (>99.995%, Sigma-Aldrich), manganese(II) chloride tetrahydrate (99%, Alfa Aesar), cobalt(II) chloride hexahydrate (99%, Riedel-de Haën) and methylene blue (82%, Panreac), were purchased from commercial sources. All chemicals were used without any further purification. All manipulations were performed in air atmosphere.

2. Synthesis of TiO_2 nanocrystals

The TiO_2 NCs analysed in this work consist of two groups of samples synthesized by a method adapted from the procedure described by Lusvardi *et al.*[30] Interestingly, this synthesis procedure produces crystalline anatase and brookite TiO_2 NCs. Briefly, titanium isopropoxide was added dropwise to an aqueous solution of urea (1:0.5 Ti:urea ratio) and the mixture was stirred at 50 ºC for 60 minutes. Then, the solution was heated up at *ca*. 85 ºC under stirring to remove the excess water, obtaining the nanocrystalline TiO_2 powder. The TM-doped samples were prepared by adding stoichiometric amounts of the corresponding metal chloride to the urea solution. A subsequent calcination process was performed in order to remove the urea excess and increase the rutile ratio.

The first set of NCs presents three samples (T1-T3): the as-obtained NCs, NCs subjected to a thermal treatment of 600 ºC for 2 hours, and NCs calcined at 800 ºC for 2 hours. The second group of samples comprises TiO_2 NCs doped with 5 mol% of Mn and Co, both as-prepared and calcined at 600 ºC (T4-T7). Table 1 summarizes the studied NCs and the experimental parameters employed in each synthesis.

Table 1 Summary of the undoped and TM-doped TiO_2 NCs.

Sample	TM dopant	Calcination temperature (ºC)
T1	--	---
T2	--	600
T3	--	800
T4	5% Mn	---
T5	5% Mn	600
T6	5% Co	---
T7	5% Co	600

3. Preparation of the supported photocatalyst

In order to prepare the support, two types of enamels were deposited on stainless steel sheets (AC01EK quality with 0.08% carbon content): firstly, base enamel and, secondly, coat enamel. In both cases, the precursors (enamel frit, clay, $NaAlO_2$, urea and water) were ground in a ball mill to obtain a suspension with density of *ca*. 1.75-1.80 g/mL.

The base enamel was deposited onto the stainless steel sheets and dried at 100 °C. Subsequently, this base enamel was vitrified by heating at 840 °C for 3 min. After cooling down, the coat enamel was deposited on the vitrified base enamel, dried at 100 ºC and vitrified by heating at 830 °C for 3 min. The resulting vitrified coat enamel shows a thickness of *ca*. 150 μm, while the base enamel exhibits a thickness around 120 μm.

To prepare the supported photocatalyst (5% TiO_2), NCs were mixed with a serigraph-type oil (mainly composed of acrylic resins and propylene glycol ester in a 2:5 w:w ratio) to obtain an appropriate viscosity. The mixture was deposited on the prepared support (enamel onto stainless steel sheets) by indirect serigraphy and vitrified by heating at 700 ºC for 15 min.

4. Structural and optical characterization

4.1 X-ray powder diffraction

Crystal structure and particle size of all synthesized samples were studied by XRD. XRD measurements were performed either in a Bruker D8 Advanced diffractometer equipped with a Cu tube (wavelength: $<K\alpha_{1,2}>$= 1.5418 Å) and a fast Lynxeye 1D-detector, or in a Bruker D2 Phaser diffractometer with a Cu tube and a 0D Xflash detector. Both the starting synthesized NCs and the prepared supported catalysts were measured in the 10-120º range (2θ) for phase identification and quantification as well as structure refinement. The Rietveld method was applied to patterns from all the samples for the structural analysis. Microstructural parameters were determined from the whole powder pattern fitting through a

convolution procedure as implemented in the software TOPAS.[31] Average crystallite sizes were determined based on the Double Voigt approach (size and strain contributions).[32] The instrumental line broadening was determined from the Fundamental Parameters approach[33] as well as the standard method (LaB_6 sample).

4.2 Transmission electron microscopy

Morphology and size distribution of TiO_2 NCs were analysed through TEM images obtained with a JEOL JEM 1011 equipped with a high-resolution Gatan CCD camera. NCs were dispersed in ethanol and a small drop was deposited on the copper grids.

4.3 Raman spectroscopy

Raman spectra were obtained with a SM245 spectrophotometer equipped with a CCD detector, and a solid-state laser emitting at 785 nm and focused on the sample with a 20X objective. The spectra were acquired in the range 80-900 cm^{-1}, with a resolution higher than 5 cm^{-1}, a laser power of 150 mW and acquisition time of 60 seconds. Complementary analyses were performed with a T64000 Raman spectrometer (Horiba), employing as detector a nitrogen-equipped CCD coupled to a confocal microscopy using the 514.5 nm line of a Kr^+-Ar^+-laser.

4.4 Optical spectroscopy

Reflectance spectra were registered in the 200-1000 nm spectral range using a Varian Cary 6000i spectrophotometer equipped with a polytetrauoroethylene-coated integrating sphere, two light sources, a quartz halogen lamp for the visible region and a deuterium lamp for the ultraviolet (UV), and two detectors, a Hamamatsu R928 photomultiplier for the visible region and an InGaAs detector for the near infrared.

5. Photocatalytic study

The photocatalytic performance was analysed by studying the degradation of a MB solution under UV radiation according to the ISO 10678 International Standard method.[34] For comparison purposes, all samples were tested using the same experimental conditions as follows. TiO_2 NCs (10 mg) were dispersed in a solution of MB in water (150 mL, C_0 = 10 μM) and irradiated from the top with a UV LED lamp (395 nm, 22 W) at room temperature (RT). In the case of supported TiO_2 NCs, the catalytic material shaped like a plate (5 x 5 cm^2) was activated with the UV lamp for 48 h. Next, the solution of MB in water (100 mL, C_0 = 10 μM) was added and the degradation assay was carried out under the same conditions as described for non-supported TiO_2 NCs. In parallel, the supported photocatalyst was placed in 150 mL of a 10 μM MB solution and left in the dark for 24 h. A slight reduction of the MB solution concentration as a result of an adsorption process was observed.

The absorbance of the MB solution was measured every 1 h for 24 h, and the photocatalytic activity (*PA*) was determined from the reduction of the absorbance *A*, which is proportional to the MB solution concentration, *C*, according to $PA(\%) = \frac{C_0 - C}{C_0} \cdot 100 = \frac{A_0 - A}{A_0} \cdot 100$, where C_0 and A_0 are the initial

solution concentration and absorbance, respectively. The obtained values were appropriately corrected with the adsorption contribution in all photocatalytic activity measurements (% MB degradation).

RESULTS AND DISCUSSION

1. Optimization of TiO_2 NCs by tailoring the anatase/brookite/rutile ratio and doping with TM cations

Firstly, the influence of the thermal treatment on the anatase/brookite/rutile ratio of the so-obtained TiO_2 NCs was analysed. In particular, the following samples have been studied: TiO_2 NCs without thermal treatment (T1), and calcined at 600 ºC (T2) and 800 ºC (T3). Figs. 1 and S1† show the XRD patterns of the aforementioned TiO_2 samples as raw nanocrystalline powder. Since the synthesis of TiO_2 NCs was carried out at RT, the anatase phase is predominantly generated (Table 2, entry 1). In addition, a considerable amount of brookite form was also observed. Thus, the application of thermal treatments at different temperatures was performed to generate the rutile phase and study the effect of anatase/brookite/rutile ratio on the photocatalytic activity.[35] As expected, XRD analyses show an increase in the rutile ratio after calcination. Specifically, upon heating at 600 ºC NCs present 7.8% of the rutile form, while at 800 ºC a complete transformation to rutile phase occurs (Table 2, entries 2 and 3). Moreover, the brookite form was totally removed at 600 ºC (Table 2, entry 2).

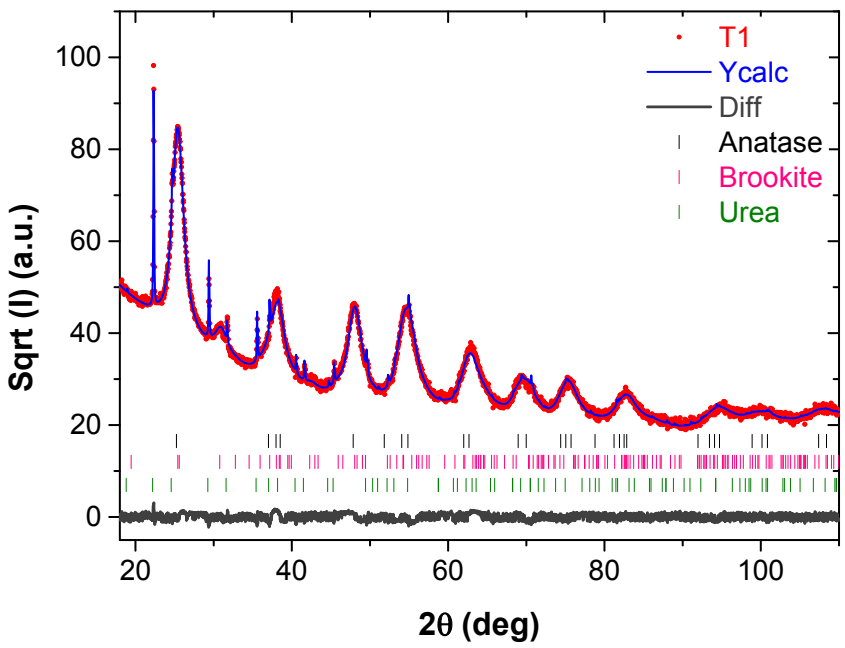

Fig. 1 XRD diffraction pattern of non-calcined undoped TiO_2 NCs (T1).

The NCs size estimation from XRD increases with the calcination temperature as a result of NCs sintering (Table 2). This trend was corroborated by TEM results (Fig. 2).

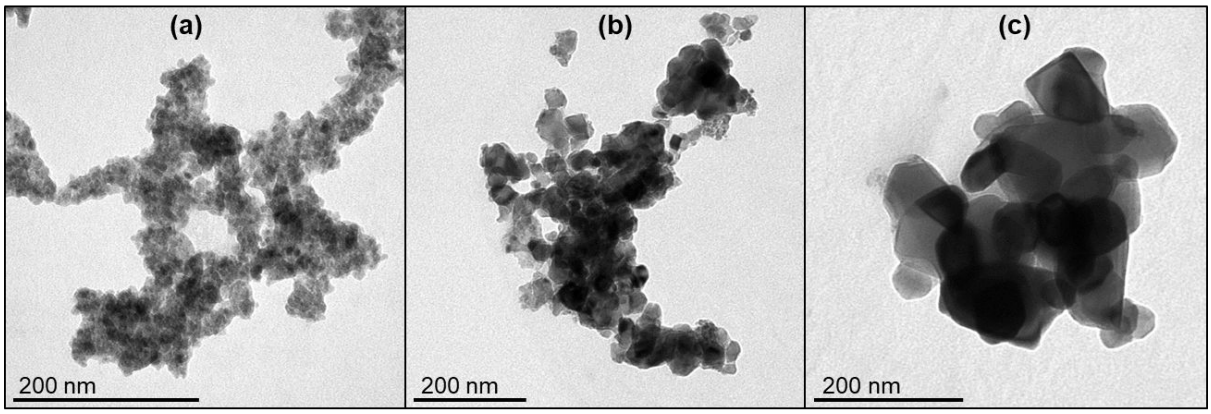

Fig. 2 TEM images of undoped (a) non-calcined TiO_2 NCs (T1); (b) TiO_2 NCs calcined at 600 ºC (T2); (c) TiO_2 NCs calcined at 800 ºC (T3).

Table 2 Summary of crystallite sizes and anatase/brookite/rutile ratios obtained by XRD and TEM for undoped TiO_2 NCs.

Sample	*T* (ºC)[a]	Ana : Ru : Bro	$Size_{Ana}$ (nm)	$Size_{Rut}$ (nm)	$Size_{Bro}$ (nm)	$Size_{TEM}$ (nm)
T1[b]	–	68.3 : – : 31.7	4.8 ± 0.1	–	3.1 ± 0.2	5.4 ± 2.9
T2	600	92.2 : 7.8 : –	29.7 ± 0.5	59 ± 2	–	34 ± 11
T3	800	0.5 : 99.5 : –	n/a	102 ± 4	–	77 ± 15

[a] Calcination temperature. [b] 10% urea.

The Raman spectra of T1-T3 samples are shown in Fig. 3. The Raman spectra of T1 and T2 are dominated by the bands associated to the anatase phase, centred at 147 (E_g), 398 (B_{1g}), 515 (A_{1g} + B_{1g}) and 638 cm^{-1} (E_g).[36] In addition, the presence of a peak located at about 312 cm^{-1} (B_{1g}) in the spectrum of T1 reveals the presence of the brookite form in this sample,[37] while the peak at 1002 cm^{-1} corresponds to the NCN symmetric stretching mode of the remaining urea.[38] On the other hand, the spectrum of T3 exhibits the typical bands at 228 (two phonon scattering), 449 (E_g) and 607 cm^{-1} (A_{1g}) belonging to the rutile phase.[37,39] The spectrum of T3 also shows a small peak at 141 cm^{-1} associated to the E_g active mode of anatase. These results are consistent with those obtained by XRD.

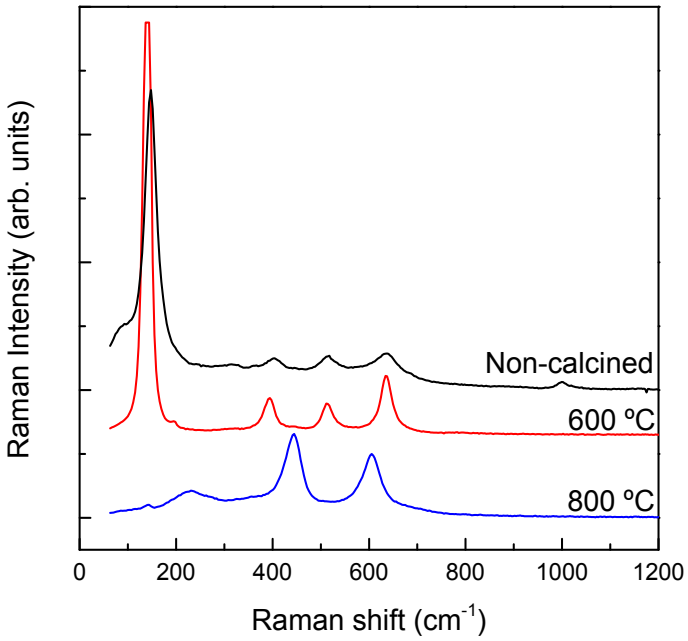

Fig. 3 Raman spectra of undoped TiO_2 NCs; black, non-calcined TiO_2 NCs (T1); red, TiO_2 NCs calcined at 600 ºC (T2); and blue, TiO_2 NCs calcined at 800 ºC (T3).

Secondly, doping with TM ions has been previously reported to be an efficient strategy to improve the photocatalytic activity of TiO_2 NCs.[40] In this work the incorporation of Co and Mn has been analysed. Figs. 4 and S2† and Table 3 show the XRD diffraction patterns and the ratios between the different TiO_2 phases and their corresponding crystallite sizes for NCs doped with 5% Co and 5% Mn. The non-calcined TiO_2 NCs (T4 and T6, Fig. S2†) exhibit high brookite phase ratios (>30%) and small crystallite sizes (<5 nm). On the other hand, T5 and T7 (Fig. 4) consist of NCs calcined at 600 ºC and thus, as expected, the NCs show bigger sizes than non-calcined NCs. Besides, the amount of brookite phase decreased or even disappeared (Table 3), similarly to the undoped TiO_2 NCs. For Co-doped TiO_2 NCs (T7) only the anatase phase was observed upon calcination at 600 ºC. In addition, a small amount (<8%) of $CoTiO_3$ ilmenite-type structure was also detected.[41] Interestingly, the NC size was found to increase in the order brookite<anatase<rutile. Indeed, a similar trend was previously observed by other authors.[42] The nanocrystalline size has also been estimated from TEM images (Figs. S3-S6†) and included in Table 3. These sizes observed by TEM are in good agreement with those determined from XRD, indicating single domain NCs.

Table 3 Summary of crystallite sizes and anatase/brookite/rutile ratios obtained by XRD and TEM for TM-doped TiO_2 NCs.

Sample	Dopant	Calcination T (ºC)	Ana : Ru : Bro	$Size_{Ana}$ (nm)	$Size_{Rut}$ (nm)	$Size_{Bro}$ (nm)	$Size_{TEM}$ (nm)
T4	5% Mn	–	62.7 : – : 37.2	4.4 ± 0.1	–	2.6 ± 0.1	5.4 ± 2.0
T5	5% Mn	600	86.7 : 3.0 : 10.3	22.8 ± 0.5	37 ± 4	12.0 ± 0.7	30.7 ± 9.7
T6	5% Co	–	59.1 : – : 40.0	4.1 ± 0.2	–	1.7 ± 0.1	4.7 ± 1.5
T7[a]	5% Co	600	100 : – : –	27.2 ± 0.7	–	–	36 ± 29

[a] 7.9% $CoTiO_3$

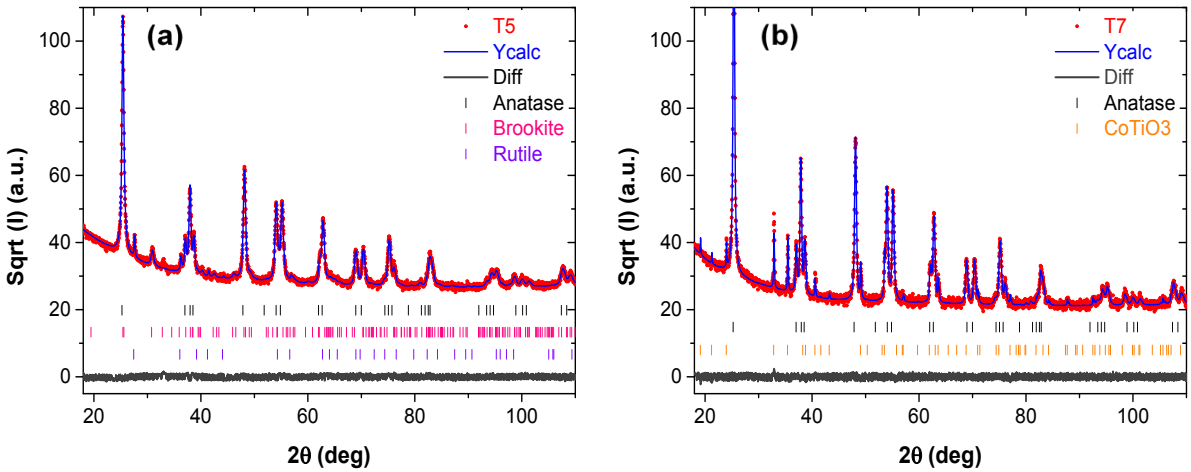

Fig. 4 XRD diffraction patterns of (a) Mn-doped TiO_2 NCs calcined at 600 ºC (T5); (b) Co-doped TiO_2 NCs calcined at 600 ºC (T7).

Fig. 5 shows the Raman spectra of TiO_2 NCs doped with Mn and Co, as-prepared and calcined at 600 ºC (T4-T7). The Raman spectra are dominated by the bands corresponding to the anatase phase, in good agreement with XRD data, similarly to T1-T3 samples. In the case of Mn-doped TiO_2 NCs, T4 (Fig. 5(a)) displays the characteristic bands of anatase phase, which are located at 149, 395, 514 and 631 cm^{-1}.[36] In addition, the peak at *ca.* 310 cm^{-1} can be attributed to the B_{1g} active mode of brookite.[37] As expected, an increase in the intensity of anatase bands is observed for T5 (from 62.7 to 86.7% anatase by XRD). The small peak at 315 cm^{-1} corresponds to brookite (10.3% brookite by XRD), while no rutile fingerprints are detected (below 3%).

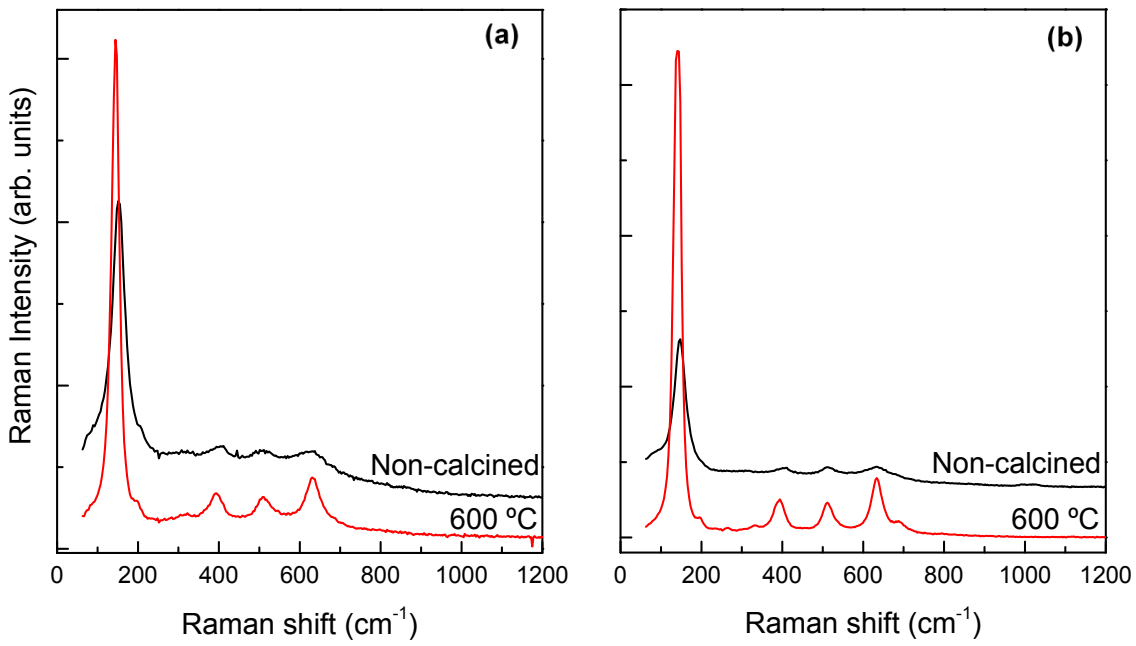

Fig. 5 Raman spectra of (a) Mn-doped TiO_2 NCs (T4 and T5); (b) Co-doped TiO_2 NCs (T6 and T7). Black, non-calcined TM-doped TiO_2 NCs; red, TM-doped TiO_2 NCs calcined at 600 ºC.

A similar result was obtained with Co-doped TiO_2 NCs. Both T6 and T7 spectra are dominated by the peaks belonging to the anatase phase, with an increase in the intensity of these bands in T7 as a consequence of the higher anatase content due to the calcination process. Interestingly, T7 also shows a series of small peaks at 196, 263 and 332 and 687 cm^{-1} corresponding to $CoTiO_3$ ilmenite structure,[41] which supports the XRD observations.

2. Optical characterization of undoped and TM-doped TiO_2 nanocrystals

The optical characterization of the bandgap of undoped TiO_2 NCs, non-calcined and heated at 600 ºC and 800 ºC, by reflectance spectroscopy is summarized in Fig. 6. The spectra clearly illustrate how the NCs absorption bandgap is influenced by the calcination treatment. Specifically, the absorption edge is centred at *ca*. 373 nm for the as-prepared sample (T1), and 391 nm and 408 nm for the NCs treated at 600 ºC (T2) and 800 ºC (T3), respectively. The red-shift of the bandgap towards the visible region with the increase of calcination temperature is mainly ascribed to the presence of rutile phase,[43] in agreement with XRD and Raman results.

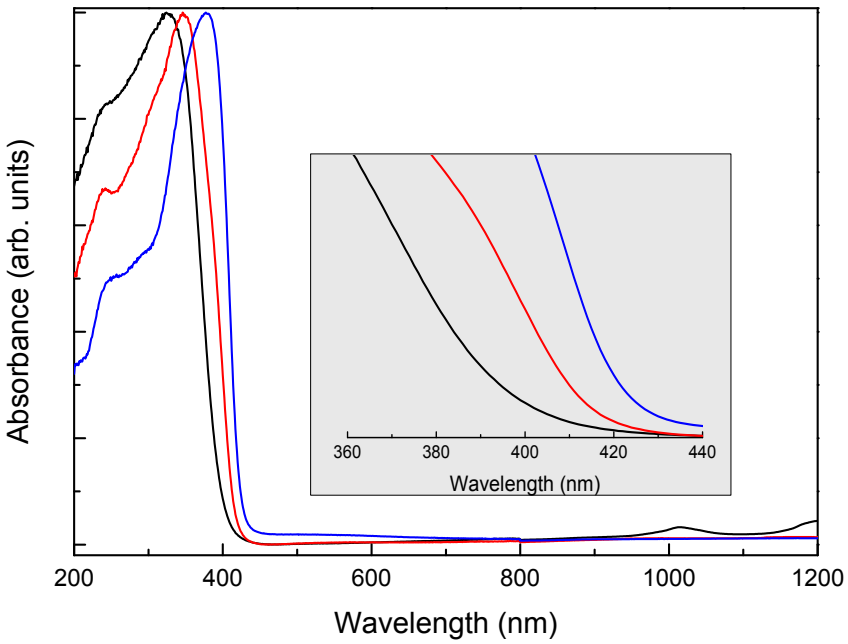

Fig. 6 Optical reflectance of undoped TiO_2 NCs; black, non-calcined TiO_2 NCs (T1); red, TiO_2 NCs calcined at 600 ºC (T2); and blue, TiO_2 NCs calcined at 800 ºC (T3).

Figs. 7(a) and 7(b) show the optical reflectance spectra of TiO_2 NCs doped with 5% of Mn (T4 and T5) and 5% of Co (T6 and T7), respectively. The main differences with respect to non-doped TiO_2 NCs (in black) are the red-shift of the absorption edge and the presence of broad bands, which appear as a shoulder overlapping the absorption edge. These bands can be ascribed to either TM ions absorption or charge-transfer transitions between TM ions and the TiO_2 conduction or valence band, confirming the incorporation of the TM into the TiO_2 structure.[44] For Mn-doped TiO_2 NCs, the reflectance spectrum of the sample calcined at 600 ºC (T5) is clearly different from the one obtained at RT (T4). This fact can be related to the presence of different Mn oxidation states. Specifically, previous X-ray photoelectron spectroscopy studies have shown that while the Mn oxidation state is 2+ for Mn-doped TiO_2 samples prepared at RT, the presence of Mn^{3+} and Mn^{4+} is observed for samples calcined at temperatures higher than 550 ºC.[45] On the contrary, the shape of the reflectance spectra for Co-doped NCs is mostly independent of the calcination treatment. This indicates that Co presents the most stable valence, 2+, which is corroborated by the presence of a well-defined absorption band centred at 610 nm, related to a *d-d* Co^{2+} transition.[44a] Thus, the potential enhancement of the photocatalytic activity by doping with these cations is associated not only with a displacement of the energy bandgap to the visible region, but also to the introduction of additional energy states within the TiO_2 energy bandgap, particularly in the case of Co-doped samples, which induces visible light absorption bands at higher wavelengths in the visible range.

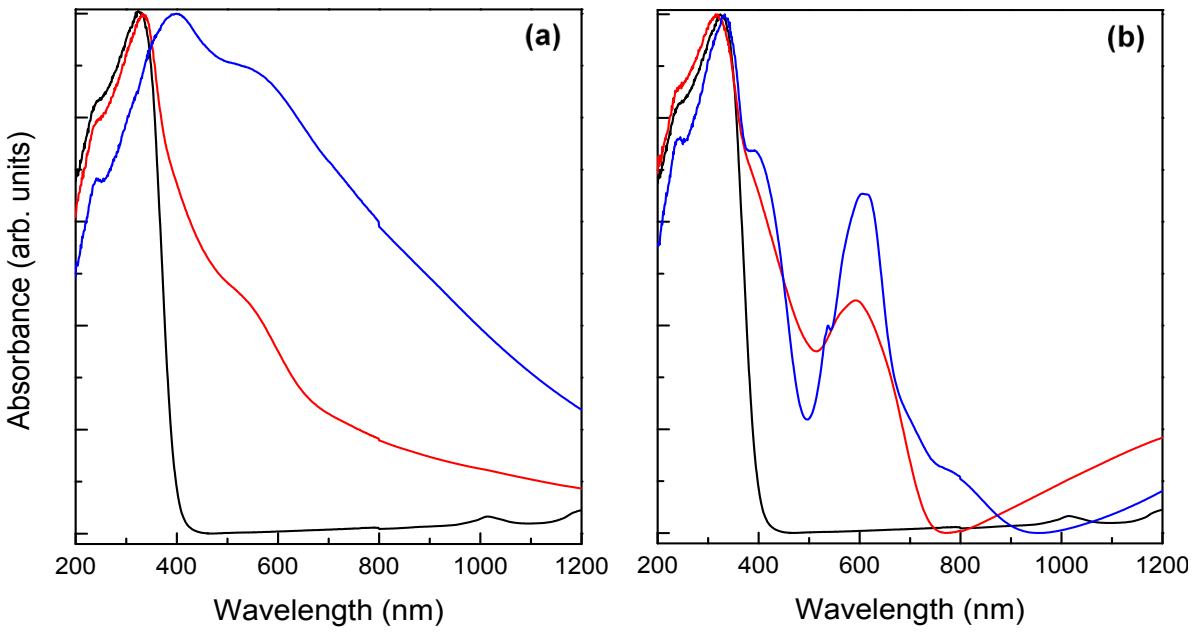

Fig. 7 Optical reflectance of (a) TiO_2 NCs doped with 5% Mn; (b) TiO_2 NCs doped with 5% Co. Red, non-calcined TM-doped TiO_2 NCs; blue, TM-doped TiO_2 NCs calcined at 600 ºC. For comparison purposes, non-calcined undoped TiO_2 NCs are shown in black.

3. Catalytic activity of TiO_2 NCs

We have investigated the photocatalytic activity of undoped and Co or Mn-doped TiO_2 NCs using the degradation of MB in water under UV irradiation (395 nm) as a model reaction (Scheme 1),[16a,46] since the use of this synthetic dye is recommended by the ISO/CD10678 regulation.[34]

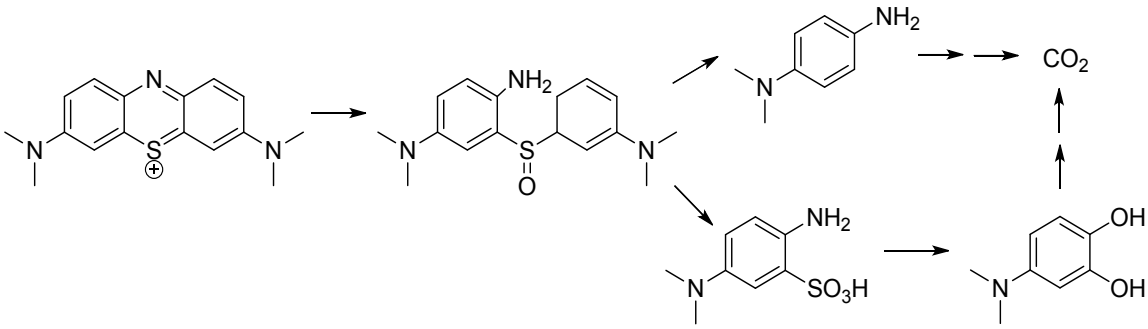

Scheme 1 Photocatalytic degradation route of methylene blue.

The degradation occurs when TiO_2 absorbs radiation of higher energy than its bandgap, which produces the promotion of an electron from the valence band to the conduction band (e^-_{CB}) and creates a positive hole (h_{VB}^+), thus generating an electron/hole (e^-_{CB}/h^+_{VB}) pair (eq. 1). Positive holes can oxidize water or OH^- and form $^{\bullet}OH$ radicals at TiO_2 NCs surface (eq. 2–3). In addition, e^-_{CB} electrons can interact with O_2 and generate superoxide ($O_2^{\bullet-}$) and hydroperoxyl ($^{\bullet}OOH$) radical anions (eq. 5 and 7). These radicals are extremely reactive oxidants and may degrade pollutants or organic compounds through an oxidation process (eq. 4, 6 and 8).[5,24,47]

$$TiO_2 + h\nu \longrightarrow h^+_{VB} + e^-_{CB} \quad (1)$$

$$h^+_{VB} + H_2O \longrightarrow H^+ + {}^{\bullet}OH \quad (2)$$

$$h^+_{VB} + OH^- \longrightarrow {}^{\bullet}OH \quad (3)$$

$${}^{\bullet}OH + \text{organic molecule} \longrightarrow \longrightarrow \longrightarrow CO_2 + H_2O \quad (4)$$

$$e^-_{CB} + O_2 \longrightarrow O_2^{\bullet -} \quad (5)$$

$$O_2^{\bullet -} + \text{organic molecule} \longrightarrow \longrightarrow \longrightarrow CO_2 + H_2O \quad (6)$$

$$O_2^{\bullet -} + H^+ \longrightarrow {}^{\bullet}OOH \quad (7)$$

$${}^{\bullet}OOH + \text{organic molecule} \longrightarrow \longrightarrow \longrightarrow CO_2 + H_2O \quad (8)$$

To this end, TiO_2 NCs were dispersed in a solution of MB in water (for further details see Experimental section) and irradiated from the top with a UV lamp (22 W, λ = 395 nm LED). After a given time, the concentration of MB solution (*C*) was determined using the absorption of the characteristic band of MB at 664 ± 5 nm in the acquired UV–vis spectrum (Fig. 8). The photocatalytic efficiency for each TiO_2 NCs is represented by the decomposition rate of MB, which is estimated by the equation:

$$d = \frac{C_0 - C_t}{C_0} \times 100 = \frac{A_0 - A_t}{A_0} \quad (9)$$

where *d* is the degradation rate, C_0 is the initial concentration of MB solution and C_t is the concentration of MB solution after a specific irradiation time, *t*. A_0 and A_t are the absorbance values at the maximum absorption band at time *t*=0 and time *t*.

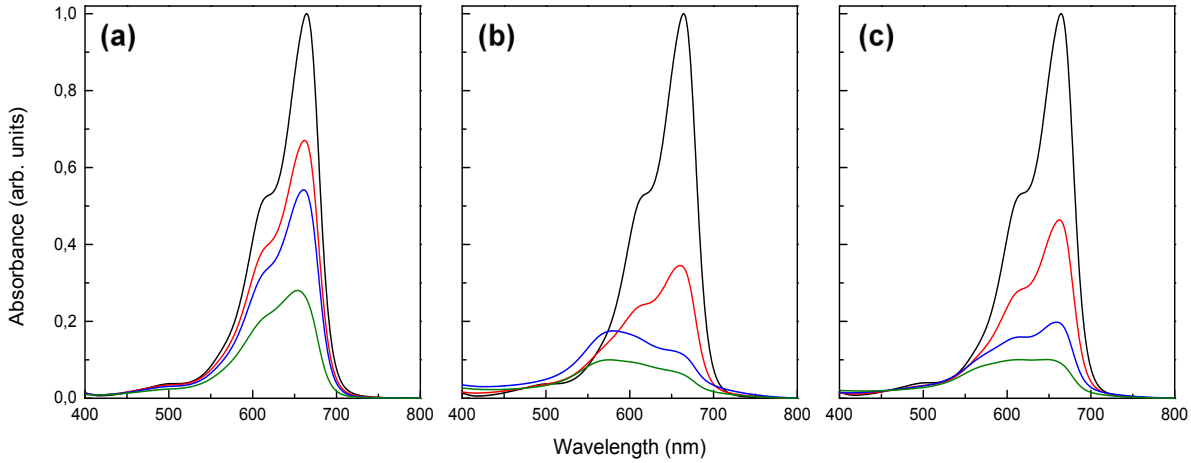

Fig. 8 Evolution of MB solution absorbance with time in a catalytic experiment mediated by (a) T1, (b) T2, and (c) T3 undoped TiO_2 NCs. Conditions: MB (150 mL, 10 μM), TiO_2 NCs (10 mg), 22 W, λ = 395 nm, at RT; black, *t* = 0 h; red, *t* = 1 h; blue, *t* = 8 h; green, *t* = 24 h.

Thus, a set of catalytic experiments was carried out to study the influence of NCs size, anatase/rutile ratio and presence of TM dopants on the photocatalytic activity of TiO_2 NCs. Firstly, non-calcined TiO_2 NCs (T1, Table 4), which contain a 68.3:31.7 anatase/brookite ratio and do not present rutile phase, showed good catalytic performance and 72% MB degradation was observed after 24 h of reaction (Fig. 8(a)). Despite the much bigger size, the NCs calcined at 600 ºC (T2) displayed higher photocatalytic activity, leading to 93% MB degradation (Fig. 8(b)). This is attributable to both the increase in the highly active anatase ratio and the formation of rutile phase as a result of the calcination process.[35] Indeed, it is reported that a mixture of anatase and rutile produces a synergistic effect for which photoexcited electrons in anatase are transferred to the rutile conduction band.[26] This promotes the separation of photogenerated charge carriers and thus reduces the recombination of electrons and holes, which is the main limitation in semiconductor-mediated photocatalysis.[5,48] In this context, Besenbacher *et al.* described an optimal 40-80% anatase content (with the remaining amount of rutile) for MB photooxidation catalysed by TiO_2 films.[26] Nevertheless, Du, Yang *et al.* reported that the photocatalytic activity of TiO_2 NPs is maximized for a composition of *ca*. 70% anatase and 30% rutile,[25] while other authors claim that there is no synergistic effect at all between anatase and rutile.[27]

TiO_2 NCs calcined at 800 ºC (T3) led to a slight decrease in the MB degradation in comparison with T2 (Fig. 8(c)). This can be related to the decrease in the anatase phase content, since, as previously described, the photocatalytic activity of a combination of anatase and rutile polymorphs is higher than that of the pure rutile.[48] Specifically, T2 exhibits 92.2% anatase, while T3 presents 99.5% rutile form. In addition, T3 shows much bigger NCs than T2, which also diminishes the catalytic activity. It should be noted that the brookite form is also photocatalytically active and its effect must be considered.[28] However, in this study the presence of brookite seems to be detrimental as compared with the catalytic performance shown by anatase and rutile phases, as the activity increases with the decrease of brookite content (Table 4).

Table 4 Photocatalytic degradation of MB mediated by TiO_2 NCs.[a]

Sample	TM dopant	Ana : Rut : Bro	$Size_{Ana}$ (nm)	$Size_{Rut}$ (nm)	$Size_{Bro}$ (nm)	MB degradation (%)
T1[b]	–	68.3 : 0 : 31.7	4.8	–	3.1	72
T2	–	92.2 : 7.8 : 0	29.7	59.0	–	93
T3	–	0.5 : 99.5 : 0	60.0	102.0	–	90
T4	5% Mn	62.7 : 0 : 37.2	4.4	–	2.6	79
T5	5% Mn	86.7 : 3.0 : 10.3	22.8	37.0	12.0	82
T6	5% Co	59.1 : 0 : 40.0	4.1	–	1.7	75
T7[c]	5% Co	100 : 0 : 0	27.2	–	–	86

[a] Reagents and conditions: MB (150 mL, 10 μM), catalyst (10 mg), 22 W, λ = 395 nm, RT, 24 h.[b] 10% urea.[c] 7.9% $CoTiO_3$.

Next, an experiment catalysed by TiO_2 NCs doped with 5% Mn was performed. The doping of TiO_2 NCs with TM may lead to a decrease in the bandgap as a result of the formation of new energy levels, which shifts the absorption edge towards the visible region and increase the activity of photocatalytic TiO_2 NCs. Moreover, the presence of a TM can enhance the electron-hole pair separation, and thus reduce the recombination of photogenerated charge carriers and increase their lifetime.[5,48] In line with the displacement observed in the absorption edge towards the visible zone (Fig. 7(a)), an increase in the MB degradation (79%) was achieved with Mn-doped TiO_2 NCs (T4), as compared to 72% degradation obtained in the experiment catalysed by non-doped NCs (T1). In fact, the TM-doping effect on the catalytic activity is clearly highlighted considering that T1 and T4 show similar nanocrystalline size and anatase content. This trend continues when Mn-doped TiO_2 NCs calcined at 600 ºC (T5) were employed as catalyst, although the catalytic activity growth was lower than expected. Indeed, T5 displays lower activity than pure TiO_2 NCs calcined at 600 ºC (T2). Thus, the ratio of different phases may play a more important role than the NCs size here. Although T5 is formed by smaller NCs, T2 exhibits a 92:8 anatase/rutile ratio, in contrast with the 87:3:10 anatase/rutile/brookite ratio shown by T5. Therefore, T2 are again the most active NCs and it seems that there is indeed a synergistic effect between anatase and rutile. Finally, TiO_2 NCs doped with 5% Co (T6) presented also slightly higher activity (75%) than that obtained with undoped NCs (T1), in agreement with the absorption edge shift observed in Fig. 7(b). The calcination of Co-doped TiO_2 NCs (T7) had a positive effect on the activity, leading to 86% MB degradation. As T5, these NCs exhibit less activity than pure TiO_2 NCs calcined at 600 ºC (T2), which can be due to the absence of the synergistic effect provided by the combination of anatase and rutile polymorphs (100% of pure anatase form).

The results presented in this section point out the clear influence of both the anatase/brookite/rutile ratio and the presence of TM dopants on the catalytic performance of TiO_2 NCs. Specifically, the brookite phase content decrease and the formation of rutile phase lead to an enhancement of catalytic activity, which could be associated to the aforementioned synergistic effect between anatase and rutile phases. In addition, the doping with TM also produces an improvement in the catalytic performance of TiO_2 NCs. Both the optimisation of anatase/rutile ratio and the doping with TM lead to a shift in the absorption edge towards the visible spectral region and thus an increase in the activity of TiO_2 NCs is observed. Finally, it is worth noting that the employed synthesis method comprises the use of urea as N-dopant source, which could increase the catalytic activity of the synthesized NCs.[30c] However, this possible positive effect of N-dopant on the photocatalytic activity of non-calcined NCs (T1, T4 and T6) is not significant as these samples show lower activities than those of calcined NCs (T2, T3, T5 and T7), which are obtained after a calcination treatment that eliminates such a component.

4. Structural and optical characterization of photocatalysts based on pure and TM-doped TiO_2 NCs incorporated in enamel coatings on a steel sheet

In this section several photocatalysts based on T1, T4 and T6 TiO_2 NCs immobilised on enamels deposited onto steel sheets are presented (Fig. S7†). Figs. 9 and S8† show the XRD patterns of the aforementioned supported photocatalysts based on T1, T4 and T6 samples. In comparison with the starting NCs, several differences are observed in the diffractograms. The NCs in powder form exhibit broader diffraction peaks due to the small nanocrystalline size, while the supported NCs present narrower peaks and considerably worse signal to noise ratio probably due to the lower amount of TiO_2 (*ca.* 5%). Additional peaks, present in both the pure and TM-doped samples, are detected in all the diffraction patterns. They can be assigned to different phases, mainly silicates, arising from the mixture used for the enamel preparation. No features from crystalline phases incorporating TM dopants (particularly $CoTiO_3$) have been found. All the non-TiO_2 phases have been considered together as a single phase to roughly estimate their abundance, representing around the 20% in all the TM-doped samples (see the refinements from Fig. 9).

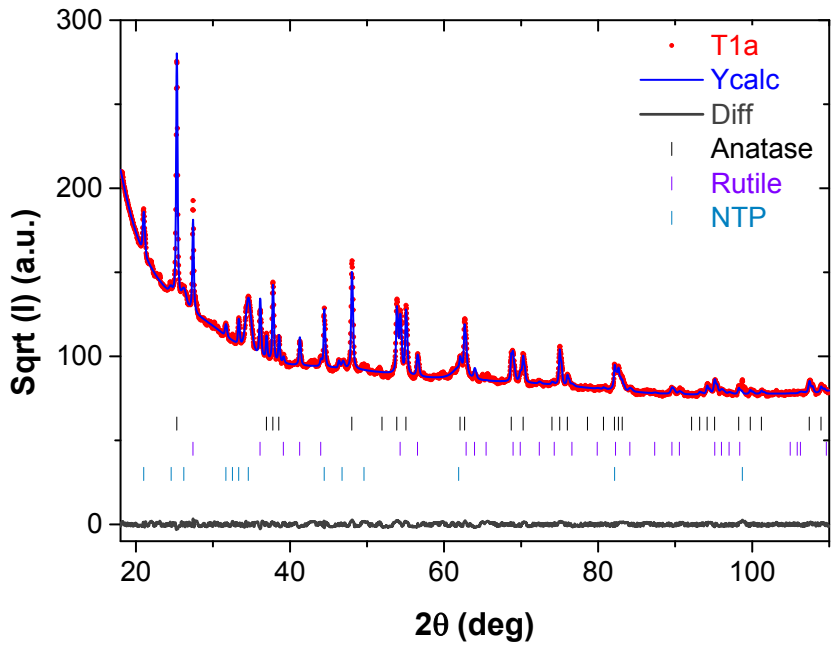

Fig. 9 Refinement of XRD diffraction pattern of pure TiO_2 NCs deposited on enamel supported onto steel sheets (T1a). Major contributions belong to rutile and anatase TiO_2 phases. The rest of the peaks appearing in the diffractogram have been modelled through a single phase for quantification purposes.

The XRD analyses (Table 5) show a growth in the particle sizes of the supported NCs with respect to those of non-calcined TiO_2 NCs in powder form (Tables 2 and 3). This can be ascribed to the sintering associated to the heating process carried out in the preparation of the supported photocatalysts (15 min at 700 ºC). Besides, similarly to the calcined non-supported NCs, the brookite phase was totally removed, the rutile form appeared and the anatase ratio increased in the NCs incorporation process. The three supported samples show similar relation between these phases, with *ca*. 75:25 anatase/rutile ratio.

Table 5 Summary of TiO_2 NCs sizes and anatase/rutile ratios determined by XRD of supported samples.

Sample	TM dopant	Anatase : rutile ratio	$Size_{Ana}$ (nm)	$Size_{Rut}$ (nm)
T1a	---	72 : 28	45	44
T4a	5% Mn	75 : 25	42	61
T6a	5% Co	76 : 24	23	25

The Raman spectra of T1a, T4a and T6a supported samples (Fig. 10) exhibit the typical peaks corresponding to the anatase phase (144 (E_g), 397 (B_{1g}), 514 ($A_{1g} + B_{1g}$) and 639 cm^{-1} (E_g)).[36] In addition, one band with lower intensity at 449 cm^{-1} associated to the E_g active mode of rutile phase is also observed.[37,39] As expected, the Raman analyses are in good agreement with XRD results.

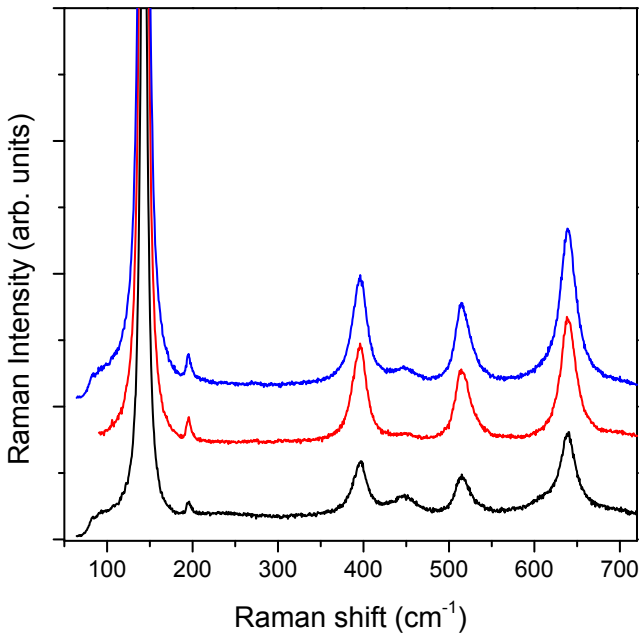

Fig. 10 Raman spectra of TiO_2 NCs deposited on enamel supported onto steel sheets; black, pure TiO_2 NCs (T1a); red, Mn-doped TiO_2 NCs (T4a); blue, Co-doped TiO_2 NCs (T6a).

Fig. 11(a) shows the optical reflectance spectra of undoped TiO_2 NCs both as nanocrystalline powder (T1) and supported photocatalyst (T1a). The absorption edge is centred at *ca*. 377 nm for the supported system, thus appearing slightly shifted to the visible region, compared to original TiO_2 NCs (373 nm). This shift can be ascribed to the appearance of 28% of rutile phase at the temperature employed in the NCs immobilization process on the enamel-coated steel sheet (700 ºC). Fig. 11(b) compares the optical reflectance of the enamel samples containing T1, T4 and T6 TiO_2 NCs deposited on steel sheets (T1a, T4a and T6a, respectively). The absorption edge is centred at 372 nm and 382 nm for the enamels obtained after the incorporation of NCs doped with Mn (T4a) and Co (T6a), respectively. Thus, the three supported samples display comparable absorption edge values, in agreement with their similar anatase/rutile ratio (Table 5). Besides, both the aforementioned charge-transfer transitions and the *d*-

d Co absorption band centred at 610 nm are also observed in the TM-doped samples, although the relative intensity is lower than the one observed for the starting powder NCs.

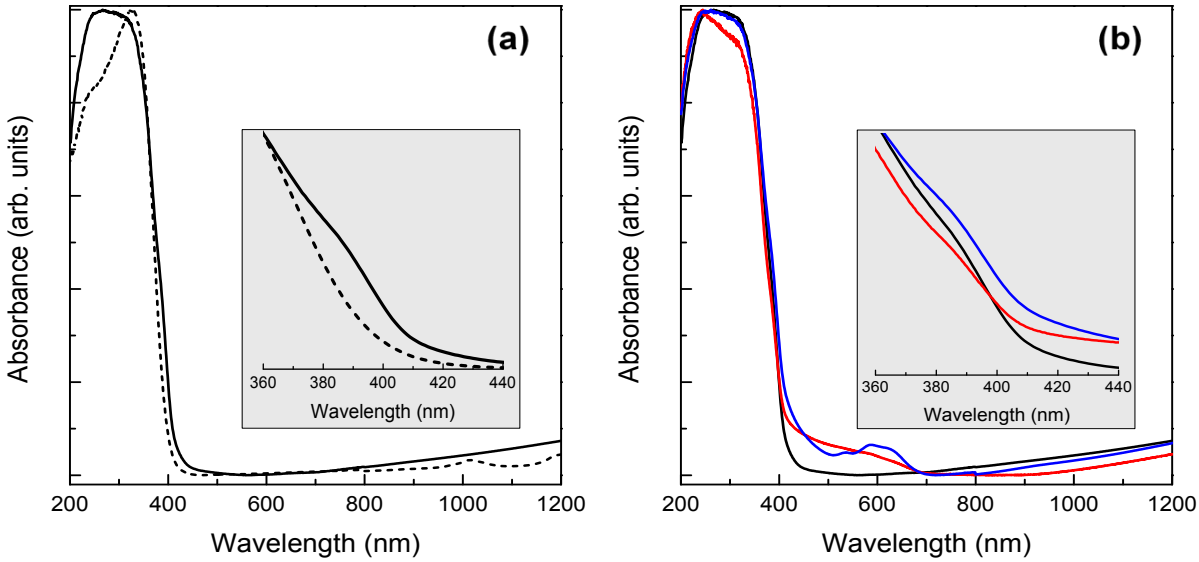

Fig. 11 (a) Optical reflectance of synthesized (T1) (dashed line) and supported (T1a) (solid line) non-doped TiO_2 NCs. (b) Optical reflectance of supported TiO_2 NCs; black, pure TiO_2 NCs (T1a); red, Mn-doped TiO_2 NCs (T4a); blue, Co-doped TiO_2 NCs (T6a).

5. Catalytic activity of TiO_2 NCs deposited on enamel supported onto stainless steel

Finally, the supported samples containing pure and TM-doped TiO_2 NCs were employed as photocatalysts. The main results are presented in Table 6 and Fig. 12. 16% MB degradation was observed after 8 h of reaction (54% at 24 h) in the experiment catalysed by the sample T1a containing non-doped TiO_2 NCs (Fig. 12a). By comparison, the sample T6a prepared with Co-doped TiO_2 NCs exhibits higher activity, leading to an increase in the MB decomposition (35% after 8 h of reaction, Fig. 12c). Since the three samples show similar anatase/rutile ratio (Table 6), the enhancement of catalytic activity can be attributed to the effect of the TM dopant. In addition, T1a contains bigger NCs than T6a and thus the size may play a role here. On the other hand, the sample containing Mn-doped TiO_2 NCs (T4a) is less active (9% MB degradation after 8 h of reaction, Fig. 12b) than both T1a and T6a, which could be due to the higher nanocrystalline size of rutile phase in T4a.[49]

We also carried out a number of experiments to study the recyclability of the TiO_2 NCs deposited on enamel supported onto stainless steel. Through extraction of the MB solution followed by reactivation with the LED lamp for 48 h, the supported photocatalysts T4a and T6a were reused in successive cycles. A substantial reduction in the activity was noted in the third cycle (Figs. S9-S10†), which can be due to a gradual loss of the supported TiO_2 NCs as a consequence of the repeated catalytic cycles. Thus, the supported samples display a limited potential for recyclability.

Table 6 Photocatalytic degradation of MB mediated by TiO_2 NCs deposited on enamel supported onto steel sheets.[a]

Sample	% TM dopant	Anatase : Rutile	$Size_{Ana}$ (nm)	$Size_{Rut}$ (nm)	MB degradation (%)	
					8 h	24 h
T1a	--	72 : 28	45	44	16	54
T4a	5% Mn	75 : 25	42	61	9	35
T6a	5% Co	76 : 24	23	25	35	55

[a] Reagents and conditions: MB (100 mL, 10 μM), catalyst (5 x 5 cm^2), 22 W, λ = 395 nm, RT.

Although the results described herein might seem moderate when compared with those reported for other nanosized TiO_2 systems either supported on glazed surfaces[13b,17a,19b-c,20a-c,21b-c] or contained in enamels,[17b,23a,24] it is important to note that: (i) the supported samples employed in this study contains only 5% of catalyst, and (ii) the experiments were performed under near-visible light (λ = 395 nm) with a low power LED lamp (22 W). Indeed, the use of a sunlight source with light intensity of *ca.* 500 lux would certainly improve the catalytic results. Thus, we suggest that the presented photocatalyst based on TiO_2 NCs show potential for a variety of applications as indoor and outdoor construction elements like floorings, walls, tunnels or subway panels.

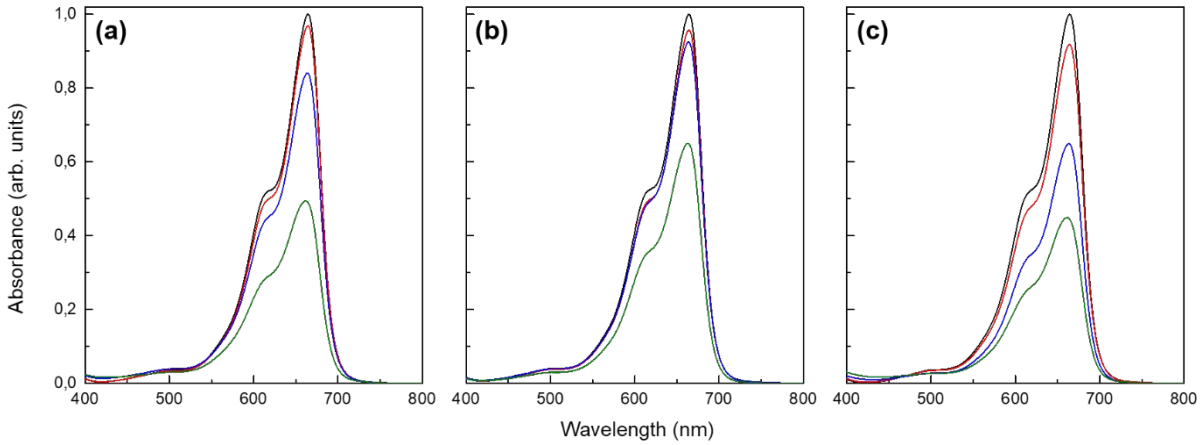

Fig. 12 Evolution of MB solution absorbance with time in a catalytic experiment mediated by (a) T1a, (b) T4a, and (c) T6a. Conditions: MB (150 mL, 10 μM), catalyst (5 x 5 cm^2), 22 W, λ = 395 nm, at RT; black, t = 0 h; red, t = 1 h; blue, t = 8 h; green, t = 24 h.

CONCLUSIONS

In summary, we have successfully employed a new family of undoped and Co- and Mn-doped TiO_2 NCs as catalysts for the photocatalytic degradation of MB. In line with the displacement of the absorption edge to the visible region, a clear positive effect of anatase/rutile ratio and TM dopants on the catalytic activity was observed. Specifically, the calcination of TiO_2 NCs involves an increase in the anatase ratio and the formation of rutile form, leading to a rise in activity that is attributed to a

synergistic effect between these phases. Similarly, the doping with Mn and Co gave rise to an enhancement of the catalytic performance.

Such NCs were used as an active material for the fabrication of an enamel immobilised onto stainless steel. The resulting supported photocatalyst was fully characterized through XRD as well as Raman and reflectance spectroscopies. This system showed good photocatalytic activity and, as in the case of non-supported NCs, an influence of the TM dopant was observed. Specifically, the sample prepared with Co-doped TiO_2 NCs exhibits the highest activity.

In conclusion, a new type of smart photocatalytic surface with very exciting properties has been devised. In this first application the catalytic system was employed in the photodegradation of MB, but after this thorough study the road seems open for many applications as a self-cleaning coating and potential use for NOx photodegradation.

AUTHOR INFORMATION

Corresponding Authors

*E-mail: icrico@us.es (Israel Cano)

*E-mail: rosa.martin@unican.es (Rosa Martín-Rodríguez)

ORCID

Andrea Diego-Rucabado: 0000-0002-8806-8784

Marina T. Candela: 0000-0002-8532-3735

Fernando Aguado: 0000-0003-2912-0228

Jesús González: 0000-0002-0381-6393

Rafael Valiente: 0000-0001-9855-8309

Israel Cano: 0000-0003-3727-9327

Rosa Martín-Rodríguez: 0000-0003-1568-592

AUTHOR CONTRIBUTIONS

Synthesis of TiO_2 NCs and photocatalytic experiments, Andrea Diego-Rucabado and Israel Cano; TEM images, Israel Cano; Preparation of enamel coatings on stainless steel, Eugenio Gómez; XRD analyses, Marina T. Candela and Fernando Aguado; Raman measurements, Andrea Diego-Rucabado and Jesús González; Reflectance, Andrea Diego-Rucabado and Rosa Martín-Rodríguez; Supervision and design of experiments, Rafael Valiente, Israel Cano and Rosa Martín-Rodríguez; Writing–original draft preparation, Israel Cano and Rosa Martín-Rodríguez; Writing–review and editing, Andrea Diego-Rucabado, Israel Cano and Rosa Martín-Rodríguez; Manuscript review, Andrea Diego-Rucabado, Fernando Aguado and Rafael Valiente; Project administration, Rafael Valiente; Funding acquisition, Eugenio Gómez, Rafael Valiente and Rosa Martín-Rodríguez. All authors have read and agreed to the published version of the manuscript.

CONFLICTS OF INTEREST

There are no conflicts of interest to declare.

FUNDING

This work was funded by the company VITRISPAN S.A.

ACKNOWLEDGMENTS

The authors acknowledge financial support from company VITRISPAN S.A. M.T.C. would like to thank University of Cantabria and the Government of Cantabria for her pre-doctoral grant "Concepción Arenal".

NOTES AND REFERENCES

1 (*a*) J. Balbuena, M. Cruz-Yusta and L. Sánchez, Nanomaterials to combat NO_x pollution, *J. Nanosci. Nanotechnol.*, 2015, **15**, 6373–6385; (*b*) A. J. Ebele, M. A.-E. Abdallah and S. Harrad, Pharmaceuticals and personal care products (PPCPs) in the freshwater aquatic environment, *Emerg. Contam.*, 2017, **3**, 1–16; (*c*) J. Li, H. Liu and J. P. Chen, Microplastics in freshwater systems: A review on occurrence, environmental effects, and methods for microplastics detection, *Water Res.*, 2018, **137**, 362–374.

2 (*a*) F. I. Khan and A. K. Ghoshal, Removal of Volatile Organic Compounds from polluted air, *J. Loss Prev. Process Ind.*, 2000, **13**, 527–545; (*b*) T. Masciangoli and W.-X. Zhang, Environmental technologies at the nanoscale, *Environ. Sci. Technol.*, 2003, **37**, 102–108; (*c*) P. G. Tratnyek and R. L. Johnson, Nanotechnologies for environmental cleanup, *Nano Today*, 2006, **1**, 44–48; (*d*) A. Vaseashta, M. Vaclavikova, S. Vaseashta, G. Gallios, P. Roy and O. Pummakarnchana, Nanostructures in environmental pollution detection, monitoring, and remediation, *Sci. Technol. Adv. Mater.*, 2007, **8**, 47–59.

3 F. Petronella, A. Truppi, C. Ingrosso, T. Placido, M. Striccoli, M. L. Curri, A. Agostiano and R. Comparelli, Nanocomposite materials for photocatalytic degradation of pollutants, *Catal. Today*, 2017, **281**, 85-100.

4 (*a*) Y. Paz, Application of TiO_2 photocatalysis for air treatment: Patents' overview, *Appl. Catal. B*, 2010, **99**, 448–460; (*b*) M. Lazar, S. Varguese and S. Nair, Photocatalytic water treatment by titanium dioxide: recent updates, *Catalysts*, 2012, **2**, 572–601; (*c*) S. W. Verbruggen, TiO_2 photocatalysis for the degradation of pollutants in gas phase: From morphological design to plasmonic enhancement, *J. Photochem. Photobiol. C-Photochem. Rev.*, 2015, **24**, 64–82.

5 M. Pelaez, N. T. Nolan, S. C. Pillai, M. K. Seery, P. Falaras, A. G. Kontos, P. S. M. Dunlop, J. W. J. Hamilton, J. A. Byrne, K. O`Shea, M. H. Entezari and D. D. Dionysiou, A review on the visible light

active titanium dioxide photocatalysts for environmental applications, *Appl. Catal. B*, 2012, **125**, 331–349.

6 (*a*) H. Choi, S. R. Al-Abed, D. D. Dionysiou, E. Stathatos and P. Lianos, TiO_2-based advanced oxidation nanotechnologies for water purification and reuse, *Sustain. Sci. Eng.*, 2010, **8**, 229–254; (*b*) A. Ajmal, I. Majeed, R. N. Malik, H. Idriss and M. A. Nadeem, Principles and mechanisms of photocatalytic dye degradation on TiO_2 based photocatalysts: a comparative overview, *RSC Adv.*, 2014, **4**, 37003–37026.

7 (*a*) S. N. Frank and A. J. Bard, Heterogeneous photocatalytic oxidation of cyanide ion in aqueous solutions at titanium dioxide powder, *J. Am. Chem. Soc.*, 1977, **99**, 303–304; (*b*) S. N. Frank and A. J. Bard, Heterogeneous photocatalytic oxidation of cyanide and sulfite in aqueous solutions at semiconductor powders, *J. Phys. Chem.*, 1977, **81**, 1484–1488.

8 A. Truppi, F. Petronella, T. Placido, M. Striccoli, A. Agostiano, M. L. Curri and R. Comparelli, Visible-light-active TiO_2-based hybrid nanocatalysts for environmental applications, *Catalysts*, 2017, **7**, 100.

9 (*a*) H.-J. Kim, Y.-G. Shul and H. Han, Photocatalytic properties of silica-supported TiO_2, *Top. Catal.*, 2005, **35**, 287–293; (*b*) D. Maučec, A. Šuligoj, A. Ristić, G. Dražić, A. Pintar and N. N. Tušar, Titania versus zinc oxide nanoparticles on mesoporous silica supports as photocatalysts for removal of dyes from wastewater at neutral pH, *Catal. Today*, 2018, **310**, 32–41.

10 J. Chen, F. Qiu, W. Xua, S. Cao and H. Zhu, Recent progress in enhancing photocatalytic efficiency of TiO_2-based materials, *Appl. Catal. A-Gen.*, 2015, **495**, 131–140.

11 M. Zarezade, S. Ghasemi and M. R. Gholami, The effect of multiwalled carbon nanotubes and activated carbon on the morphology and photocatalytic activity of TiO_2/C hybrid materials, *Catal. Sci. Technol.*, 2011, **1**, 279–284.

12 (*a*) Z. Zhang, Y. Xu, X. Ma, F. Li, D. Liu, Z. Chen, F. Zhang and D. D. Dionysiou, Microwave degradation of methyl orange dye in aqueous solution in the presence of nano-TiO_2-supported activated carbon (supported-TiO_2/AC/MW), *J. Hazard Mater.*, 2012, **209-210**, 271–277; (*b*) M. Ouzzine, A. J. Romero-Anaya, M. A. Lillo-Ródenas and A. Linares-Solano, Spherical activated carbon as an enhanced support for TiO_2/AC photocatalysts, *Carbon*, 2014, **67**, 104–118; (*c*) D. Liu, Z. Wu, F. Tian, B.-C. Ye and Y. Tong, Synthesis of N and La co-doped TiO_2/AC photocatalyst by microwave irradiation for the photocatalytic degradation of naphthalene, *J. Alloy Compd.*, 2016, **676**, 489–498; (*d*) S. Ali, Z. Li, S. Chen, A. Zada, I. Khan, I. Khan, W. Ali, S. Shaheen, Y. Qu and L. Jing, Synthesis of activated carbon-supported TiO_2-based nano-photocatalysts with well recycling for efficiently degrading high-concentration pollutants, *Catal. Today*, 2019, **335**, 557–564.

13 (*a*) K. Tennakone and K.G.U. Wijayantha, Photocatalysis of CFC degradation by titanium dioxide, *Appl. Catal. B*, 2005, **57**, 9–12; (*b*) K. Sirirerkratana, P. Kemacheevakul and S. Chuangchote, Color

removal from wastewater by photocatalytic process using titanium dioxide-coated glass, ceramic tile, and stainless-steel sheets, *J. Clean. Prod.*, 2019, **215**, 123–130.

14 (*a*) L. Torkian, M. M. Amini and E. Amereh, Sol-gel synthesised silver doped TiO_2 nanoparticles supported on NaX zeolite for photocatalytic applications, *Mater. Technol.*, 2013, **28**, 111–116; (*b*) M. N. Chong, Z. Y. Tneu, P. E. Poh, B. Jin and R. Aryal, Synthesis, characterization and application of TiO_2-zeolite nanocomposites for the advanced treatment of industrial dye wastewater, *J. Taiwan Inst. Chem. Eng.*, 2015, **50**, 288–296; (*c*) N. U. Saqib, R. Adnan and I. Shah, Zeolite supported TiO_2 with enhanced degradation efficiency for organic dye under household compact fluorescent light, *Mater. Res. Express*, 2019, **6**, 095506.

15 (*a*) H. B. Hadjltaief, M. B. Zina, M. E. Galvez and P. D. Costa, Photocatalytic degradation of methyl green dye in aqueous solution over natural clay-supported ZnO-TiO_2 catalysts, *J. Photochem. Photobiol., A*, 2016, **315**, 25–33; (*b*) A. Mishra, A. Mehta and S. Basu, Clay supported TiO_2 nanoparticles for photocatalytic degradation of environmental pollutants: A review, *J. Environ. Chem. Eng.*, 2018, **6**, 6088–6107.

16 (*a*) R. Zuo, G. Du, W. Zhang, L. Liu, Y. Liu, L. Mei and Z. Li, Photocatalytic degradation of methylene blue using TiO_2 impregnated diatomite, *Adv. Mater. Sci. Eng.*, 2014, 170148; (*b*) B. Wang, G. Zhang, Z. Sun and S. Zheng, Synthesis of natural porous minerals supported TiO_2 nanoparticles and their photocatalytic performance towards Rhodamine B degradation, *Powder Technol.*, 2014, **262**, 1–8.

17 (*a*) S. Ke, X. Cheng, Q. Wang, Y. Wang and Z. Pan, Preparation of a photocatalytic TiO_2/$ZnTiO_3$ coating on glazed ceramic tiles, *Ceram. Int.*, 2014, **40**, 8891–8895; (*b*) L. Baltes, S. Patachia, M. Tierean, O. Ekincioglu and H. M. Ozkul, Photoactive glazed polymer-cement composite, *Appl. Surf. Sci.*, 2018, **438**, 84–95.

18 (*a*) A. Fernández, G. Lassaletta, V. M. Jiménez, A. Justo, A. R. González-Elipe, J.-M. Herrmann, H. Tahiri and Y. Ait-Ichou, Preparation and characterization of TiO_2 photocatalysts supported on various rigid supports (glass, quartz and stainless steel). Comparative studies of photocatalytic activity in water purification, *Appl. Catal. B*, 1995, **7**, 49–63; (*b*) L. Zhang, Y. Zhu, Y. He, W. Li and H. Sun, Preparation and performances of mesoporous TiO_2 film photocatalyst supported on stainless steel, *Appl. Catal. B*, 2003, **40**, 287–292; (*c*) S. Permpoon, M. Fallet, G. Berthomé, B. Baroux, J. C. Joud and M. Langlet, Photoinduced hydrophilicity of TiO_2 films deposited on stainless steel via sol-gel technique, *J. Sol-Gel Sci. Technol.*, 2005, **35**, 127–136; (*d*) J.-P. Nikkanen, E. Huttunen-Saarivirta, T. Salminen, L. Hyvärinen, M. Honkanen, E. Isotahdon, S. Heinonen and E. Levänen, Enhanced photoactive and photoelectrochemical properties of TiO_2 sol–gel coated steel by the application of SiO_2 intermediate layer, *Appl. Catal. B*, 2015, **174–175**, 533–543.

19 See the following for a variety of examples of TiO_2 NPs deposited on glazed surfaces for photocatalytic applications: (*a*) V. S. Smitha, K. A. Manjumol, K. V. Baiju, S. Ghosh, P. Perumal and

K. G. K. Warrier, Sol–gel route to synthesize titania-silica nano precursors for photoactive particulates and coatings, *J. Sol-Gel Sci. Technol.*, 2010, **54**, 203–211; (*b*) B. K. Kaleji, R. Sarraf-Mamoory, K. Nakata and A. Fujishima, The effect of Sn dopant on crystal structure and photocatalytic behavior of nanostructured titania thin films, *J. Sol-Gel Sci. Technol.*, 2011, **60**, 99–107; (*c*) K. Murugana, R. Subasri, T. N. Rao, A. S. Gandhi and B. S. Murty, Synthesis, characterization and demonstration of self-cleaning TiO_2 coatings on glass and glazed ceramic tiles, *Prog. Org. Coat.*, 2013, **76**, 1756–1760.

20 See the following for a variety of examples of TiO_2 NPs deposited on glazed surfaces for environmental applications: (*a*) P. S. Marcos, J. Marto, T. Trindade and J. A. Labrincha, Screen-printing of TiO_2 photocatalytic layers on glazed ceramic tiles, *J. Photochem. Photobiol., A*, 2008, **197**, 125–131; (*b*) M. Raimondo, G. Guarini, C. Zanelli, F. Marani, L. Fossa and M. Dondi, Photocatalytic, highly hydrophilic porcelain stoneware slabs, *IOP Conf. Ser.: Mat. Sci. Eng.*, 2011, **18**, 222022; (*c*) B. K. Kaleji, N. Hosseinabadi and A. Fujishima, Enhanced photo-catalytic activity of TiO_2 nanostructured thin films under solar light by Sn and Nb co-doping, *J. Sol-Gel Sci. Technol.*, 2013, **65**, 195–203; (*d*) P. Zhang, J. Tian, R. Xu and G. Ma, Hydrophilicity, photocatalytic activity and stability of tetraethyl orthosilicate modified TiO_2 film on glazed ceramic surface, *Appl. Surf. Sci.*, 2013, **266**, 141–147; (*e*) S. de Niederhausern and M. Bondi, Self-cleaning and antibacteric ceramic tile surface, *Int. J. Appl. Ceram. Technol.*, 2013, **10**, 949–956; (*f*) R. Taurino, L. Barbieri and F. Bondioli, Surface properties of new green building material after TiO_2–SiO_2 coatings deposition, *Ceram. Int.*, 2016, **42**, 4866–4874; (*g*) A. L. da Silva, M. Dondi and D. Hotza, Self-cleaning ceramic tiles coated with Nb_2O_5-doped-TiO_2 nanoparticles, *Ceram. Int.*, 2017, **43**, 11986–11991; (*h*) A. Barmeh, M. R. Nilforoushan and S. Otroj, Wetting and photocatalytic properties of Ni-doped TiO_2 coating on glazed ceramic tiles under visible light, *Thin Solid Films*, 2018, **66**, 137–142; (*i*) H. Oladipo, C. Garlisi, K. Al-Ali, E. Azar and G. Palmisano, Combined photocatalytic properties and energy efficiency via multifunctional glass, *J. Environ. Chem. Eng.*, 2019, **7**, 102980.

21 (*a*) M. Machida, K. Norimoto and T. Kimura, Antibacterial activity of photocatalytic titanium dioxide thin films with photodeposited silver on the surface of sanitary ware, *J. Am. Ceram. Soc.*, 2005, **88**, 95–100; (*b*) B. K. Kaleji, R. Sarraf-Mamoory and S. Sanjabi, Photocatalytic evaluation of a titania thin film on glazed porcelain substrates via a $TiCl_4$ precursor, *Reac. Kinet. Mech. Cat.*, 2011, **103**, 289–298; (*c*) K. Malnieks, G. Mezinskis, I. Pavlovska, L. Bidermanis and A. Pludons, Optical, photocatalytical and structural Properties of TiO_2-SiO_2 sol-gel coatings on high content SiO_2 enamel surface, *Mat. Sci.*, 2015, **21**, 100–104.

22 (*a*) D. Onna, K. M. Fuentes, C. Spedalieri, M. Perullini, M. C. Marchi, F. Alvarez, R. J. Candal and S. A. Bilmes, Wettability, photoactivity, and antimicrobial activity of glazed ceramic tiles coated with titania films containing tungsten, *ACS Omega*, 2018, **3**, 17629–17636; (*b*) M. Piispanen, J. Määttä, S. Areva, A.-M. Sjöberg, M. Hupa and L. Hupa, Chemical resistance and cleaning properties of coated glazed surfaces, *J. Eur. Ceram. Soc.*, 2009, **29**, 1855–1860.

23 (*a*) W. Jiang, Y. Wang and L. Gu, Influence of TiO_2 film on photo-catalytic property of enamels, *J. Non-Cryst. Solids*, 2007, **353**, 4191–4194; (*b*) S.-J. Yoo, S.-I. Lee, D.-H. Kwak, K.-G. Kim, K.-J. Hwang, J.-W. Lee, U.-Y. Hwang, H.-S. Park and J.-O. Kim, Photocatalytic degradation of methylene blue and acetaldehyde by TiO_2/glaze coated porous red clay tile, *Korean J. Chem. Eng.*, 2008, **25**, 1232–1238.

24 S. Morelli, R. Pérez, A. Querejeta, J. Muñoz, L. Lusvarghi, M. L. Gualtieri, G. Bolelli and H.-J. Grande, Photocatalytic enamel/TiO_2 coatings developed by electrophoretic deposition for methyl orange decomposition, *Ceram. Int.*, 2018, **44**, 16199–16208.

25 J. He, Y.-e. Du, Y. Bai, J. An, X. Cai, Y. Chen, P. Wang, X. Yang and Q. Feng, Facile formation of anatase/rutile TiO_2 nanocomposites with enhanced photocatalytic activity, *Molecules*, 2019, **24**, 2996.

26 R. Su, R. Bechstein, L. Sø, R. T. Vang, M. Sillassen, B. Esbjörnsson, A. Palmqvist and F. Besenbacher, How the anatase-to-rutile ratio influences the photoreactivity of TiO_2, *J. Phys. Chem. C*, 2011, **115**, 24287–24292.

27 R. Ma and T. Chen, Checking the synergetic effect between anatase and rutile, *J. Phys. Chem. C*, 2019, **123**, 19479–19485.

28 A. Di Paola, M. Bellardita and L. Palmisano, Brookite, the least known TiO_2 photocatalyst, *Catalysts*, 2013, **3**, 36–73.

29 S. Yadava and G. Jaiswar, Review on undoped/doped TiO_2 nanomaterial; synthesis and photocatalytic and antimicrobial activity, *J. Chin. Chem. Soc.*, 2017, **64**, 103–116.

30 We tested different synthesis methods described in preliminary studies: (*a*) W. Choi, A. Termin and M. R. Hoffmann, The role of metal ion dopants in quantum-sized TiO_2: Correlation between photoreactivity and charge carrier recombination dynamics, *J. Phys. Chem.*, 1994, **98**, 13669–13679; (*b*) G. Oskam, A. Nellore, R. L. Penn and P. C. Searson, The growth kinetics of TiO_2 nanoparticles from titanium(IV) alkoxide at high water/titanium ratio, *J. Phys. Chem. B*, 2003, **107**, 1734–1738; (*c*) G. Lusvardi, C. Barani, F. Giubertoni and G. Paganelli, Synthesis and characterization of TiO_2 nanoparticles for the reduction of water pollutants, *Materials*, 2017, **10**, 1208, among which the latter was chosen because it allows an easy scale-up.

31 A. Kern, A. A. Coelho and R. W. Cheary, Convolution based profile fitting. *Diffraction Analysis of the Microstructure of Materials*, ed. E. J. Mittemeijer, P. Scardi, Springer, 2004.

32 D. Balzar, Voigt function model in diffraction-line broadening analysis. *Defect and Microstructure Analysis by Diffraction*, ed. R. Snyder, J. Fiala & H. J. Bunge, IUCr / Oxford University Press, 1999, 94–126.

33 R. W. Cheary, A. A. Coelho and J. P. Cline, Fundamental parameters line profile fitting in laboratory diffractometers, *J. Res. Natl. Inst. Stand. Technol.*, 2004, **109**, 1–25.

34 ISO 10678:2010. Fine ceramics (advanced ceramics, advanced technical ceramics) – Determination of photocatalytic activity of surfaces in aqueous medium by degradation of methylene blue.

35 Anatase and brookite transform to rutile at temperatures higher than 600 ºC. See: Y. Hu, H.-L. Tsai and C.-L. Huangk, Effect of brookite phase on the anatase–rutile transition in titania nanoparticles, *J. Eur. Ceram. Soc.*, 2003, **23**, 691–696.

36 (*a*) A. Felske and W. J. Plieth. Raman spectroscopy of titanium dioxide layers, *Electrochim. Acta*, 1989, **34**, 75–77; (*b*) J. S. Dalton, P. A. Janes, N. G. Jones, J. A. Nicholson, K. R. Hallam and G. C. Allen, Photocatalytic oxidation of NOx gases using TiO_2: a surface spectroscopic approach, *Environ. Pollut.*, 2002, **120**, 415–422; (*c*) A. G. Ilie, M. Scarisoreanu, E. Dutu, F. Dumitrache, A.-M. Banici, C. T. Fleaca, E. Vasile and I. Mihailescu, Study of phase development and thermal stability in as synthesized TiO_2 nanoparticles by laser pyrolysis: ethylene uptake and oxygen enrichment, *Appl. Surf. Sci.*, 2018, **427**, 798–806.

37 J.-G. Li, T. Ishigaki and X. Sun, Anatase, brookite, and rutile nanocrystals via redox reactions under mild hydrothermal conditions: phase-selective synthesis and physicochemical properties, *J. Phys. Chem. C*, 2007, **111**, 4969–4976.

38 R. L. Frost, J. Kristof, L. Rintoul and J. T. Kloprogge, Raman spectroscopy of urea and urea-intercalated kaolinites at 77 K, *Spectrochim. Acta A*, 1999, **56**, 1681–1691.

39 S. P. S. Porto, P. A. Fleury and T. C. Damen, Raman spectra of TiO_2, MgF_2, ZnF_2, FeF_2, and MnF_2, *Phys. Rev.*, 1967, **154**, 522–526.

40 (*a*) W. Choi, A. Termin and M. R. J. Hoffmann, The role of metal ion dopants in quantum-sized TiO_2: correlation between photoreactivity and charge carrier recombination dynamics, *Phys. Chem.*, 1994, **98**, 13669–13679; (*b*) M. Zhou, J. Yu and B. J. Cheng, Effects of Fe-doping on the photocatalytic activity of mesoporous TiO_2 powders prepared by an ultrasonic method, *Hazard. Mater.*, 2006, **137**, 1838–1847; (*c*) J. Yu, Q. Xiang and M. Zhou, Preparation, characterization and visible-light-driven photocatalytic activity of Fe-doped titania nanorods and first-principles study for electronic structures, *Appl. Catal. B*, 2009, **90**, 595–602; (*d*) J. Chen, M. Yao and X. Wang, Investigation of transition metal ion doping behaviours on TiO_2 nanoparticles, *J. Nanopart. Res.*, 2008, **10**, 163–171; (*e*) L. G. Devi and S. G. Kumar, Influence of physicochemical–electronic properties of transition metal ion doped polycrystalline titania on the photocatalytic degradation of Indigo Carmine and 4-nitrophenol under UV/solar light, *Appl. Surf. Sci.*, 2011, **257**, 2779–2790.

41 M. Shilpy, M. A. Ehsan, T. H. Ali, S. B. A. Hamid and Md. E. Ali, Performance of cobalt titanate towards H_2O_2 based catalytic oxidation of lignin model compound, *RSC Adv.*, 2015, **5**, 79644–79653.

42 (*a*) T. A. Kandiel, L. Robben, A. Alkaima and D. Bahnemann, Brookite *versus* anatase TiO_2 photocatalysts: phase transformations and photocatalytic activities, *Photochem. Photobiol. Sci.*, 2013, **12**, 602–609; (*b*) N. S. Allen, N. Mahdjoub, V. Vishnyakov, P. J. Kelly and R. J. Kriek, The effect of crystalline phase (anatase, brookite and rutile) and size on the photocatalytic activity of calcined polymorphic titanium dioxide (TiO_2), *Polym. Degrad. Stab.*, 2018, **150**, 31–36.

43 Y. Lan, Y. Lu and Z. Ren, Mini review on photocatalysis of titanium dioxide nanoparticles and their solar applications, *Nano Energy*, 2013, **2**, 1031–1045.

44 (*a*) T. Umebayashi, T. Yamaki, H. Itoh and K. Asai, Analysis of electronic structures of 3d transition metal-doped TiO_2 based on band calculations, *J. Phys. Chem. Solids*, 2002, **63**, 1909–1920; (*b*) B. Peng, X. Meng, F. Tang, X. Ren, D. Chen and J. Ren, General synthesis and optical properties of monodisperse multifunctional metal-ion-doped TiO_2 hollow particles, *J. Phys. Chem. C*, 2009, **113**, 20240–20245.

45 (*a*) W. Zhang, W. Zhou, J. H. Wright, Y. N. Kim, D. Liu and X. Xiao, Mn-Doped TiO_2 nanosheet-based spheres as anode materials for lithium-ion batteries with high performance at elevated temperatures, *ACS Appl. Mater. Interfaces*, 2014, **6**, 7292−7300; (*b*) I. Birlik and D. Dagdelen, Synergistic effect of manganese and nitrogen codoping on photocatalytic properties of titania nanoparticles, *Bull. Mater. Sci.*, 2020, **43**, 85.

46 A. Houas, H. Lachheb, M. Ksibi, E. Elaloui, C. Guillard and J.-M. Herrmann, Photocatalytic degradation pathway of methylene blue in water, *Appl. Catal. B*, 2001, **31**, 145–157.

47 H. A. Le, L. T. Linh, S. Chin and J. Jurng, Photocatalytic degradation of methylene blue by a combination of TiO_2-anatase and coconut shell activated carbon, *Powder Technol.*, 2012, **225**, 167–175.

48 D. A. H. Hanaor and C. C. Sorrell, Review of the anatase to rutile phase transformation, *J. Mater. Sci.*, 2011, **46**, 855–874.

49 As in the case of calcined NCs, the preparation of the supported photocatalysts involves a calcination process that discards a possible positive effect of N-dopant on the photocatalytic activity (see Experimental Section for more details).

Photocatalytic activity of ~~pur~~undoped and Mn- and Co-doped TiO_2 nanocrystals incorporated in enamel coatings on stainless steel†

Andrea Diego-Rucabado,[ab] Marina T. Candela,[bc] Fernando Aguado,[b]c Jesús González,[b]c Eugenio Gómez,[d] Rafael Valiente,[ab] Israel Cano*[ae] and Rosa Martín-Rodríguez*[bf]

ABSTRACT: A series of undoped and transition-metal (TM)-doped TiO_2 nanocrystals (NCs) were synthesized and calcined at different temperatures, and fully characterized. Such NCs were employed as catalyst for the photodegradation of methylene blue, which enabled to study the influence of both NCs size and anatase/brookite/rutile phases ratio on the photocatalytic activity, as well as the effect of different TM dopants, namely Mn and Co. Then, the NCs were used as active additive for the fabrication of a new photocatalytic system composed of an enamel incorporating these NCs supported onto a stainless-steel sheet. NCs both in powder form and incorporated in enamels deposited on steel were characterized by transmission electron microscopy, X-ray diffraction, and reflectance and Raman spectroscopies. We demonstrate how the calcination of TiO_2 NCs induces both a growth in the anatase ratio and formation of rutile form, which leads to a photocatalytic activity increase. Similarly, doping with Mn and Co gives rise to an enhancement of the catalytic performance attributed to a displacement of the energy bandgap. The obtained material combines the resistance of steel and the photocatalytic activity of TiO_2 deposited on enamel, which also operates as a corrosion protection layer for the former. The resulting smart photocatalytic surface presents many applications as a self-cleaning coating and potential use for NOx photodegradation.

Keywords: enamel · metal nanocrystals · methylene blue · photocatalytic surface · photocatalysis · photodegradation · TiO_2 nanocrystals · transition metal

[a] *Applied Physics Department, University of Cantabria, Avda. de Los Castros 48, 39005 Santander, Spain*
[b] *Nanomedicine Group, IDIVAL, Avda. Cardenal Herrera Oria s/n, 39011 Santander, Spain*
[c] *CITIMAC Department, University of Cantabria, Avda. de Los Castros 48, 39005 Santander, Spain*
[d] *VITRISPAN S.A., Barrio Rioseco, 39786 Guriezo, Spain*
[e] *Crystallography, Mineralogy and Agricultural Chemistry Department. Faculty of Chemistry, University of Seville, 41012 Seville, Spain. E-mail: icrico@us.es*
[f] *QUIPRE Department, University of Cantabria, Avda. de Los Castros 46, 39005 Santander, Spain. E-mail: rosa.martin@unican.es*

† Electronic supplementary information (ESI) available: XRD analyses, TEM images and photographs of supported photocatalysts.

INTRODUCTION

Nowadays, environmental pollution constitutes one of the most urgent problems[1] and thus the development of more efficient air and water decontamination treatments has become an increasingly important research area.[2] In this context, air and water treatment can be achieved through photo-oxidation processes catalysed by semiconductor catalysts.[3,4] Among them, titanium oxide (TiO_2) is the most widely employed photocatalyst to decompose organic and inorganic compounds in polluted water and air,[4,5,6] since the first report of Frank and Bard in 1977, where the reduction of CN^- in water catalysed by TiO_2 was reported.[7] This semiconductor exhibits multiple interesting properties that makes it a very suitable photocatalyst for this type of processes, including low cost, high photocatalytic activity, low toxicity, and high thermal and chemical stability.[5] Specifically, TiO_2 nanoparticles (NPs) have shown a particular ability to perform this transformation due to their high surface-to-volume ratio, which results in an increase of the number of active sites and thus leads to a higher catalytic activity.[8] Furthermore, the band gap of semiconductor nanomaterials is size-dependent, which can be employed to control the photocatalytic process through an effective tuning of redox potentials of generated electron/hole pairs.[8] However, a decrease or total loss of activity can be produced as a result of NPs aggregation. As a strategy to solve this problem, TiO_2 NPs can be dispersed and immobilised on a support, leading to more stable catalysts by preventing agglomeration. Different supports have been employed to immobilise TiO_2 NPs, such as SiO_2,[9] carbon nanotubes (CNTs),[10] multiwalled carbon nanotubes (MWCNTs),[11] graphene,[10] activated carbon,[11,12] glass,[13] zeolite,[14] clay,[15] diatomite,[16] ceramics,[13b,17] and stainless steel.[18] In this context, nanosized TiO_2 can be supported on glazed surfaces[13b,17a,19,20,21,22] or incorporated into enamels[17b,23,24] to generate smart photocatalytic materials with self-cleaning properties that may additionally serve as an interesting functionality for different applications. Particularly, a large body of literature has emerged describing the use of these functional materials as coating for high solar power receivers,[21c] electrical lines,[21b] reactors,[13b] sanity wares,[21a] building's indoor and outdoor applications,[22,23] and construction elements like floorings, glasses, roofing, and walls, tunnels and subway panels.[17,20,23]

In this work, we describe a new photocatalytic surface composed of an enamel containing 5% of TiO_2 NCs supported onto a stainless-steel substrate. This material combines the resistance of steel and the photocatalytic activity of TiO_2 deposited on enamel, which also acts as protecting layer for the former. The resulting smart photocatalytic surface holds great potential for use in a variety of applications such as self-cleaning coating used in means of transport (ships, trains), reactors to remove dye pollutants in wastewater from textile industry, water tanks, or boilers and vessels for food and water.

Firstly, the influence of both NCs size and anatase/brookite/rutile phases ratio in the photocatalytic properties has been analysed. It is generally accepted that although anatase shows better performance due to its higher Fermi level and indirect gap, the photocatalytic activity is maximized for a composition of *ca*. 70% anatase and 30% rutile.[25] However, there is still an open controversy and contradictory

results regarding this synergistic effect between anatase and rutile phases.[26,27] In addition, the brookite form is also photocatalytically active, and thus its effect in a mixture of different TiO_2 phases should not be ignored.[28] Secondly, the effect of different transition metal (TM) dopants on the catalytic performance was studied, since the modification of TiO_2 bandgap with TM may induce a shift of its spectral response towards the visible region and increase the activity of the photocatalytic material.[6b,10,29] To this end, not only undoped but also Mn- and Co-doped TiO_2 NCs were synthesized, integrated on the surface of an enamel, and supported onto stainless steel sheets. NCs both in powder form and immobilised on enamels deposited onto steel were fully characterized by different techniques, such as X-ray diffraction (XRD), transmission electron microscopy (TEM), as well as Raman and reflectance spectroscopy. The photocatalytic activity of the designed systems was evaluated using the photodegradation of methylene blue (MB) in water as a model reaction.

EXPERIMENTAL

1. Materials

Urea (99.5%, Merck), titanium (IV) isopropoxide (>99.995%, Sigma-Aldrich), manganese(II) chloride tetrahydrate (99%, Alfa Aesar), cobalt(II) chloride hexahydrate (99%, Riedel-de Haën) and methylene blue (82%, Panreac), were purchased from commercial sources. All chemicals were used without any further purification. All manipulations were performed in air atmosphere.

2. Synthesis of TiO_2 nanocrystals

The TiO_2 NCs analysed in this work consist of two groups of samples synthesized by a method adapted from the procedure described by Lusvardi *et al.*[30] Interestingly, this synthesis procedure produces crystalline anatase and brookite TiO_2 NCs. Briefly, titanium isopropoxide was added dropwise to an aqueous solution of urea (1:0.5 Ti:urea ratio) and the mixture was stirred at 50 ºC for 60 minutes. Then, the solution was heated up at *ca*. 85 ºC under stirring to remove the excess water, obtaining the nanocrystalline TiO_2 powder. The TM-doped samples were prepared by adding stoichiometric amounts of the corresponding metal chloride to the urea solution. A subsequent calcination process was performed in order to remove the urea excess and increase the rutile ratio.

The first set of NCs presents three samples (T1-T3): the as-obtained NCs, NCs subjected to a thermal treatment of 600 ºC for 2 hours, and NCs calcined at 800 ºC for 2 hours. The second group of samples comprises TiO_2 NCs doped with 5 mol% of Mn and Co, both as-prepared and calcined at 600 ºC (T4-T7). Table 1 summarizes the studied NCs and the experimental parameters employed in each synthesis.

Table 1 Summary of the undoped and TM-doped TiO_2 NCs.

Sample	TM dopant	Calcination temperature (ºC)
T1	--	---
T2	--	600
T3	--	800
T4	5% Mn	---
T5	5% Mn	600
T6	5% Co	---
T7	5% Co	600

3. Preparation of the supported photocatalyst

In order to prepare the support, two types of enamels were deposited on stainless steel sheets (AC01EK quality with 0.08% carbon content): firstly, base enamel and, secondly, coat enamel. In both cases, the precursors (enamel frit, clay, $NaAlO_2$, urea and water) were ground in a ball mill to obtain a suspension with density of *ca*. 1.75-1.80 g/mL.

The base enamel was deposited onto the stainless steel sheets and dried at 100 °C. Subsequently, this base enamel was vitrified by heating at 840 °C for 3 min. After cooling down, the coat enamel was deposited on the vitrified base enamel, dried at 100 ºC and vitrified by heating at 830 °C for 3 min. The resulting vitrified coat enamel shows a thickness of *ca*. 150 μm, while the base enamel exhibits a thickness around 120 μm.

To prepare the supported photocatalyst (5% TiO_2), NCs were mixed with a serigraph-type oil (mainly composed of acrylic resins and propylene glycol ester in a 2:5 w:w ratio) to obtain an appropriate viscosity. The mixture was deposited on the prepared support (enamel onto stainless steel sheets) by indirect serigraphy and vitrified by heating at 700 ºC for 15 min.

4. Structural and optical characterization

4.1 X-ray powder diffraction

Crystal structure and particle size of all synthesized samples were studied by XRD. XRD measurements were performed either in a Bruker D8 Advanced diffractometer equipped with a Cu tube (wavelength: $<K\alpha_{1,2}>$= 1.5418 Å) and a fast Lynxeye 1D-detector, or in a Bruker D2 Phaser diffractometer with a Cu tube and a 0D Xflash detector. Both the starting synthesized NCs and the prepared supported catalysts were measured in the 10-120º range (2θ) for phase identification and quantification as well as structure refinement. The Rietveld method was applied to patterns from all the samples for the structural analysis. Microstructural parameters were determined from the whole powder pattern fitting through a

convolution procedure as implemented in the software TOPAS.[31] Average crystallite sizes were determined based on the Double Voigt approach (size and strain contributions).[32] The instrumental line broadening was determined from the Fundamental Parameters approach[33] as well as the standard method (LaB_6 sample).

4.2 Transmission electron microscopy

Morphology and size distribution of TiO_2 NCs were analysed through TEM images obtained with a JEOL JEM 1011 equipped with a high-resolution Gatan CCD camera. NCs were dispersed in ethanol and a small drop was deposited on the copper grids.

4.3 Raman spectroscopy

Raman spectra were obtained with a SM245 spectrophotometer equipped with a CCD detector, and a solid-state laser emitting at 785 nm and focused on the sample with a 20X objective. The spectra were acquired in the range 80-900 cm^{-1}, with a resolution higher than 5 cm^{-1}, a laser power of 150 mW and acquisition time of 60 seconds. Complementary analyses were performed with a T64000 Raman spectrometer (Horiba), employing as detector a nitrogen-equipped CCD coupled to a confocal microscopy using the 514.5 nm line of a Kr^+-Ar^+-laser.

4.4 Optical spectroscopy

Reflectance spectra were registered in the 200-1000 nm spectral range using a Varian Cary 6000i spectrophotometer equipped with a polytetrauoroethylene-coated integrating sphere, two light sources, a quartz halogen lamp for the visible region and a deuterium lamp for the ultraviolet (UV), and two detectors, a Hamamatsu R928 photomultiplier for the visible region and an InGaAs detector for the near infrared.

5. Photocatalytic study

The photocatalytic performance was analysed by studying the degradation of a MB solution under UV radiation according to the ISO 10678 International Standard method.[34] For comparison purposes, all samples were tested using the same experimental conditions as follows. TiO_2 NCs (10 mg) were dispersed in a solution of MB in water (150 mL, C_0 = 10 μM) and irradiated from the top with a UV LED lamp (395 nm, 22 W) at room temperature (RT). In the case of supported TiO_2 NCs, the catalytic material shaped like a plate (5 x 5 cm^2) was activated with the UV lamp for 48 h. Next, the solution of MB in water (100 mL, C_0 = 10 μM) was added and the degradation assay was carried out under the same conditions as described for non-supported TiO_2 NCs. In parallel, the supported photocatalyst was placed in 150 mL of a 10 μM MB solution and left in the dark for 24 h. A slight reduction of the MB solution concentration as a result of an adsorption process was observed.

The absorbance of the MB solution was measured every 1 h for 24 h, and the photocatalytic activity (*PA*) was determined from the reduction of the absorbance *A*, which is proportional to the MB solution concentration, *C*, according to $PA(\%) = \frac{C_0 - C}{C_0} \cdot 100 = \frac{A_0 - A}{A_0} \cdot 100$, where C_0 and A_0 are the initial

solution concentration and absorbance, respectively. The obtained values were appropriately corrected with the adsorption contribution in all photocatalytic activity measurements (% MB degradation).

RESULTS AND DISCUSSION

1. Optimization of TiO_2 NCs by tailoring the anatase/brookite/rutile ratio and doping with TM cations

Firstly, the influence of the thermal treatment on the anatase/brookite/rutile ratio of the so-obtained TiO_2 NCs was analysed. In particular, the following samples have been studied: TiO_2 NCs without thermal treatment (T1), and calcined at 600 ºC (T2) and 800 ºC (T3). Figs. 1 and S1† show the XRD patterns of the aforementioned TiO_2 samples as raw nanocrystalline powder. Since the synthesis of TiO_2 NCs was carried out at RT, the anatase phase is predominantly generated (Table 2, entry 1). In addition, a considerable amount of brookite form was also observed. Thus, the application of thermal treatments at different temperatures was performed to generate the rutile phase and study the effect of anatase/brookite/rutile ratio on the photocatalytic activity.[35] As expected, XRD analyses show an increase in the rutile ratio after calcination. Specifically, upon heating at 600 ºC NCs present 7.8% of the rutile form, while at 800 ºC a complete transformation to rutile phase occurs (Table 2, entries 2 and 3). Moreover, the brookite form was totally removed at 600 ºC (Table 2, entry 2).

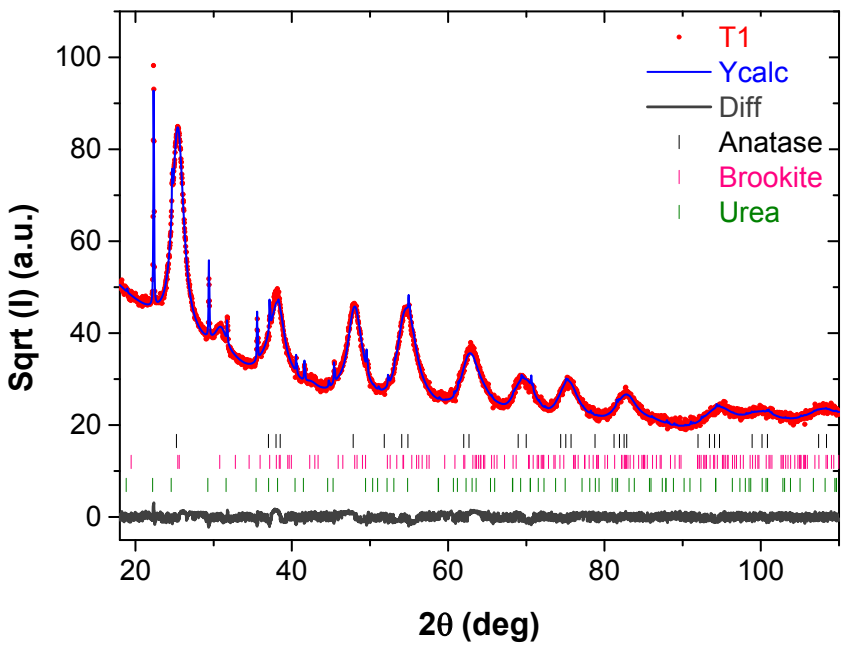

Fig. 1 XRD diffraction pattern of non-calcined undoped TiO_2 NCs (T1).

The NCs size estimation from XRD increases with the calcination temperature as a result of NCs sintering (Table 2). This trend was corroborated by TEM results (Fig. 2).

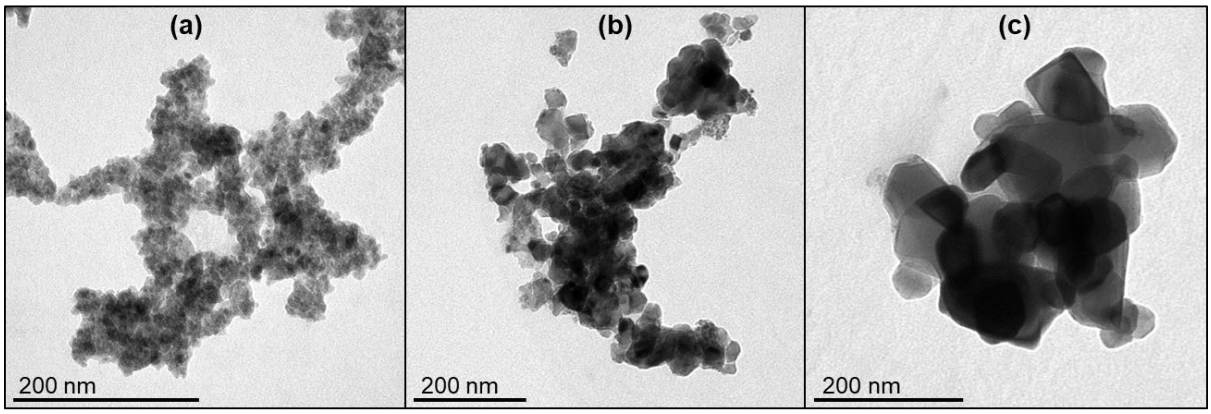

Fig. 2 TEM images of undoped (a) non-calcined TiO_2 NCs (T1); (b) TiO_2 NCs calcined at 600 ºC (T2); (c) TiO_2 NCs calcined at 800 ºC (T3).

Table 2 Summary of crystallite sizes and anatase/brookite/rutile ratios obtained by XRD and TEM for undoped TiO_2 NCs.

Sample	*T* (ºC)[a]	Ana : Ru : Bro	$Size_{Ana}$ (nm)	$Size_{Rut}$ (nm)	$Size_{Bro}$ (nm)	$Size_{TEM}$ (nm)
T1[b]	–	68.3 : – : 31.7	4.8 ± 0.1	–	3.1 ± 0.2	5.4 ± 2.9
T2	600	92.2 : 7.8 : –	29.7 ± 0.5	59 ± 2	–	34 ± 11
T3	800	0.5 : 99.5 : –	n/a	102 ± 4	–	77 ± 15

[a] Calcination temperature. [b] 10% urea.

The Raman spectra of T1-T3 samples are shown in Fig. 3. The Raman spectra of T1 and T2 are dominated by the bands associated to the anatase phase, centred at 147 (E_g), 398 (B_{1g}), 515 (A_{1g} + B_{1g}) and 638 cm^{-1} (E_g).[36] In addition, the presence of a peak located at about 312 cm^{-1} (B_{1g}) in the spectrum of T1 reveals the presence of the brookite form in this sample,[37] while the peak at 1002 cm^{-1} corresponds to the NCN symmetric stretching mode of the remaining urea.[38] On the other hand, the spectrum of T3 exhibits the typical bands at 228 (two phonon scattering), 449 (E_g) and 607 cm^{-1} (A_{1g}) belonging to the rutile phase.[37,39] The spectrum of T3 also shows a small peak at 141 cm^{-1} associated to the E_g active mode of anatase. These results are consistent with those obtained by XRD.

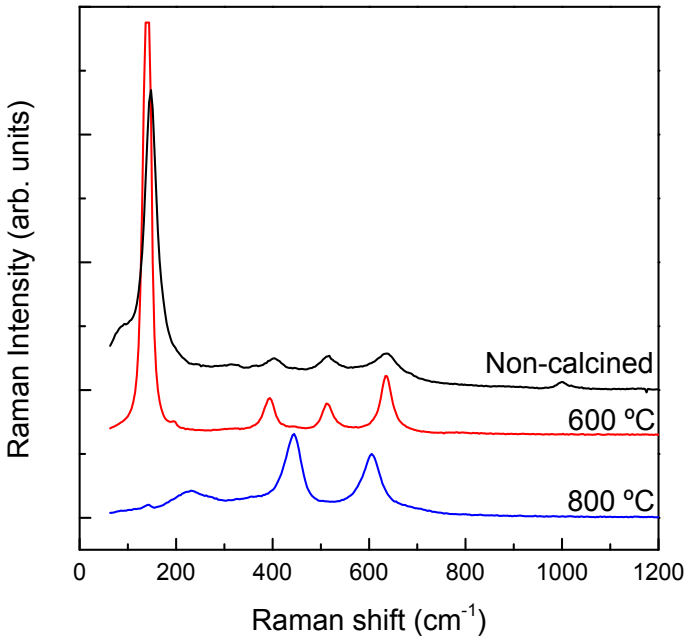

Fig. 3 Raman spectra of undoped TiO_2 NCs; black, non-calcined TiO_2 NCs (T1); red, TiO_2 NCs calcined at 600 ºC (T2); and blue, TiO_2 NCs calcined at 800 ºC (T3).

Secondly, doping with TM ions has been previously reported to be an efficient strategy to improve the photocatalytic activity of TiO_2 NCs.[40] In this work the incorporation of Co and Mn has been analysed. Figs. 4 and S2† and Table 3 show the XRD diffraction patterns and the ratios between the different TiO_2 phases and their corresponding crystallite sizes for NCs doped with 5% Co and 5% Mn. The non-calcined TiO_2 NCs (T4 and T6, Fig. S2†) exhibit high brookite phase ratios (>30%) and small crystallite sizes (<5 nm). On the other hand, T5 and T7 (Fig. 4) consist of NCs calcined at 600 ºC and thus, as expected, the NCs show bigger sizes than non-calcined NCs. Besides, the amount of brookite phase decreased or even disappeared (Table 3), similarly to the undoped TiO_2 NCs. For Co-doped TiO_2 NCs (T7) only the anatase phase was observed upon calcination at 600 ºC. In addition, a small amount (<8%) of $CoTiO_3$ ilmenite-type structure was also detected.[41] Interestingly, the NC size was found to increase in the order brookite<anatase<rutile. Indeed, a similar trend was previously observed by other authors.[42] The nanocrystalline size has also been estimated from TEM images (Figs. S3-S6†) and included in Table 3. These sizes observed by TEM are in good agreement with those determined from XRD, indicating single domain NCs.

Table 3 Summary of crystallite sizes and anatase/brookite/rutile ratios obtained by XRD and TEM for TM-doped TiO_2 NCs.

Sample	Dopant	Calcination T (ºC)	Ana : Ru : Bro	$Size_{Ana}$ (nm)	$Size_{Rut}$ (nm)	$Size_{Bro}$ (nm)	$Size_{TEM}$ (nm)
T4	5% Mn	–	62.7 : – : 37.2	4.4 ± 0.1	–	2.6 ± 0.1	5.4 ± 2.0
T5	5% Mn	600	86.7 : 3.0 : 10.3	22.8 ± 0.5	37 ± 4	12.0 ± 0.7	30.7 ± 9.7
T6	5% Co	–	59.1 : – : 40.0	4.1 ± 0.2	–	1.7 ± 0.1	4.7 ± 1.5
T7[a]	5% Co	600	100 : – : –	27.2 ± 0.7	–	–	36 ± 29

[a] 7.9% $CoTiO_3$

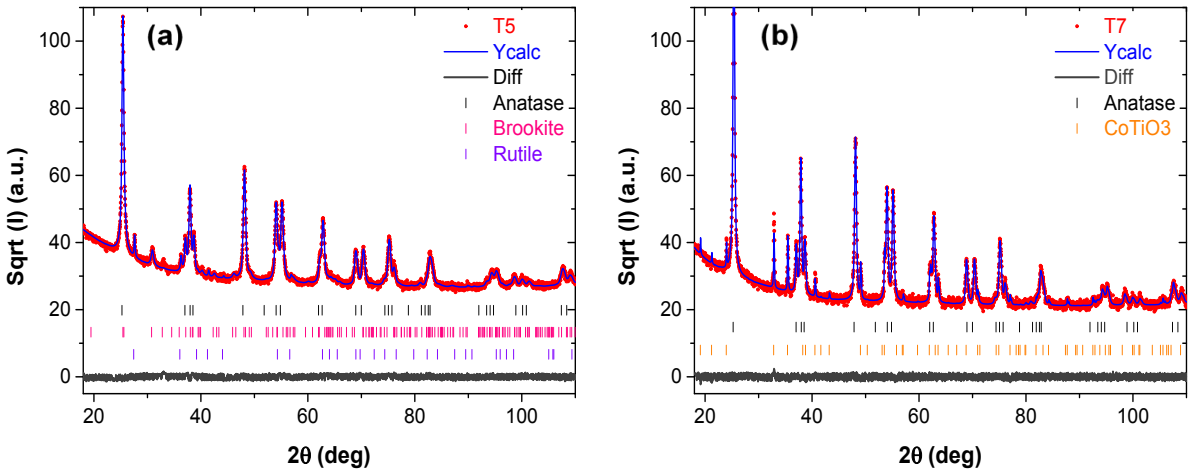

Fig. 4 XRD diffraction patterns of (a) Mn-doped TiO_2 NCs calcined at 600 ºC (T5); (b) Co-doped TiO_2 NCs calcined at 600 ºC (T7).

Fig. 5 shows the Raman spectra of TiO_2 NCs doped with Mn and Co, as-prepared and calcined at 600 ºC (T4-T7). The Raman spectra are dominated by the bands corresponding to the anatase phase, in good agreement with XRD data, similarly to T1-T3 samples. In the case of Mn-doped TiO_2 NCs, T4 (Fig. 5(a)) displays the characteristic bands of anatase phase, which are located at 149, 395, 514 and 631 cm^{-1}.[36] In addition, the peak at *ca.* 310 cm^{-1} can be attributed to the B_{1g} active mode of brookite.[37] As expected, an increase in the intensity of anatase bands is observed for T5 (from 62.7 to 86.7% anatase by XRD). The small peak at 315 cm^{-1} corresponds to brookite (10.3% brookite by XRD), while no rutile fingerprints are detected (below 3%).

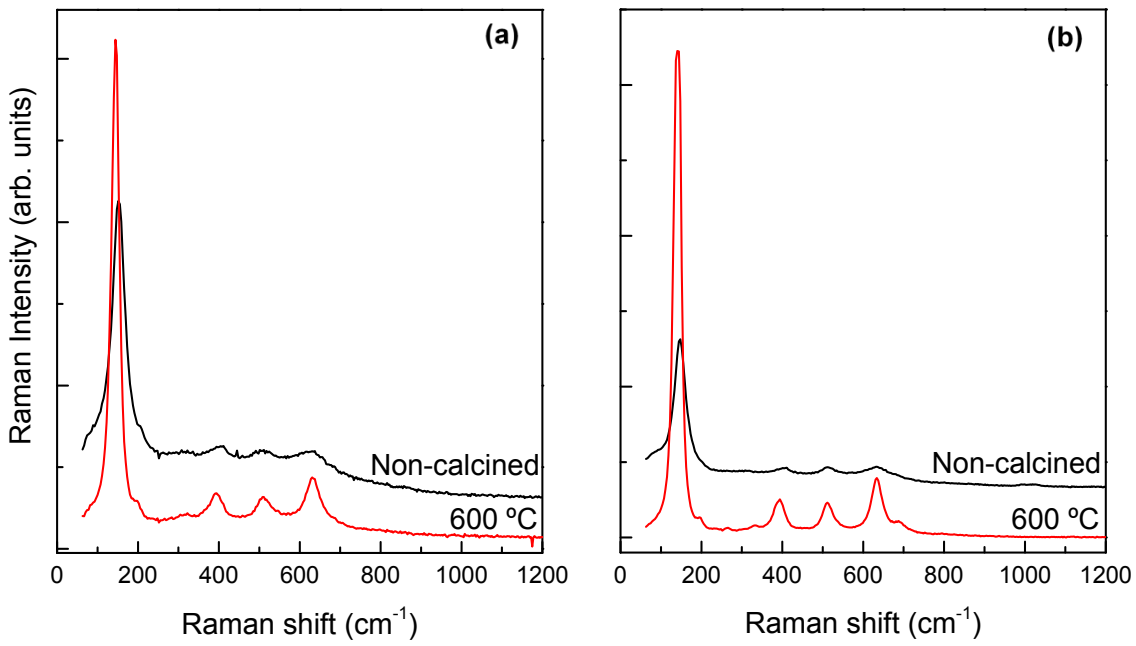

Fig. 5 Raman spectra of (a) Mn-doped TiO_2 NCs (T4 and T5); (b) Co-doped TiO_2 NCs (T6 and T7). Black, non-calcined TM-doped TiO_2 NCs; red, TM-doped TiO_2 NCs calcined at 600 ºC.

A similar result was obtained with Co-doped TiO_2 NCs. Both T6 and T7 spectra are dominated by the peaks belonging to the anatase phase, with an increase in the intensity of these bands in T7 as a consequence of the higher anatase content due to the calcination process. Interestingly, T7 also shows a series of small peaks at 196, 263 and 332 and 687 cm^{-1} corresponding to $CoTiO_3$ ilmenite structure,[41] which supports the XRD observations.

2. Optical characterization of ~~pure~~undoped and TM-doped TiO_2 nanocrystals

The optical characterization of the bandgap of undoped TiO_2 NCs, non-calcined and heated at 600 ºC and 800 ºC, by reflectance spectroscopy is summarized in Fig. 6. The spectra clearly illustrate how the NCs absorption bandgap is influenced by the calcination treatment. Specifically, the absorption edge is centred at *ca*. 373 nm for the as-prepared sample (T1), and 391 nm and 408 nm for the NCs treated at 600 ºC (T2) and 800 ºC (T3), respectively. The red-shift of the bandgap towards the visible region with the increase of calcination temperature is mainly ascribed to the presence of rutile phase,[43] in agreement with XRD and Raman results.

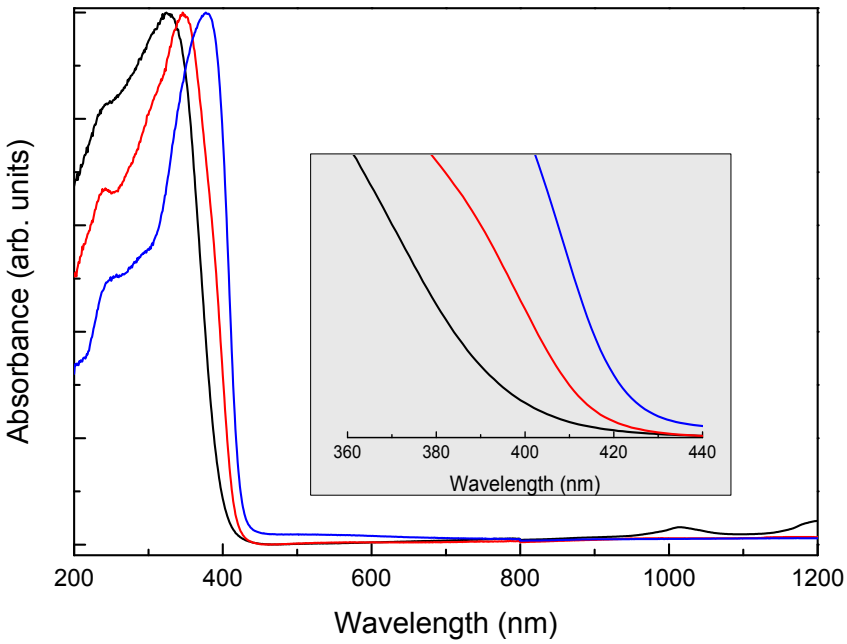

Fig. 6 Optical reflectance of undoped TiO_2 NCs; black, non-calcined TiO_2 NCs (T1); red, TiO_2 NCs calcined at 600 ºC (T2); and blue, TiO_2 NCs calcined at 800 ºC (T3).

Figs. 7(a) and 7(b) show the optical reflectance spectra of TiO_2 NCs doped with 5% of Mn (T4 and T5) and 5% of Co (T6 and T7), respectively. The main differences with respect to non-doped TiO_2 NCs (in black) are the red-shift of the absorption edge and the presence of broad bands, which appear as a shoulder overlapping the absorption edge. These bands can be ascribed to either TM ions absorption or charge-transfer transitions between TM ions and the TiO_2 conduction or valence band, confirming the incorporation of the TM into the TiO_2 structure.[44] For Mn-doped TiO_2 NCs, the reflectance spectrum of the sample calcined at 600 ºC (T5) is clearly different from the one obtained at RT (T4). This fact can be related to the presence of different Mn oxidation states. Specifically, previous X-ray photoelectron spectroscopy studies have shown that while the Mn oxidation state is 2+ for Mn-doped TiO_2 samples prepared at RT, the presence of Mn^{3+} and Mn^{4+} is observed for samples calcined at temperatures higher than 550 ºC.[45] On the contrary, the shape of the reflectance spectra for Co-doped NCs is mostly independent of the calcination treatment. This indicates that Co presents the most stable valence, 2+, which is corroborated by the presence of a well-defined absorption band centred at 610 nm, related to a *d-d* Co^{2+} transition.[44a] Thus, the potential enhancement of the photocatalytic activity by doping with these cations is associated not only with a displacement of the energy bandgap to the visible region, but also to the introduction of additional energy states within the TiO_2 energy bandgap, particularly in the case of Co-doped samples, which induces visible light absorption bands at higher wavelengths in the visible range.

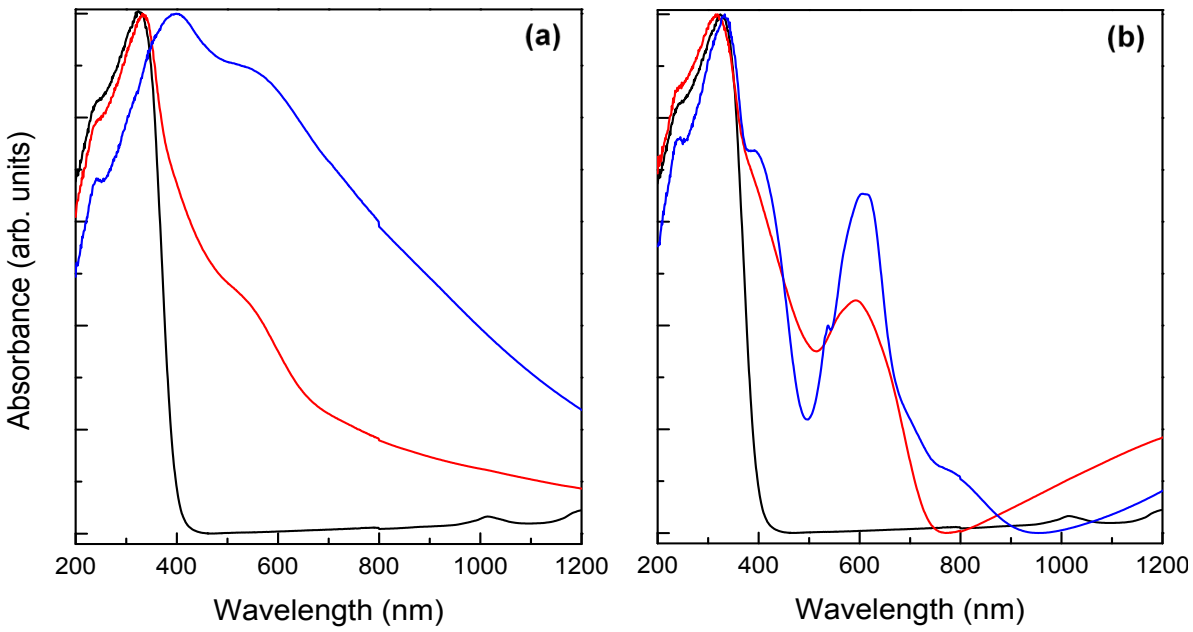

Fig. 7 Optical reflectance of (a) TiO_2 NCs doped with 5% Mn; (b) TiO_2 NCs doped with 5% Co. Red, non-calcined TM-doped TiO_2 NCs; blue, TM-doped TiO_2 NCs calcined at 600 ºC. For comparison purposes~~Black~~, non-calcined undoped TiO_2 NCs are shown in black.

3. Catalytic activity of TiO_2 NCs

We have investigated the photocatalytic activity of undoped and Co or Mn-doped TiO_2 NCs using the degradation of MB in water under UV irradiation (395 nm) as a model reaction (Scheme 1),[16a,46] since the use of this synthetic dye is recommended by the ISO/CD10678 regulation.[34]

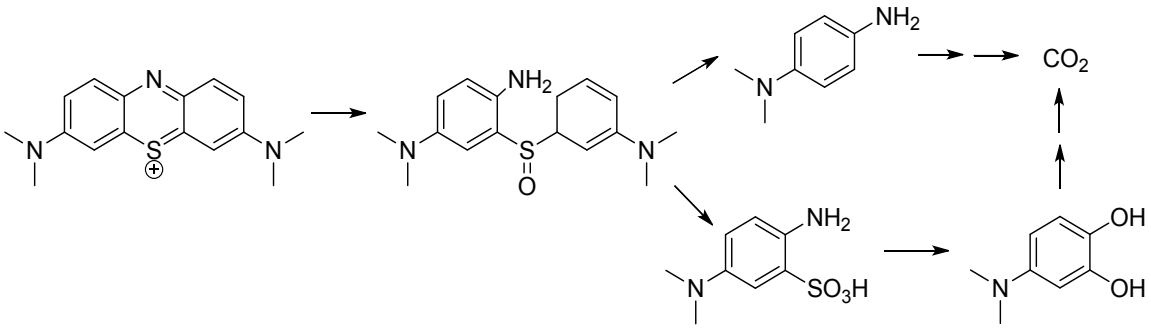

Scheme 1 Photocatalytic degradation route of methylene blue.

The degradation occurs when TiO_2 absorbs radiation of higher energy than its bandgap, which produces the promotion of an electron from the valence band to the conduction band (e^-_{CB}) and creates a positive hole (h_{VB}^+), thus generating an electron/hole (e^-_{CB}/h^+_{VB}) pair (eq. 1). Positive holes can oxidize water or OH^- and form $^{\bullet}OH$ radicals at TiO_2 NCs surface (eq. 2–3). In addition, e^-_{CB} electrons can interact with O_2 and generate superoxide ($O_2^{\bullet-}$) and hydroperoxyl ($^{\bullet}OOH$) radical anions (eq. 5 and 7). These radicals are extremely reactive oxidants and may degrade pollutants or organic compounds through an oxidation process (eq. 4, 6 and 8).[5,24,47]

$$TiO_2 + h\nu \longrightarrow h^+_{VB} + e^-_{CB} \quad (1)$$

$$h^+_{VB} + H_2O \longrightarrow H^+ + {}^{\bullet}OH \quad (2)$$

$$h^+_{VB} + OH^- \longrightarrow {}^{\bullet}OH \quad (3)$$

$${}^{\bullet}OH + \text{organic molecule} \longrightarrow \longrightarrow \longrightarrow CO_2 + H_2O \quad (4)$$

$$e^-_{CB} + O_2 \longrightarrow O_2^{\bullet -} \quad (5)$$

$$O_2^{\bullet -} + \text{organic molecule} \longrightarrow \longrightarrow \longrightarrow CO_2 + H_2O \quad (6)$$

$$O_2^{\bullet -} + H^+ \longrightarrow {}^{\bullet}OOH \quad (7)$$

$${}^{\bullet}OOH + \text{organic molecule} \longrightarrow \longrightarrow \longrightarrow CO_2 + H_2O \quad (8)$$

To this end, TiO_2 NCs were dispersed in a solution of MB in water (for further details see Experimental section) and irradiated from the top with a UV lamp (22 W, λ = 395 nm LED). After a given time, the concentration of MB solution (*C*) was determined using the absorption of the characteristic band of MB at 664 ± 5 nm in the acquired UV–vis spectrum (Fig. 8). The photocatalytic efficiency for each TiO_2 NCs is represented by the decomposition rate of MB, which is estimated by the equation:

$$d = \frac{C_0 - C_t}{C_0} \times 100 = \frac{A_0 - A_t}{A_0} \quad (9)$$

where *d* is the degradation rate, C_0 is the initial concentration of MB solution and C_t is the concentration of MB solution after a specific irradiation time, *t*. A_0 and A_t are the absorbance values at the maximum absorption band at time *t*=0 and time *t*.

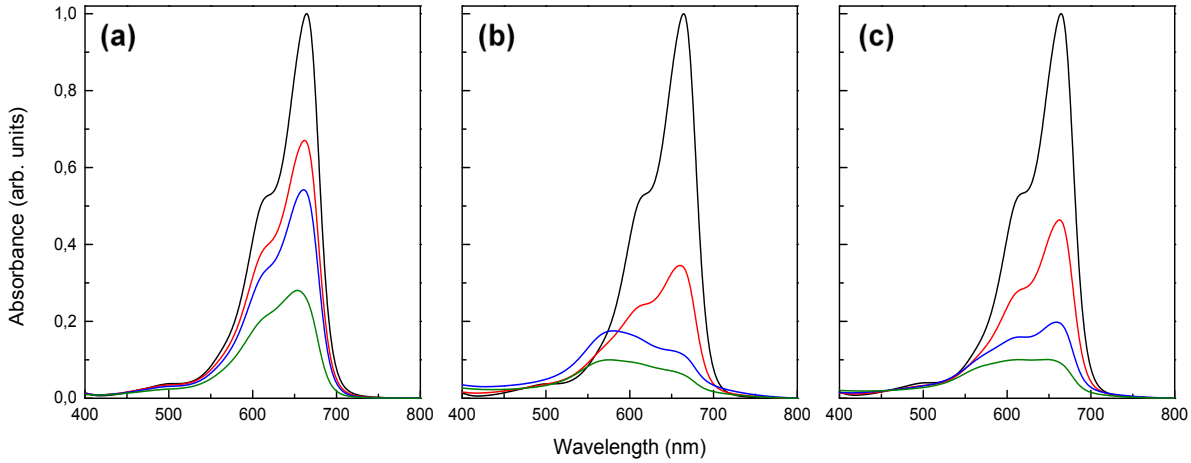

Fig. 8 Evolution of MB solution absorbance with time in a catalytic experiment mediated by (a) T1, (b) T2, and (c) T3 undoped TiO_2 NCs. Conditions: MB (150 mL, 10 μM), TiO_2 NCs (10 mg), 22 W, λ = 395 nm, at RT; black, *t* = 0 h; red, *t* = 1 h; blue, *t* = 8 h; green, *t* = 24 h.

Thus, a set of catalytic experiments was carried out to study the influence of NCs size, anatase/rutile ratio and presence of TM dopants on the photocatalytic activity of TiO_2 NCs. Firstly, non-calcined TiO_2 NCs (T1, Table 4), which contain a 68.3:31.7 anatase/brookite ratio and do not present rutile phase, showed good catalytic performance and 72% MB degradation was observed after 24 h of reaction (Fig. 8(a)). Despite the much bigger size, the NCs calcined at 600 ºC (T2) displayed higher photocatalytic activity, leading to 93% MB degradation (Fig. 8(b)). This is attributable to both the increase in the highly active anatase ratio and the formation of rutile phase as a result of the calcination process.[35] Indeed, it is reported that a mixture of anatase and rutile produces a synergistic effect for which photoexcited electrons in anatase are transferred to the rutile conduction band.[26] This promotes the separation of photogenerated charge carriers and thus reduces the recombination of electrons and holes, which is the main limitation in semiconductor-mediated photocatalysis.[5,48] In this context, Besenbacher *et al.* described an optimal 40-80% anatase content (with the remaining amount of rutile) for MB photooxidation catalysed by TiO_2 films.[26] Nevertheless, Du, Yang *et al.* reported that the photocatalytic activity of TiO_2 NPs is maximized for a composition of *ca*. 70% anatase and 30% rutile,[25] while other authors claim that there is no synergistic effect at all between anatase and rutile.[27]

TiO_2 NCs calcined at 800 ºC (T3) led to a slight decrease in the MB degradation in comparison with T2 (Fig. 8(c)). This can be related to the decrease in the anatase phase content, since, as previously described, the photocatalytic activity of a combination of anatase and rutile polymorphs is higher than that of the pure rutile.[48] Specifically, T2 exhibits 92.2% anatase, while T3 presents 99.5% rutile form. In addition, T3 shows much bigger NCs than T2, which also diminishes the catalytic activity. It should be noted that the brookite form is also photocatalytically active and its effect must be considered.[28] However, in this study the presence of brookite seems to be detrimental as compared with the catalytic performance shown by anatase and rutile phases, as the activity increases with the decrease of brookite content (Table 4).

Table 4 Photocatalytic degradation of MB mediated by TiO_2 NCs.[a]

Sample	TM dopant	Ana : Rut : Bro	$Size_{Ana}$ (nm)	$Size_{Rut}$ (nm)	$Size_{Bro}$ (nm)	MB degradation (%)
T1[b]	–	68.3 : 0 : 31.7	4.8	–	3.1	72
T2	–	92.2 : 7.8 : 0	29.7	59.0	–	93
T3	–	0.5 : 99.5 : 0	60.0	102.0	–	90
T4	5% Mn	62.7 : 0 : 37.2	4.4	–	2.6	79
T5	5% Mn	86.7 : 3.0 : 10.3	22.8	37.0	12.0	82
T6	5% Co	59.1 : 0 : 40.0	4.1	–	1.7	75
T7[c]	5% Co	100 : 0 : 0	27.2	–	–	86

[a] Reagents and conditions: MB (150 mL, 10 μM), catalyst (10 mg), 22 W, λ = 395 nm, RT, 24 h.[b] 10% urea.[c] 7.9% $CoTiO_3$.

Next, an experiment catalysed by TiO_2 NCs doped with 5% Mn was performed. The doping of TiO_2 NCs with TM may lead to a decrease in the bandgap as a result of the formation of new energy levels, which shifts the absorption edge towards the visible region and increase the activity of photocatalytic TiO_2 NCs. Moreover, the presence of a TM can enhance the electron-hole pair separation, and thus reduce the recombination of photogenerated charge carriers and increase their lifetime.[5,48] In line with the displacement observed in the absorption edge towards the visible zone (Fig. 7(a)), an increase in the MB degradation (79%) was achieved with Mn-doped TiO_2 NCs (T4), as compared to 72% degradation obtained in the experiment catalysed by non-doped NCs (T1). In fact, the TM-doping effect on the catalytic activity is clearly highlighted considering that T1 and T4 show similar nanocrystalline size and anatase content. This trend continues when Mn-doped TiO_2 NCs calcined at 600 ºC (T5) were employed as catalyst, although the catalytic activity growth was lower than expected. Indeed, T5 displays lower activity than pure TiO_2 NCs calcined at 600 ºC (T2). Thus, the ratio of different phases may play a more important role than the NCs size here. Although T5 is formed by smaller NCs, T2 exhibits a 92:8 anatase/rutile ratio, in contrast with the 87:3:10 anatase/rutile/brookite ratio shown by T5. Therefore, T2 are again the most active NCs and it seems that there is indeed a synergistic effect between anatase and rutile. Finally, TiO_2 NCs doped with 5% Co (T6) presented also slightly higher activity (75%) than that obtained with undoped NCs (T1), in agreement with the absorption edge shift observed in Fig. 7(b). The calcination of Co-doped TiO_2 NCs (T7) had a positive effect on the activity, leading to 86% MB degradation. As T5, these NCs exhibit less activity than pure TiO_2 NCs calcined at 600 ºC (T2), which can be due to the absence of the synergistic effect provided by the combination of anatase and rutile polymorphs (100% of pure anatase form).

The results presented in this section point out the clear influence of both the anatase/brookite/rutile ratio and the presence of TM dopants on the catalytic performance of TiO_2 NCs. Specifically, the brookite phase content decrease and the formation of rutile phase lead to an enhancement of catalytic activity, which could be associated to the aforementioned synergistic effect between anatase and rutile phases. In addition, the doping with TM also produces an improvement in the catalytic performance of TiO_2 NCs. Both the optimisation of anatase/rutile ratio and the doping with TM lead to a shift in the absorption edge towards the visible spectral region and thus an increase in the activity of TiO_2 NCs is observed. Finally, it is worth noting that the employed synthesis method comprises the use of urea as N-dopant source, which could increase the catalytic activity of the synthesized NCs.[30c] However, this possible positive effect of N-dopant on the photocatalytic activity of non-calcined NCs (T1, T4 and T6) is not significant as these samples show lower activities than those of calcined NCs (T2, T3, T5 and T7), which are obtained after a calcination treatment that eliminates such a component.

4. Structural and optical characterization of photocatalysts based on pure and TM-doped TiO_2 NCs incorporated in enamel coatings on a steel sheet

In this section several photocatalysts based on T1, T4 and T6 TiO_2 NCs immobilised on enamels deposited onto steel sheets are presented (Fig. S7†). Figs. 9 and S8† show the XRD patterns of the aforementioned supported photocatalysts based on T1, T4 and T6 samples. In comparison with the starting NCs, several differences are observed in the diffractograms. The NCs in powder form exhibit broader diffraction peaks due to the small nanocrystalline size, while the supported NCs present narrower peaks and considerably worse signal to noise ratio probably due to the lower amount of TiO_2 (*ca.* 5%). Additional peaks, present in both the pure and TM-doped samples, are detected in all the diffraction patterns. They can be assigned to different phases, mainly silicates, arising from the mixture used for the enamel preparation. No features from crystalline phases incorporating TM dopants (particularly $CoTiO_3$) have been found. All the non-TiO_2 phases have been considered together as a single phase to roughly estimate their abundance, representing around the 20% in all the TM-doped samples (see the refinements from Fig. 9).

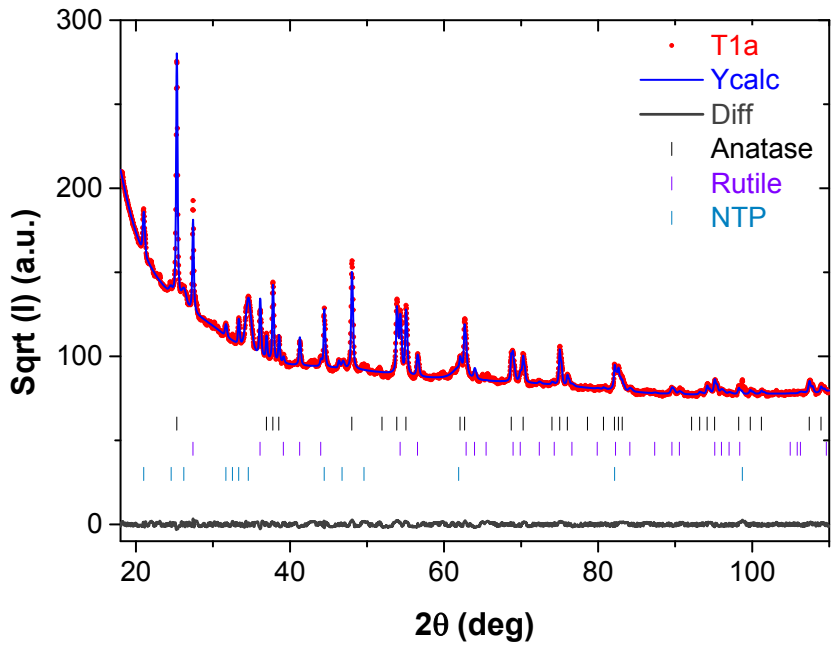

Fig. 9 Refinement of XRD diffraction pattern of pure TiO_2 NCs deposited on enamel supported onto steel sheets (T1a). Major contributions belong to rutile and anatase TiO_2 phases. The rest of the peaks appearing in the diffractogram have been modelled through a single phase for quantification purposes.

The XRD analyses (Table 5) show a growth in the particle sizes of the supported NCs with respect to those of non-calcined TiO_2 NCs in powder form (Tables 2 and 3). This can be ascribed to the sintering associated to the heating process carried out in the preparation of the supported photocatalysts (15 min at 700 ºC). Besides, similarly to the calcined non-supported NCs, the brookite phase was totally removed, the rutile form appeared and the anatase ratio increased in the NCs incorporation process. The three supported samples show similar relation between these phases, with *ca*. 75:25 anatase/rutile ratio.

Table 5 Summary of TiO_2 NCs sizes and anatase/rutile ratios determined by XRD of supported samples.

Sample	TM dopant	Anatase : rutile ratio	$Size_{Ana}$ (nm)	$Size_{Rut}$ (nm)
T1a	---	72 : 28	45	44
T4a	5% Mn	75 : 25	42	61
T6a	5% Co	76 : 24	23	25

The Raman spectra of T1a, T4a and T6a supported samples (Fig. 10) exhibit the typical peaks corresponding to the anatase phase (144 (E_g), 397 (B_{1g}), 514 ($A_{1g} + B_{1g}$) and 639 cm^{-1} (E_g)).[36] In addition, one band with lower intensity at 449 cm^{-1} associated to the E_g active mode of rutile phase is also observed.[37,39] As expected, the Raman analyses are in good agreement with XRD results.

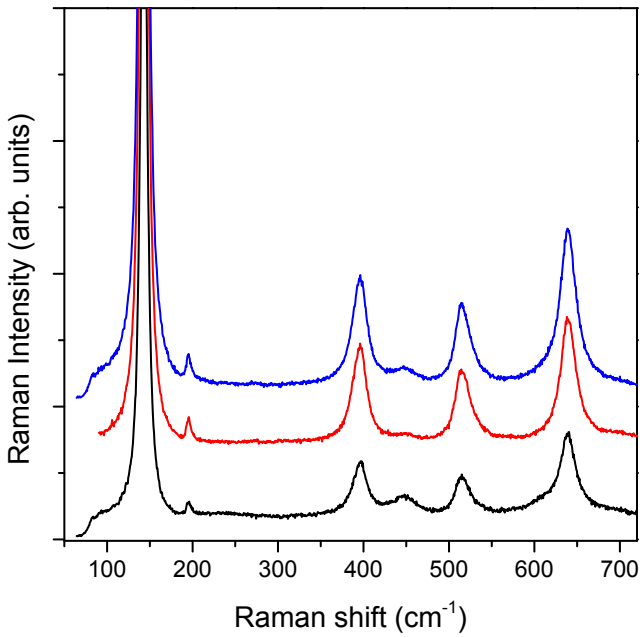

Fig. 10 Raman spectra of TiO_2 NCs deposited on enamel supported onto steel sheets; black, pure TiO_2 NCs (T1a); red, Mn-doped TiO_2 NCs (T4a); blue, Co-doped TiO_2 NCs (T6a).

Fig. 11(a) shows the optical reflectance spectra of undoped TiO_2 NCs both as nanocrystalline powder (T1) and supported photocatalyst (T1a). The absorption edge is centred at *ca*. 377 nm for the supported system, thus appearing slightly shifted to the visible region, compared to original TiO_2 NCs (373 nm). This shift can be ascribed to the appearance of 28% of rutile phase at the temperature employed in the NCs immobilization process on the enamel-coated steel sheet (700 ºC). Fig. 11(b) compares the optical reflectance of the enamel samples containing T1, T4 and T6 TiO_2 NCs deposited on steel sheets (T1a, T4a and T6a, respectively). The absorption edge is centred at 372 nm and 382 nm for the enamels obtained after the incorporation of NCs doped with Mn (T4a) and Co (T6a), respectively. Thus, the three supported samples display comparable absorption edge values, in agreement with their similar anatase/rutile ratio (Table 5). Besides, both the aforementioned charge-transfer transitions and the *d*-

d Co absorption band centred at 610 nm are also observed in the TM-doped samples, although the relative intensity is lower than the one observed for the starting powder NCs.

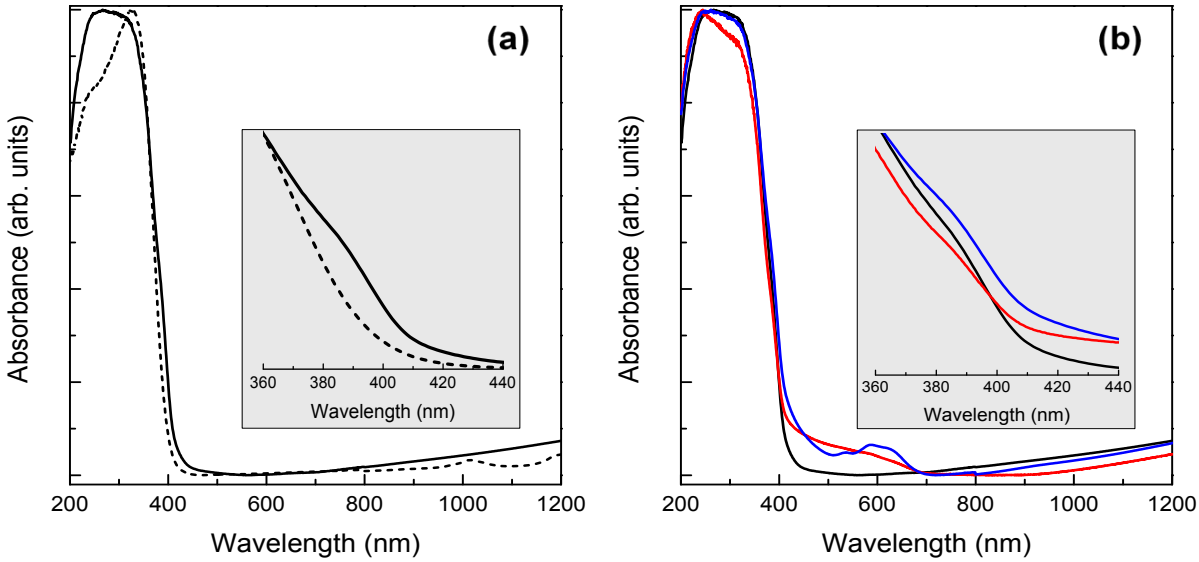

Fig. 11 (a) Optical reflectance of synthesized (T1) (dashed line) and supported (T1a) (solid line) non-doped TiO_2 NCs. (b) Optical reflectance of supported TiO_2 NCs; black, pure TiO_2 NCs (T1a); red, Mn-doped TiO_2 NCs (T4a); blue, Co-doped TiO_2 NCs (T6a).

5. Catalytic activity of TiO_2 NCs deposited on enamel supported onto stainless steel

Finally, the supported samples containing pure and TM-doped TiO_2 NCs were employed as photocatalysts. The main results are presented in Table 6 and Fig. 12. 16% MB degradation was observed after 8 h of reaction (54% at 24 h) in the experiment catalysed by the sample T1a containing non-doped TiO_2 NCs (Fig. 12a). By comparison, the sample T6a prepared with Co-doped TiO_2 NCs exhibits higher activity, leading to an increase in the MB decomposition (35% after 8 h of reaction, Fig. 12c). Since the three samples show similar anatase/rutile ratio (Table 6), the enhancement of catalytic activity can be attributed to the effect of the TM dopant. In addition, T1a contains bigger NCs than T6a and thus the size may play a role here. On the other hand, the sample containing Mn-doped TiO_2 NCs (T4a) is less active (9% MB degradation after 8 h of reaction, Fig. 12b) than both T1a and T6a, which could be due to the higher nanocrystalline size of rutile phase in T4a.[49]

We also carried out a number of experiments to study the recyclability of the TiO_2 NCs deposited on enamel supported onto stainless steel. Through extraction of the MB solution followed by reactivation with the LED lamp for 48 h, the supported photocatalysts T4a and T6a were reused in successive cycles. A substantial reduction in the activity was noted in the third cycle (Figs. S9-S10†), which can be due to a gradual loss of the supported TiO_2 NCs as a consequence of the repeated catalytic cycles. Thus, the supported samples display a limited potential for recyclability.

Table 6 Photocatalytic degradation of MB mediated by TiO_2 NCs deposited on enamel supported onto steel sheets.[a]

Sample	% TM dopant	Anatase : Rutile	$Size_{Ana}$ (nm)	$Size_{Rut}$ (nm)	MB degradation (%)	
					8 h	24 h
T1a	--	72 : 28	45	44	16	54
T4a	5% Mn	75 : 25	42	61	9	35
T6a	5% Co	76 : 24	23	25	35	55

[a] Reagents and conditions: MB (100 mL, 10 μM), catalyst (5 x 5 cm^2), 22 W, λ = 395 nm, RT.

Although the results described herein might seem moderate when compared with those reported for other nanosized TiO_2 systems either supported on glazed surfaces[13b,17a,19b-c,20a-c,21b-c] or contained in enamels,[17b,23a,24] it is important to note that: (i) the supported samples employed in this study contains only 5% of catalyst, and (ii) the experiments were performed under near-visible light (λ = 395 nm) with a low power LED lamp (22 W). Indeed, the use of a sunlight source with light intensity of *ca.* 500 lux would certainly improve the catalytic results. Thus, we suggest that the presented photocatalyst based on TiO_2 NCs show potential for a variety of applications as indoor and outdoor construction elements like floorings, walls, tunnels or subway panels.

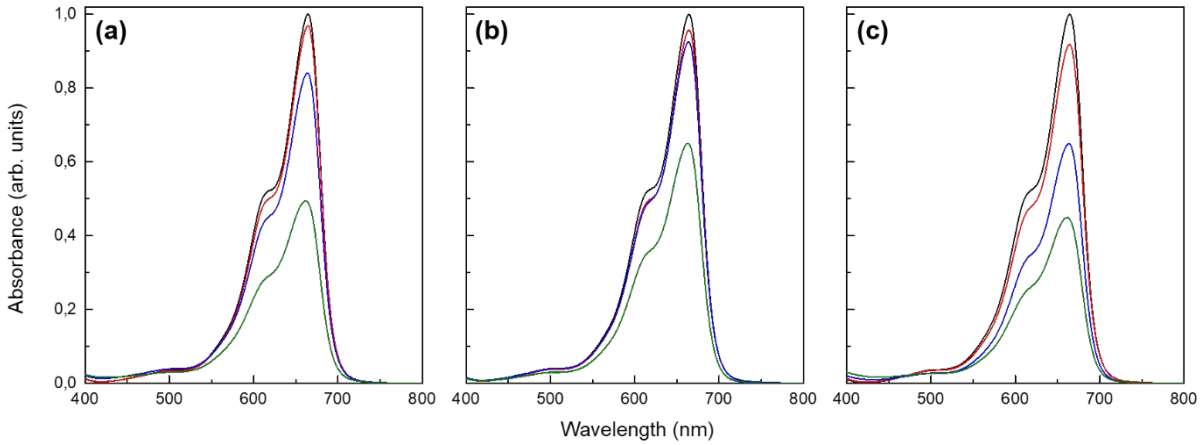

Fig. 12 Evolution of MB solution absorbance with time in a catalytic experiment mediated by (a) T1a, (b) T4a, and (c) T6a. Conditions: MB (150 mL, 10 μM), catalyst (5 x 5 cm^2), 22 W, λ = 395 nm, at RT; black, t = 0 h; red, t = 1 h; blue, t = 8 h; green, t = 24 h.

CONCLUSIONS

In summary, we have successfully employed a new family of undoped and Co- and Mn-doped TiO_2 NCs as catalysts for the photocatalytic degradation of MB. In line with the displacement of the absorption edge to the visible region, a clear positive effect of anatase/rutile ratio and TM dopants on the catalytic activity was observed. Specifically, the calcination of TiO_2 NCs involves an increase in the anatase ratio and the formation of rutile form, leading to a rise in activity that is attributed to a

synergistic effect between these phases. Similarly, the doping with Mn and Co gave rise to an enhancement of the catalytic performance.

Such NCs were used as an active material for the fabrication of an enamel immobilised onto stainless steel. The resulting supported photocatalyst was fully characterized through XRD as well as Raman and reflectance spectroscopies. This system showed good photocatalytic activity and, as in the case of non-supported NCs, an influence of the TM dopant was observed. Specifically, the sample prepared with Co-doped TiO_2 NCs exhibits the highest activity.

In conclusion, a new type of smart photocatalytic surface with very exciting properties has been devised. In this first application the catalytic system was employed in the photodegradation of MB, but after this thorough study the road seems open for many applications as a self-cleaning coating and potential use for NOx photodegradation.

AUTHOR INFORMATION

Corresponding Authors

*E-mail: icrico@us.es (Israel Cano)

*E-mail: rosa.martin@unican.es (Rosa Martín-Rodríguez)

ORCID

Andrea Diego-Rucabado: 0000-0002-8806-8784

Marina T. Candela: 0000-0002-8532-3735

Fernando Aguado: 0000-0003-2912-0228

Jesús González: 0000-0002-0381-6393

Rafael Valiente: 0000-0001-9855-8309

Israel Cano: 0000-0003-3727-9327

Rosa Martín-Rodríguez: 0000-0003-1568-592

AUTHOR CONTRIBUTIONS

Synthesis of TiO_2 NCs and photocatalytic experiments, Andrea Diego-Rucabado and Israel Cano; TEM images, Israel Cano; Preparation of enamel coatings on stainless steel, Eugenio Gómez; XRD analyses, Marina T. Candela and Fernando Aguado; Raman measurements, Andrea Diego-Rucabado and Jesús González; Reflectance, Andrea Diego-Rucabado and Rosa Martín-Rodríguez; Supervision and design of experiments, Rafael Valiente, Israel Cano and Rosa Martín-Rodríguez; Writing–original draft preparation, Israel Cano and Rosa Martín-Rodríguez; Writing–review and editing, Andrea Diego-Rucabado, Israel Cano and Rosa Martín-Rodríguez; Manuscript review, Andrea Diego-Rucabado, Fernando Aguado and Rafael Valiente; Project administration, Rafael Valiente; Funding acquisition, Eugenio Gómez, Rafael Valiente and Rosa Martín-Rodríguez. All authors have read and agreed to the published version of the manuscript.

CONFLICTS OF INTEREST

There are no conflicts of interest to declare.

FUNDING

This work was funded by the company VITRISPAN S.A.

ACKNOWLEDGMENTS

The authors acknowledge financial support from company VITRISPAN S.A. M.T.C. would like to thank University of Cantabria and the Government of Cantabria for her pre-doctoral grant "Concepción Arenal".

NOTES AND REFERENCES

1 (*a*) J. Balbuena, M. Cruz-Yusta and L. Sánchez, Nanomaterials to combat NO_x pollution, *J. Nanosci. Nanotechnol.*, 2015, **15**, 6373–6385; (*b*) A. J. Ebele, M. A.-E. Abdallah and S. Harrad, Pharmaceuticals and personal care products (PPCPs) in the freshwater aquatic environment, *Emerg. Contam.*, 2017, **3**, 1–16; (*c*) J. Li, H. Liu and J. P. Chen, Microplastics in freshwater systems: A review on occurrence, environmental effects, and methods for microplastics detection, *Water Res.*, 2018, **137**, 362–374.

2 (*a*) F. I. Khan and A. K. Ghoshal, Removal of Volatile Organic Compounds from polluted air, *J. Loss Prev. Process Ind.*, 2000, **13**, 527–545; (*b*) T. Masciangoli and W.-X. Zhang, Environmental technologies at the nanoscale, *Environ. Sci. Technol.*, 2003, **37**, 102–108; (*c*) P. G. Tratnyek and R. L. Johnson, Nanotechnologies for environmental cleanup, *Nano Today*, 2006, **1**, 44–48; (*d*) A. Vaseashta, M. Vaclavikova, S. Vaseashta, G. Gallios, P. Roy and O. Pummakarnchana, Nanostructures in environmental pollution detection, monitoring, and remediation, *Sci. Technol. Adv. Mater.*, 2007, **8**, 47–59.

3 F. Petronella, A. Truppi, C. Ingrosso, T. Placido, M. Striccoli, M. L. Curri, A. Agostiano and R. Comparelli, Nanocomposite materials for photocatalytic degradation of pollutants, *Catal. Today*, 2017, **281**, 85-100.

4 (*a*) Y. Paz, Application of TiO_2 photocatalysis for air treatment: Patents' overview, *Appl. Catal. B*, 2010, **99**, 448–460; (*b*) M. Lazar, S. Varguese and S. Nair, Photocatalytic water treatment by titanium dioxide: recent updates, *Catalysts*, 2012, **2**, 572–601; (*c*) S. W. Verbruggen, TiO_2 photocatalysis for the degradation of pollutants in gas phase: From morphological design to plasmonic enhancement, *J. Photochem. Photobiol. C-Photochem. Rev.*, 2015, **24**, 64–82.

5 M. Pelaez, N. T. Nolan, S. C. Pillai, M. K. Seery, P. Falaras, A. G. Kontos, P. S. M. Dunlop, J. W. J. Hamilton, J. A. Byrne, K. O`Shea, M. H. Entezari and D. D. Dionysiou, A review on the visible light

active titanium dioxide photocatalysts for environmental applications, *Appl. Catal. B*, 2012, **125**, 331–349.

6 (*a*) H. Choi, S. R. Al-Abed, D. D. Dionysiou, E. Stathatos and P. Lianos, TiO_2-based advanced oxidation nanotechnologies for water purification and reuse, *Sustain. Sci. Eng.*, 2010, **8**, 229–254; (*b*) A. Ajmal, I. Majeed, R. N. Malik, H. Idriss and M. A. Nadeem, Principles and mechanisms of photocatalytic dye degradation on TiO_2 based photocatalysts: a comparative overview, *RSC Adv.*, 2014, **4**, 37003–37026.

7 (*a*) S. N. Frank and A. J. Bard, Heterogeneous photocatalytic oxidation of cyanide ion in aqueous solutions at titanium dioxide powder, *J. Am. Chem. Soc.*, 1977, **99**, 303–304; (*b*) S. N. Frank and A. J. Bard, Heterogeneous photocatalytic oxidation of cyanide and sulfite in aqueous solutions at semiconductor powders, *J. Phys. Chem.*, 1977, **81**, 1484–1488.

8 A. Truppi, F. Petronella, T. Placido, M. Striccoli, A. Agostiano, M. L. Curri and R. Comparelli, Visible-light-active TiO_2-based hybrid nanocatalysts for environmental applications, *Catalysts*, 2017, **7**, 100.

9 (*a*) H.-J. Kim, Y.-G. Shul and H. Han, Photocatalytic properties of silica-supported TiO_2, *Top. Catal.*, 2005, **35**, 287–293; (*b*) D. Maučec, A. Šuligoj, A. Ristić, G. Dražić, A. Pintar and N. N. Tušar, Titania versus zinc oxide nanoparticles on mesoporous silica supports as photocatalysts for removal of dyes from wastewater at neutral pH, *Catal. Today*, 2018, **310**, 32–41.

10 J. Chen, F. Qiu, W. Xua, S. Cao and H. Zhu, Recent progress in enhancing photocatalytic efficiency of TiO_2-based materials, *Appl. Catal. A-Gen.*, 2015, **495**, 131–140.

11 M. Zarezade, S. Ghasemi and M. R. Gholami, The effect of multiwalled carbon nanotubes and activated carbon on the morphology and photocatalytic activity of TiO_2/C hybrid materials, *Catal. Sci. Technol.*, 2011, **1**, 279–284.

12 (*a*) Z. Zhang, Y. Xu, X. Ma, F. Li, D. Liu, Z. Chen, F. Zhang and D. D. Dionysiou, Microwave degradation of methyl orange dye in aqueous solution in the presence of nano-TiO_2-supported activated carbon (supported-TiO_2/AC/MW), *J. Hazard Mater.*, 2012, **209-210**, 271–277; (*b*) M. Ouzzine, A. J. Romero-Anaya, M. A. Lillo-Ródenas and A. Linares-Solano, Spherical activated carbon as an enhanced support for TiO_2/AC photocatalysts, *Carbon*, 2014, **67**, 104–118; (*c*) D. Liu, Z. Wu, F. Tian, B.-C. Ye and Y. Tong, Synthesis of N and La co-doped TiO_2/AC photocatalyst by microwave irradiation for the photocatalytic degradation of naphthalene, *J. Alloy Compd.*, 2016, **676**, 489–498; (*d*) S. Ali, Z. Li, S. Chen, A. Zada, I. Khan, I. Khan, W. Ali, S. Shaheen, Y. Qu and L. Jing, Synthesis of activated carbon-supported TiO_2-based nano-photocatalysts with well recycling for efficiently degrading high-concentration pollutants, *Catal. Today*, 2019, **335**, 557–564.

13 (*a*) K. Tennakone and K.G.U. Wijayantha, Photocatalysis of CFC degradation by titanium dioxide, *Appl. Catal. B*, 2005, **57**, 9–12; (*b*) K. Sirirerkratana, P. Kemacheevakul and S. Chuangchote, Color

removal from wastewater by photocatalytic process using titanium dioxide-coated glass, ceramic tile, and stainless-steel sheets, *J. Clean. Prod.*, 2019, **215**, 123–130.

14 (*a*) L. Torkian, M. M. Amini and E. Amereh, Sol-gel synthesised silver doped TiO_2 nanoparticles supported on NaX zeolite for photocatalytic applications, *Mater. Technol.*, 2013, **28**, 111–116; (*b*) M. N. Chong, Z. Y. Tneu, P. E. Poh, B. Jin and R. Aryal, Synthesis, characterization and application of TiO_2-zeolite nanocomposites for the advanced treatment of industrial dye wastewater, *J. Taiwan Inst. Chem. Eng.*, 2015, **50**, 288–296; (*c*) N. U. Saqib, R. Adnan and I. Shah, Zeolite supported TiO_2 with enhanced degradation efficiency for organic dye under household compact fluorescent light, *Mater. Res. Express*, 2019, **6**, 095506.

15 (*a*) H. B. Hadjltaief, M. B. Zina, M. E. Galvez and P. D. Costa, Photocatalytic degradation of methyl green dye in aqueous solution over natural clay-supported ZnO-TiO_2 catalysts, *J. Photochem. Photobiol., A*, 2016, **315**, 25–33; (*b*) A. Mishra, A. Mehta and S. Basu, Clay supported TiO_2 nanoparticles for photocatalytic degradation of environmental pollutants: A review, *J. Environ. Chem. Eng.*, 2018, **6**, 6088–6107.

16 (*a*) R. Zuo, G. Du, W. Zhang, L. Liu, Y. Liu, L. Mei and Z. Li, Photocatalytic degradation of methylene blue using TiO_2 impregnated diatomite, *Adv. Mater. Sci. Eng.*, 2014, 170148; (*b*) B. Wang, G. Zhang, Z. Sun and S. Zheng, Synthesis of natural porous minerals supported TiO_2 nanoparticles and their photocatalytic performance towards Rhodamine B degradation, *Powder Technol.*, 2014, **262**, 1–8.

17 (*a*) S. Ke, X. Cheng, Q. Wang, Y. Wang and Z. Pan, Preparation of a photocatalytic TiO_2/$ZnTiO_3$ coating on glazed ceramic tiles, *Ceram. Int.*, 2014, **40**, 8891–8895; (*b*) L. Baltes, S. Patachia, M. Tierean, O. Ekincioglu and H. M. Ozkul, Photoactive glazed polymer-cement composite, *Appl. Surf. Sci.*, 2018, **438**, 84–95.

18 (*a*) A. Fernández, G. Lassaletta, V. M. Jiménez, A. Justo, A. R. González-Elipe, J.-M. Herrmann, H. Tahiri and Y. Ait-Ichou, Preparation and characterization of TiO_2 photocatalysts supported on various rigid supports (glass, quartz and stainless steel). Comparative studies of photocatalytic activity in water purification, *Appl. Catal. B*, 1995, **7**, 49–63; (*b*) L. Zhang, Y. Zhu, Y. He, W. Li and H. Sun, Preparation and performances of mesoporous TiO_2 film photocatalyst supported on stainless steel, *Appl. Catal. B*, 2003, **40**, 287–292; (*c*) S. Permpoon, M. Fallet, G. Berthomé, B. Baroux, J. C. Joud and M. Langlet, Photoinduced hydrophilicity of TiO_2 films deposited on stainless steel via sol-gel technique, *J. Sol-Gel Sci. Technol.*, 2005, **35**, 127–136; (*d*) J.-P. Nikkanen, E. Huttunen-Saarivirta, T. Salminen, L. Hyvärinen, M. Honkanen, E. Isotahdon, S. Heinonen and E. Levänen, Enhanced photoactive and photoelectrochemical properties of TiO_2 sol–gel coated steel by the application of SiO_2 intermediate layer, *Appl. Catal. B*, 2015, **174–175**, 533–543.

19 See the following for a variety of examples of TiO_2 NPs deposited on glazed surfaces for photocatalytic applications: (*a*) V. S. Smitha, K. A. Manjumol, K. V. Baiju, S. Ghosh, P. Perumal and

K. G. K. Warrier, Sol–gel route to synthesize titania-silica nano precursors for photoactive particulates and coatings, *J. Sol-Gel Sci. Technol.*, 2010, **54**, 203–211; (*b*) B. K. Kaleji, R. Sarraf-Mamoory, K. Nakata and A. Fujishima, The effect of Sn dopant on crystal structure and photocatalytic behavior of nanostructured titania thin films, *J. Sol-Gel Sci. Technol.*, 2011, **60**, 99–107; (*c*) K. Murugana, R. Subasri, T. N. Rao, A. S. Gandhi and B. S. Murty, Synthesis, characterization and demonstration of self-cleaning TiO_2 coatings on glass and glazed ceramic tiles, *Prog. Org. Coat.*, 2013, **76**, 1756–1760.

20 See the following for a variety of examples of TiO_2 NPs deposited on glazed surfaces for environmental applications: (*a*) P. S. Marcos, J. Marto, T. Trindade and J. A. Labrincha, Screen-printing of TiO_2 photocatalytic layers on glazed ceramic tiles, *J. Photochem. Photobiol., A*, 2008, **197**, 125–131; (*b*) M. Raimondo, G. Guarini, C. Zanelli, F. Marani, L. Fossa and M. Dondi, Photocatalytic, highly hydrophilic porcelain stoneware slabs, *IOP Conf. Ser.: Mat. Sci. Eng.*, 2011, **18**, 222022; (*c*) B. K. Kaleji, N. Hosseinabadi and A. Fujishima, Enhanced photo-catalytic activity of TiO_2 nanostructured thin films under solar light by Sn and Nb co-doping, *J. Sol-Gel Sci. Technol.*, 2013, **65**, 195–203; (*d*) P. Zhang, J. Tian, R. Xu and G. Ma, Hydrophilicity, photocatalytic activity and stability of tetraethyl orthosilicate modified TiO_2 film on glazed ceramic surface, *Appl. Surf. Sci.*, 2013, **266**, 141–147; (*e*) S. de Niederhausern and M. Bondi, Self-cleaning and antibacteric ceramic tile surface, *Int. J. Appl. Ceram. Technol.*, 2013, **10**, 949–956; (*f*) R. Taurino, L. Barbieri and F. Bondioli, Surface properties of new green building material after TiO_2–SiO_2 coatings deposition, *Ceram. Int.*, 2016, **42**, 4866–4874; (*g*) A. L. da Silva, M. Dondi and D. Hotza, Self-cleaning ceramic tiles coated with Nb_2O_5-doped-TiO_2 nanoparticles, *Ceram. Int.*, 2017, **43**, 11986–11991; (*h*) A. Barmeh, M. R. Nilforoushan and S. Otroj, Wetting and photocatalytic properties of Ni-doped TiO_2 coating on glazed ceramic tiles under visible light, *Thin Solid Films*, 2018, **66**, 137–142; (*i*) H. Oladipo, C. Garlisi, K. Al-Ali, E. Azar and G. Palmisano, Combined photocatalytic properties and energy efficiency via multifunctional glass, *J. Environ. Chem. Eng.*, 2019, **7**, 102980.

21 (*a*) M. Machida, K. Norimoto and T. Kimura, Antibacterial activity of photocatalytic titanium dioxide thin films with photodeposited silver on the surface of sanitary ware, *J. Am. Ceram. Soc.*, 2005, **88**, 95–100; (*b*) B. K. Kaleji, R. Sarraf-Mamoory and S. Sanjabi, Photocatalytic evaluation of a titania thin film on glazed porcelain substrates via a $TiCl_4$ precursor, *Reac. Kinet. Mech. Cat.*, 2011, **103**, 289–298; (*c*) K. Malnieks, G. Mezinskis, I. Pavlovska, L. Bidermanis and A. Pludons, Optical, photocatalytical and structural Properties of TiO_2-SiO_2 sol-gel coatings on high content SiO_2 enamel surface, *Mat. Sci.*, 2015, **21**, 100–104.

22 (*a*) D. Onna, K. M. Fuentes, C. Spedalieri, M. Perullini, M. C. Marchi, F. Alvarez, R. J. Candal and S. A. Bilmes, Wettability, photoactivity, and antimicrobial activity of glazed ceramic tiles coated with titania films containing tungsten, *ACS Omega*, 2018, **3**, 17629–17636; (*b*) M. Piispanen, J. Määttä, S. Areva, A.-M. Sjöberg, M. Hupa and L. Hupa, Chemical resistance and cleaning properties of coated glazed surfaces, *J. Eur. Ceram. Soc.*, 2009, **29**, 1855–1860.

23 (*a*) W. Jiang, Y. Wang and L. Gu, Influence of TiO_2 film on photo-catalytic property of enamels, *J. Non-Cryst. Solids*, 2007, **353**, 4191–4194; (*b*) S.-J. Yoo, S.-I. Lee, D.-H. Kwak, K.-G. Kim, K.-J. Hwang, J.-W. Lee, U.-Y. Hwang, H.-S. Park and J.-O. Kim, Photocatalytic degradation of methylene blue and acetaldehyde by TiO_2/glaze coated porous red clay tile, *Korean J. Chem. Eng.*, 2008, **25**, 1232–1238.

24 S. Morelli, R. Pérez, A. Querejeta, J. Muñoz, L. Lusvarghi, M. L. Gualtieri, G. Bolelli and H.-J. Grande, Photocatalytic enamel/TiO_2 coatings developed by electrophoretic deposition for methyl orange decomposition, *Ceram. Int.*, 2018, **44**, 16199–16208.

25 J. He, Y.-e. Du, Y. Bai, J. An, X. Cai, Y. Chen, P. Wang, X. Yang and Q. Feng, Facile formation of anatase/rutile TiO_2 nanocomposites with enhanced photocatalytic activity, *Molecules*, 2019, **24**, 2996.

26 R. Su, R. Bechstein, L. Sø, R. T. Vang, M. Sillassen, B. Esbjörnsson, A. Palmqvist and F. Besenbacher, How the anatase-to-rutile ratio influences the photoreactivity of TiO_2, *J. Phys. Chem. C*, 2011, **115**, 24287–24292.

27 R. Ma and T. Chen, Checking the synergetic effect between anatase and rutile, *J. Phys. Chem. C*, 2019, **123**, 19479–19485.

28 A. Di Paola, M. Bellardita and L. Palmisano, Brookite, the least known TiO_2 photocatalyst, *Catalysts*, 2013, **3**, 36–73.

29 S. Yadava and G. Jaiswar, Review on undoped/doped TiO_2 nanomaterial; synthesis and photocatalytic and antimicrobial activity, *J. Chin. Chem. Soc.*, 2017, **64**, 103–116.

30 We tested different synthesis methods described in preliminary studies: (*a*) W. Choi, A. Termin and M. R. Hoffmann, The role of metal ion dopants in quantum-sized TiO_2: Correlation between photoreactivity and charge carrier recombination dynamics, *J. Phys. Chem.*, 1994, **98**, 13669–13679; (*b*) G. Oskam, A. Nellore, R. L. Penn and P. C. Searson, The growth kinetics of TiO_2 nanoparticles from titanium(IV) alkoxide at high water/titanium ratio, *J. Phys. Chem. B*, 2003, **107**, 1734–1738; (*c*) G. Lusvardi, C. Barani, F. Giubertoni and G. Paganelli, Synthesis and characterization of TiO_2 nanoparticles for the reduction of water pollutants, *Materials*, 2017, **10**, 1208, among which the latter was chosen because it allows an easy scale-up.

31 A. Kern, A. A. Coelho and R. W. Cheary, Convolution based profile fitting. *Diffraction Analysis of the Microstructure of Materials*, ed. E. J. Mittemeijer, P. Scardi, Springer, 2004.

32 D. Balzar, Voigt function model in diffraction-line broadening analysis. *Defect and Microstructure Analysis by Diffraction*, ed. R. Snyder, J. Fiala & H. J. Bunge, IUCr / Oxford University Press, 1999, 94–126.

33 R. W. Cheary, A. A. Coelho and J. P. Cline, Fundamental parameters line profile fitting in laboratory diffractometers, *J. Res. Natl. Inst. Stand. Technol.*, 2004, **109**, 1–25.

34 ISO 10678:2010. Fine ceramics (advanced ceramics, advanced technical ceramics) – Determination of photocatalytic activity of surfaces in aqueous medium by degradation of methylene blue.

35 Anatase and brookite transform to rutile at temperatures higher than 600 ºC. See: Y. Hu, H.-L. Tsai and C.-L. Huangk, Effect of brookite phase on the anatase–rutile transition in titania nanoparticles, *J. Eur. Ceram. Soc.*, 2003, **23**, 691–696.

36 (*a*) A. Felske and W. J. Plieth. Raman spectroscopy of titanium dioxide layers, *Electrochim. Acta*, 1989, **34**, 75–77; (*b*) J. S. Dalton, P. A. Janes, N. G. Jones, J. A. Nicholson, K. R. Hallam and G. C. Allen, Photocatalytic oxidation of NOx gases using TiO_2: a surface spectroscopic approach, *Environ. Pollut.*, 2002, **120**, 415–422; (*c*) A. G. Ilie, M. Scarisoreanu, E. Dutu, F. Dumitrache, A.-M. Banici, C. T. Fleaca, E. Vasile and I. Mihailescu, Study of phase development and thermal stability in as synthesized TiO_2 nanoparticles by laser pyrolysis: ethylene uptake and oxygen enrichment, *Appl. Surf. Sci.*, 2018, **427**, 798–806.

37 J.-G. Li, T. Ishigaki and X. Sun, Anatase, brookite, and rutile nanocrystals via redox reactions under mild hydrothermal conditions: phase-selective synthesis and physicochemical properties, *J. Phys. Chem. C*, 2007, **111**, 4969–4976.

38 R. L. Frost, J. Kristof, L. Rintoul and J. T. Kloprogge, Raman spectroscopy of urea and urea-intercalated kaolinites at 77 K, *Spectrochim. Acta A*, 1999, **56**, 1681–1691.

39 S. P. S. Porto, P. A. Fleury and T. C. Damen, Raman spectra of TiO_2, MgF_2, ZnF_2, FeF_2, and MnF_2, *Phys. Rev.*, 1967, **154**, 522–526.

40 (*a*) W. Choi, A. Termin and M. R. J. Hoffmann, The role of metal ion dopants in quantum-sized TiO_2: correlation between photoreactivity and charge carrier recombination dynamics, *Phys. Chem.*, 1994, **98**, 13669–13679; (*b*) M. Zhou, J. Yu and B. J. Cheng, Effects of Fe-doping on the photocatalytic activity of mesoporous TiO_2 powders prepared by an ultrasonic method, *Hazard. Mater.*, 2006, **137**, 1838–1847; (*c*) J. Yu, Q. Xiang and M. Zhou, Preparation, characterization and visible-light-driven photocatalytic activity of Fe-doped titania nanorods and first-principles study for electronic structures, *Appl. Catal. B*, 2009, **90**, 595–602; (*d*) J. Chen, M. Yao and X. Wang, Investigation of transition metal ion doping behaviours on TiO_2 nanoparticles, *J. Nanopart. Res.*, 2008, **10**, 163–171; (*e*) L. G. Devi and S. G. Kumar, Influence of physicochemical–electronic properties of transition metal ion doped polycrystalline titania on the photocatalytic degradation of Indigo Carmine and 4-nitrophenol under UV/solar light, *Appl. Surf. Sci.*, 2011, **257**, 2779–2790.

41 M. Shilpy, M. A. Ehsan, T. H. Ali, S. B. A. Hamid and Md. E. Ali, Performance of cobalt titanate towards H_2O_2 based catalytic oxidation of lignin model compound, *RSC Adv.*, 2015, **5**, 79644–79653.

42 (*a*) T. A. Kandiel, L. Robben, A. Alkaima and D. Bahnemann, Brookite *versus* anatase TiO_2 photocatalysts: phase transformations and photocatalytic activities, *Photochem. Photobiol. Sci.*, 2013, **12**, 602–609; (*b*) N. S. Allen, N. Mahdjoub, V. Vishnyakov, P. J. Kelly and R. J. Kriek, The effect of crystalline phase (anatase, brookite and rutile) and size on the photocatalytic activity of calcined polymorphic titanium dioxide (TiO_2), *Polym. Degrad. Stab.*, 2018, **150**, 31–36.

43 Y. Lan, Y. Lu and Z. Ren, Mini review on photocatalysis of titanium dioxide nanoparticles and their solar applications, *Nano Energy*, 2013, **2**, 1031–1045.

44 (*a*) T. Umebayashi, T. Yamaki, H. Itoh and K. Asai, Analysis of electronic structures of 3d transition metal-doped TiO_2 based on band calculations, *J. Phys. Chem. Solids*, 2002, **63**, 1909–1920; (*b*) B. Peng, X. Meng, F. Tang, X. Ren, D. Chen and J. Ren, General synthesis and optical properties of monodisperse multifunctional metal-ion-doped TiO_2 hollow particles, *J. Phys. Chem. C*, 2009, **113**, 20240–20245.

45 (*a*) W. Zhang, W. Zhou, J. H. Wright, Y. N. Kim, D. Liu and X. Xiao, Mn-Doped TiO_2 nanosheet-based spheres as anode materials for lithium-ion batteries with high performance at elevated temperatures, *ACS Appl. Mater. Interfaces*, 2014, **6**, 7292−7300; (*b*) I. Birlik and D. Dagdelen, Synergistic effect of manganese and nitrogen codoping on photocatalytic properties of titania nanoparticles, *Bull. Mater. Sci.*, 2020, **43**, 85.

46 A. Houas, H. Lachheb, M. Ksibi, E. Elaloui, C. Guillard and J.-M. Herrmann, Photocatalytic degradation pathway of methylene blue in water, *Appl. Catal. B*, 2001, **31**, 145–157.

47 H. A. Le, L. T. Linh, S. Chin and J. Jurng, Photocatalytic degradation of methylene blue by a combination of TiO_2-anatase and coconut shell activated carbon, *Powder Technol.*, 2012, **225**, 167–175.

48 D. A. H. Hanaor and C. C. Sorrell, Review of the anatase to rutile phase transformation, *J. Mater. Sci.*, 2011, **46**, 855–874.

49 As in the case of calcined NCs, the preparation of the supported photocatalysts involves a calcination process that discards a possible positive effect of N-dopant on the photocatalytic activity (see Experimental Section for more details).

ELECTRONIC SUPPLEMENTARY INFORMATION

Photocatalytic activity of TiO_2 nanocrystals incorporated in enamel coatings on stainless steel

Andrea Diego-Rucabado,[ab] Marina T. Candela,[bc] Fernando Aguado,[bc] Jesús González,[bc] Eugenio Gómez,[d] Rafael Valiente,[ab] Israel Cano*[ae] and Rosa Martín-Rodríguez*[bf]

[a]Applied Physics Department, University of Cantabria, Avda. de Los Castros 48, 39005 Santander, Spain

[b]Nanomedicine Group, IDIVAL, Avda. Cardenal Herrera Oria s/n, 39011 Santander, Spain

[c]CITIMAC Department, University of Cantabria, Avda. de Los Castros 48, 39005 Santander, Spain

[d]VITRISPAN S.A., Barrio Rioseco, 39786 Guriezo, Spain

[e]Crystallography, Mineralogy and Agricultural Chemistry Department. Faculty of Chemistry, University of Seville, 41012 Seville, Spain

[f]QUIPRE Department, University of Cantabria, Avda. de Los Castros 46, 39005 Santander, Spain

Contents

1. X-ray diffraction analyses of TiO_2 NCs

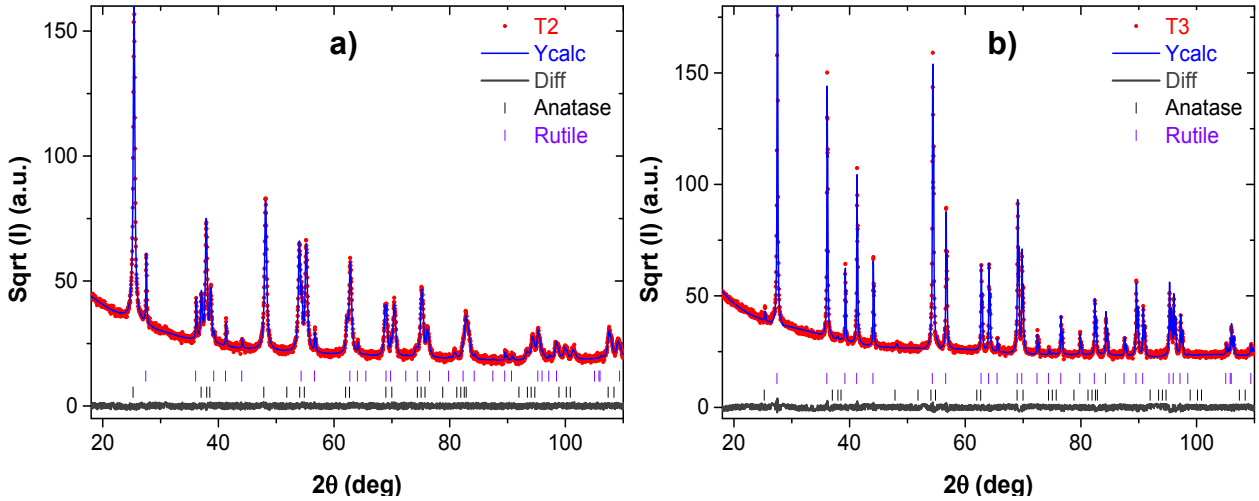

Fig. S1 XRD diffraction patterns of (a) pure TiO_2 NCs calcined at 600 ºC (T2); (b) pure TiO_2 NCs calcined at 800 ºC (T3).

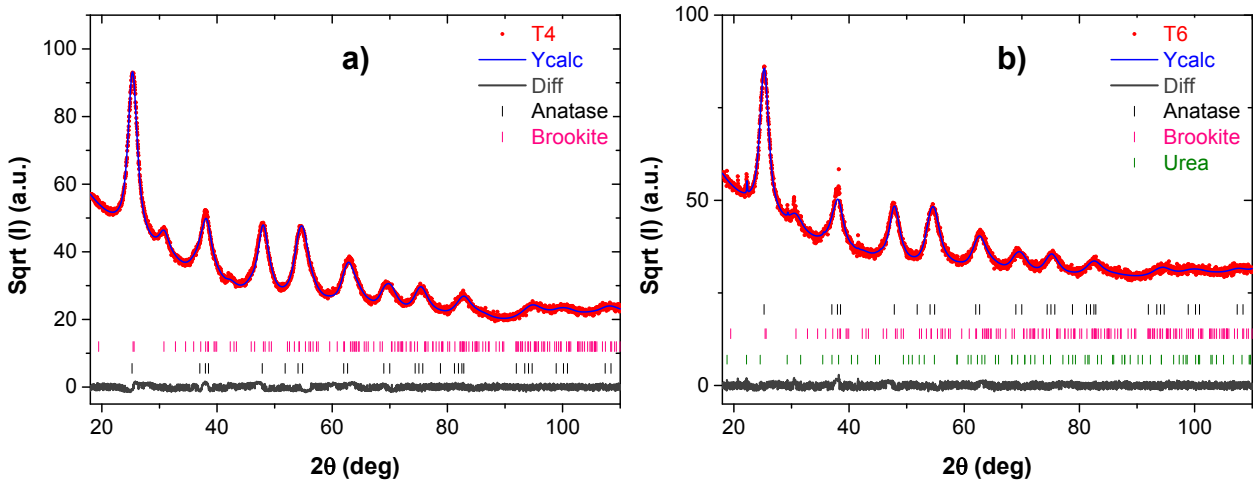

Fig. S2 XRD diffraction patterns of (a) non-calcined Mn-doped TiO_2 NCs (T4); (b) non-calcined Co-doped TiO_2 NCs (T6).

2. TEM images of TiO_2 NCs

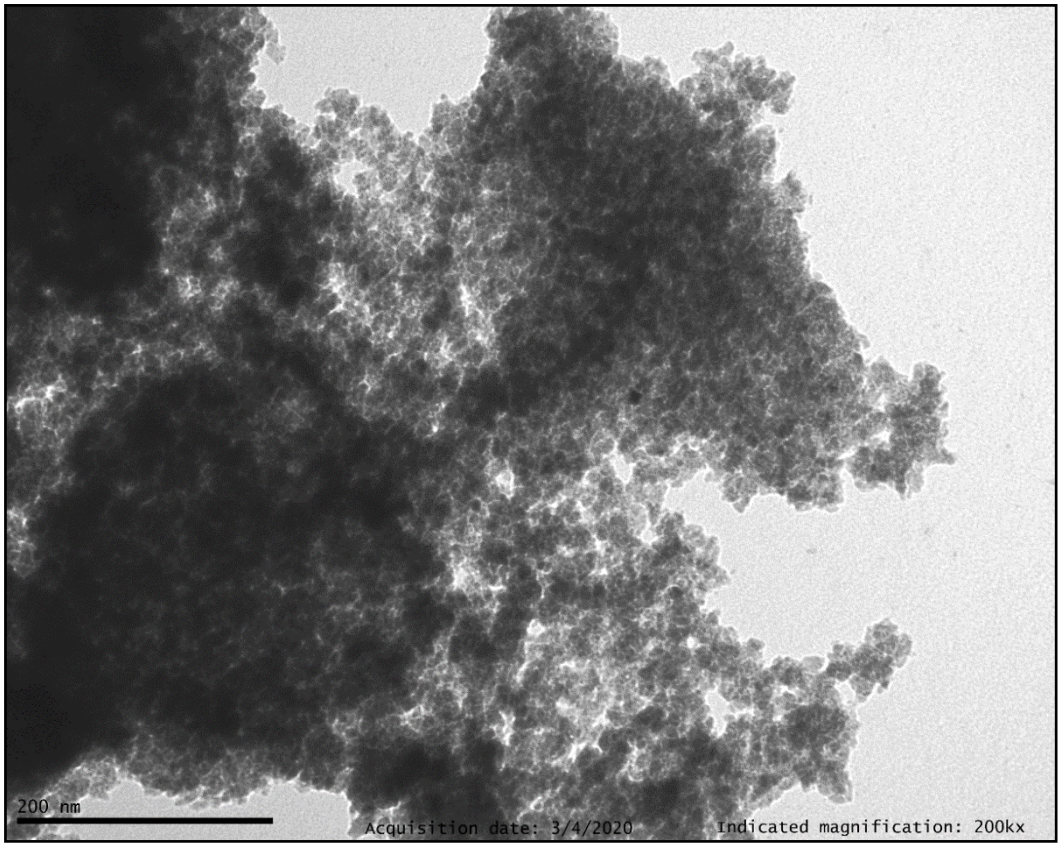

Fig. S3 TEM image of **T4**.

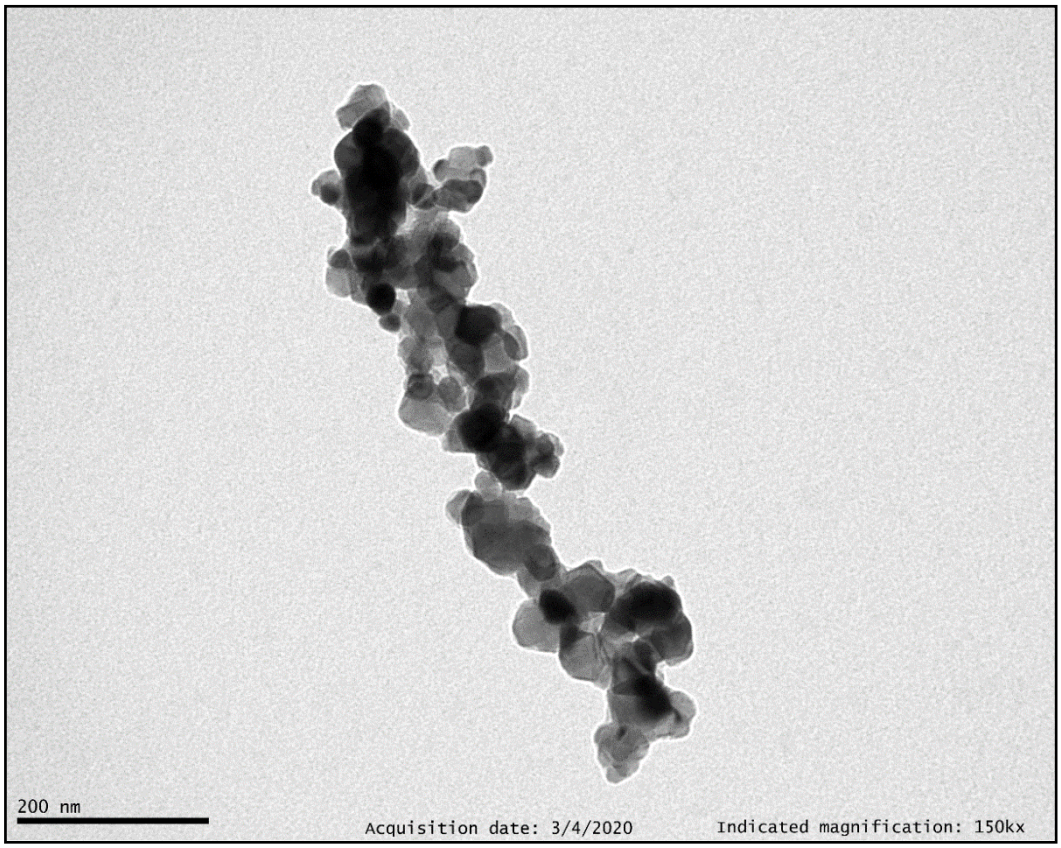

Fig. S4 TEM image of **T5**.

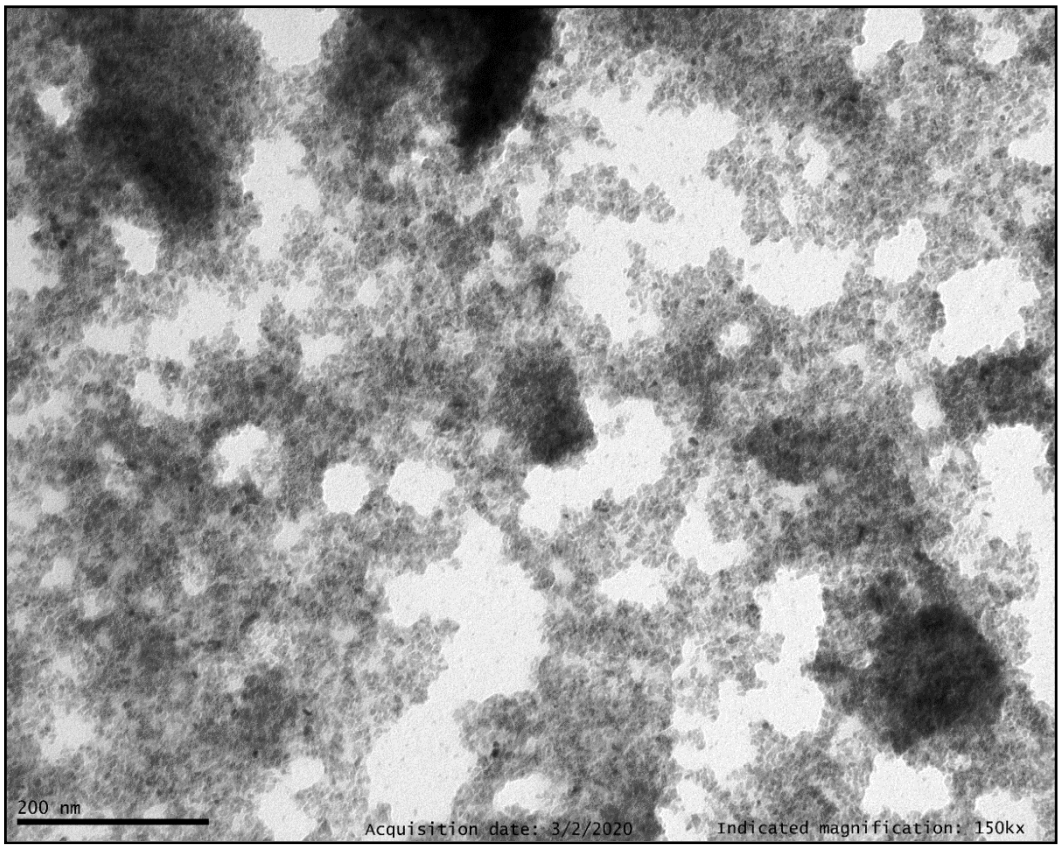

Fig. S5 TEM image of **T6**.

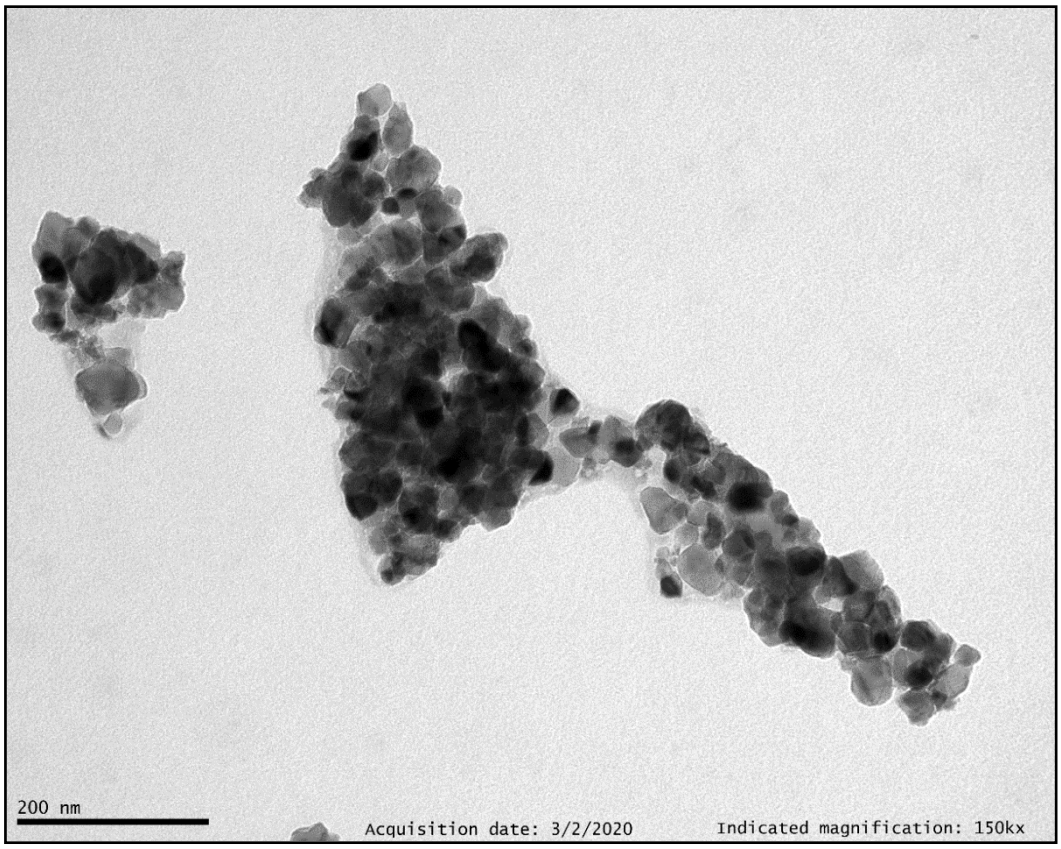

Fig. S6 TEM image of **T7**.

3. Photographs of supported photocatalysts

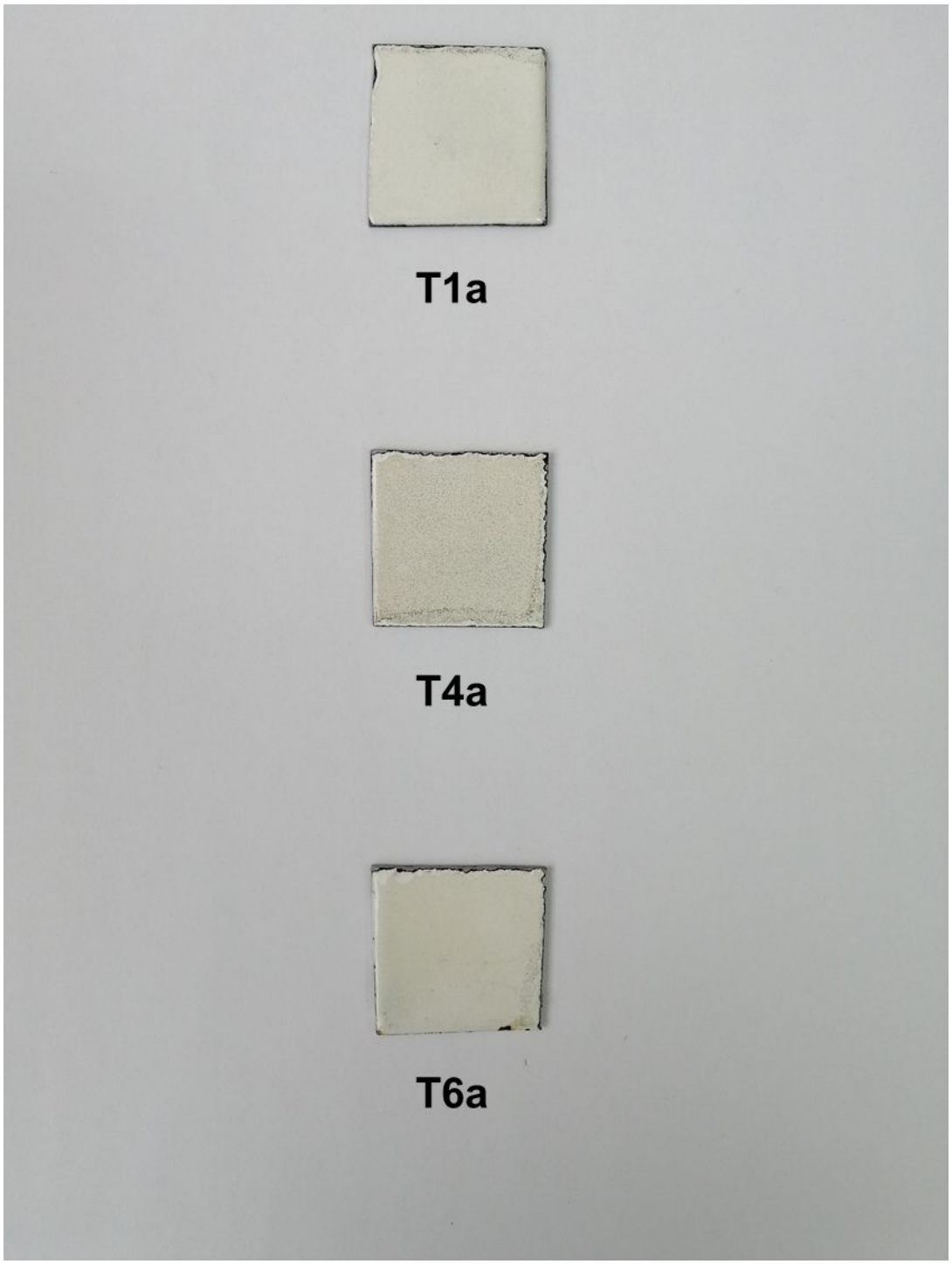

Fig. S7 Photographs of supported photocatalysts containing TiO_2 NCs. T1a: pure TiO_2 NCs; T4a: Mn-doped TiO_2 NCs; T6a: Co-doped TiO_2 NCs.

4. X-ray diffraction analyses of TiO_2 NCs deposited on enamel supported onto steel sheets

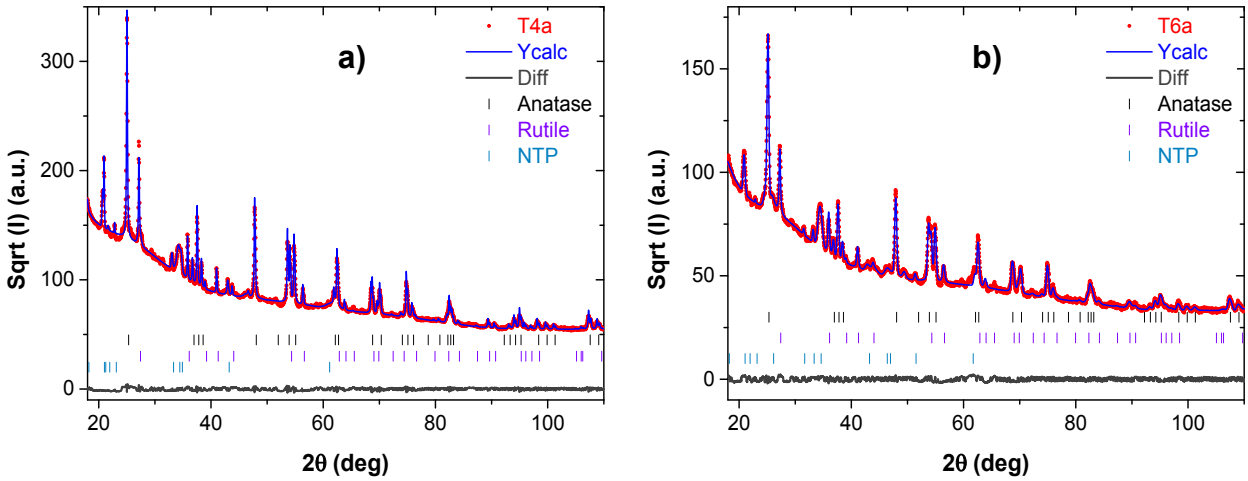

Fig. S8 XRD diffraction patterns of (a) Mn-doped TiO_2 NCs deposited on enamel supported onto steel sheets (T4a). (b) Co-doped TiO_2 NCs deposited on enamel supported onto steel sheets (T6a).

5. Recycling experiments

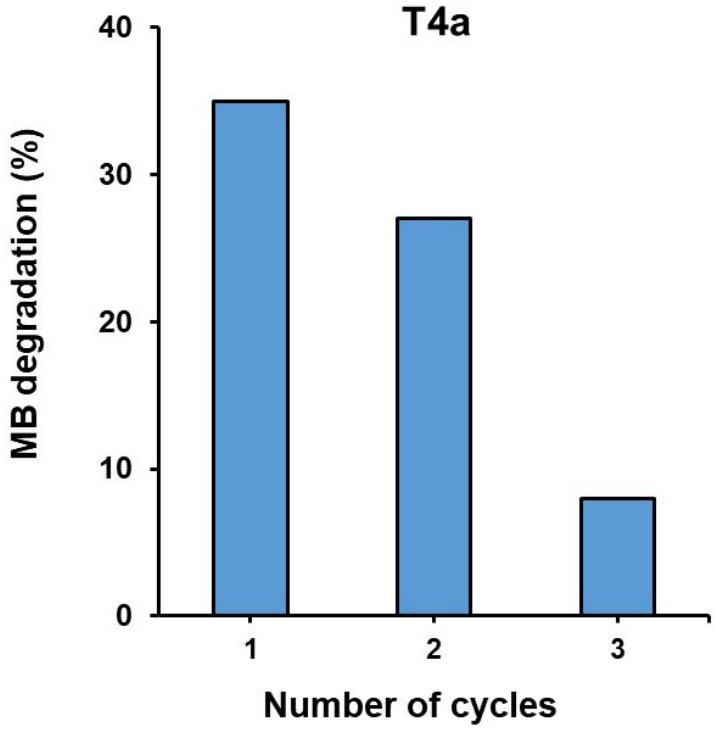

Fig. S9 Reuse of T4a in the degradation of MB. Conditions: MB (150 mL, 10 μM), catalyst (5 x 5 cm^2), 22 W, λ = 395 nm, at RT.

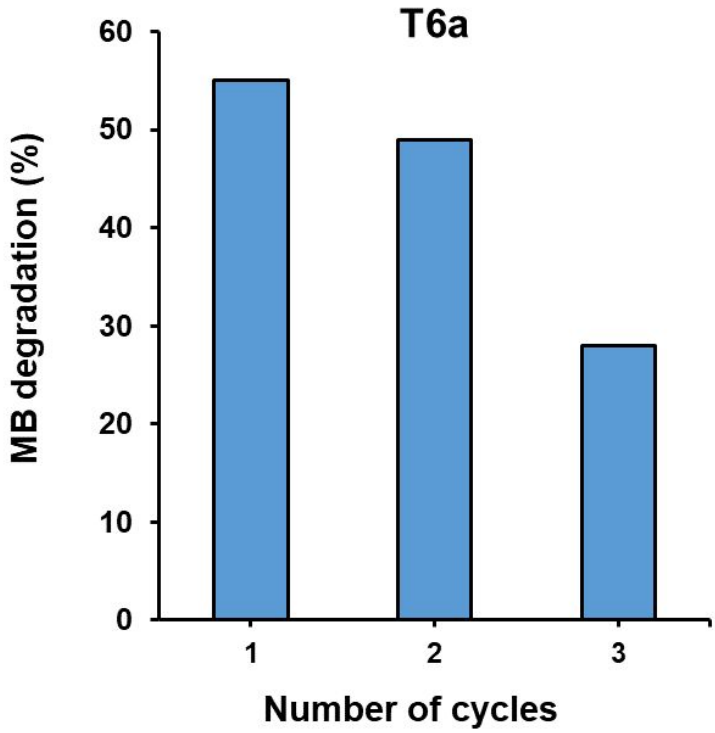

Fig. S10 Reuse of T6a in the degradation of MB. Conditions: MB (150 mL, 10 μM), catalyst (5 x 5 cm^2), 22 W, λ = 395 nm, at RT.

ELECTRONIC SUPPLEMENTARY INFORMATION

Photocatalytic activity of TiO_2 nanocrystals incorporated in enamel coatings on stainless steel

Andrea Diego-Rucabado,[ab] Marina T. Candela,[bc] Fernando Aguado,[bc] Jesús González,[bc] Eugenio Gómez,[d] Rafael Valiente,[ab] Israel Cano*[ae] and Rosa Martín-Rodríguez*[bf]

[a]Applied Physics Department, University of Cantabria, Avda. de Los Castros 48, 39005 Santander, Spain

[b]Nanomedicine Group, IDIVAL, Avda. Cardenal Herrera Oria s/n, 39011 Santander, Spain

[c]CITIMAC Department, University of Cantabria, Avda. de Los Castros 48, 39005 Santander, Spain

[d]VITRISPAN S.A., Barrio Rioseco, 39786 Guriezo, Spain

[e]Crystallography, Mineralogy and Agricultural Chemistry Department. Faculty of Chemistry, University of Seville, 41012 Seville, Spain

[f]QUIPRE Department, University of Cantabria, Avda. de Los Castros 46, 39005 Santander, Spain

Contents

1. X-ray diffraction analyses of TiO_2 NCs

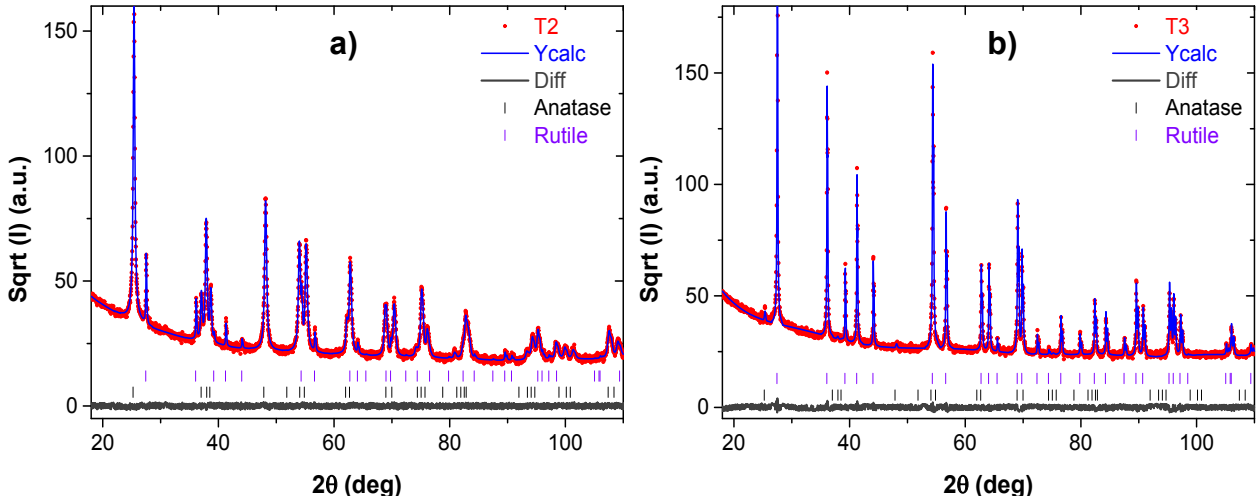

Fig. S1 XRD diffraction patterns of (a) pure TiO_2 NCs calcined at 600 ºC (T2); (b) pure TiO_2 NCs calcined at 800 ºC (T3).

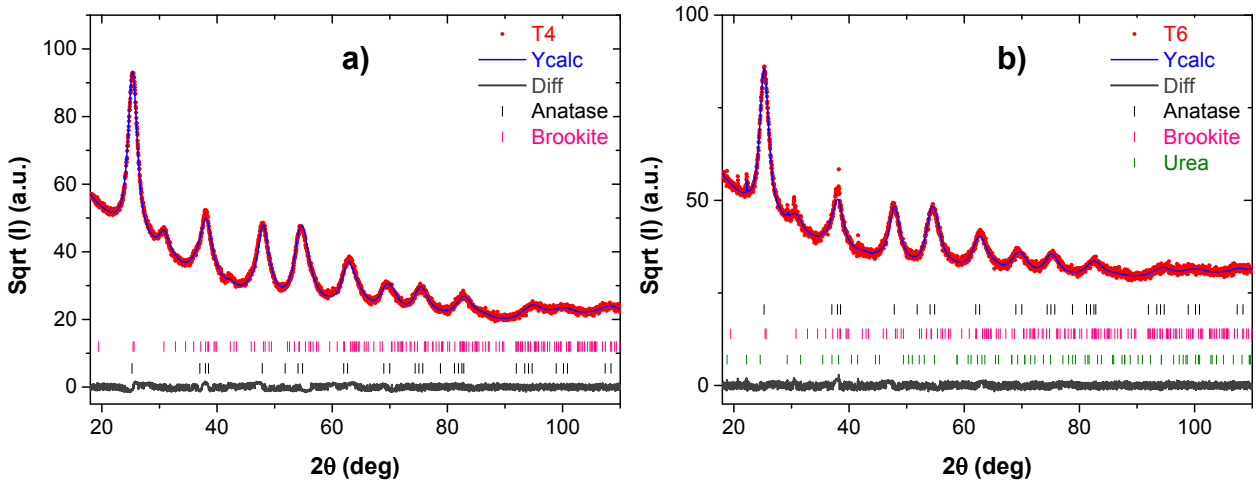

Fig. S2 XRD diffraction patterns of (a) non-calcined Mn-doped TiO_2 NCs (T4); (b) non-calcined Co-doped TiO_2 NCs (T6).

2. TEM images of TiO_2 NCs

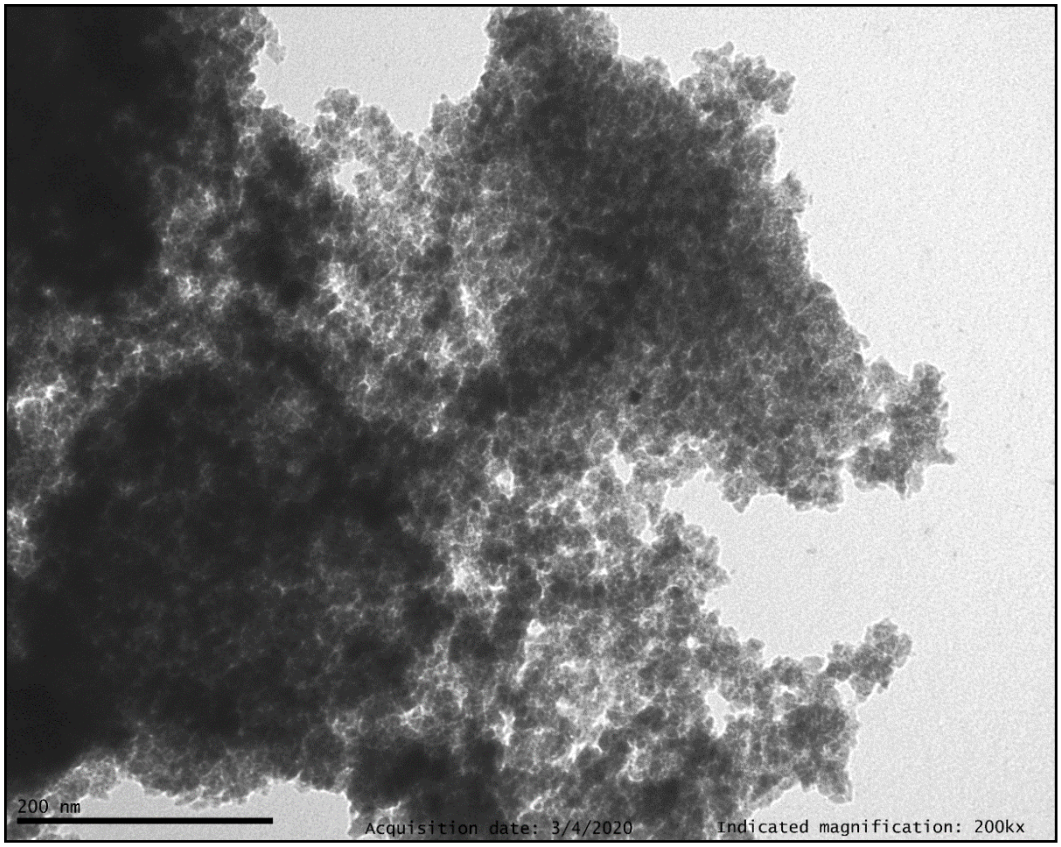

Fig. S3 TEM image of **T4**.

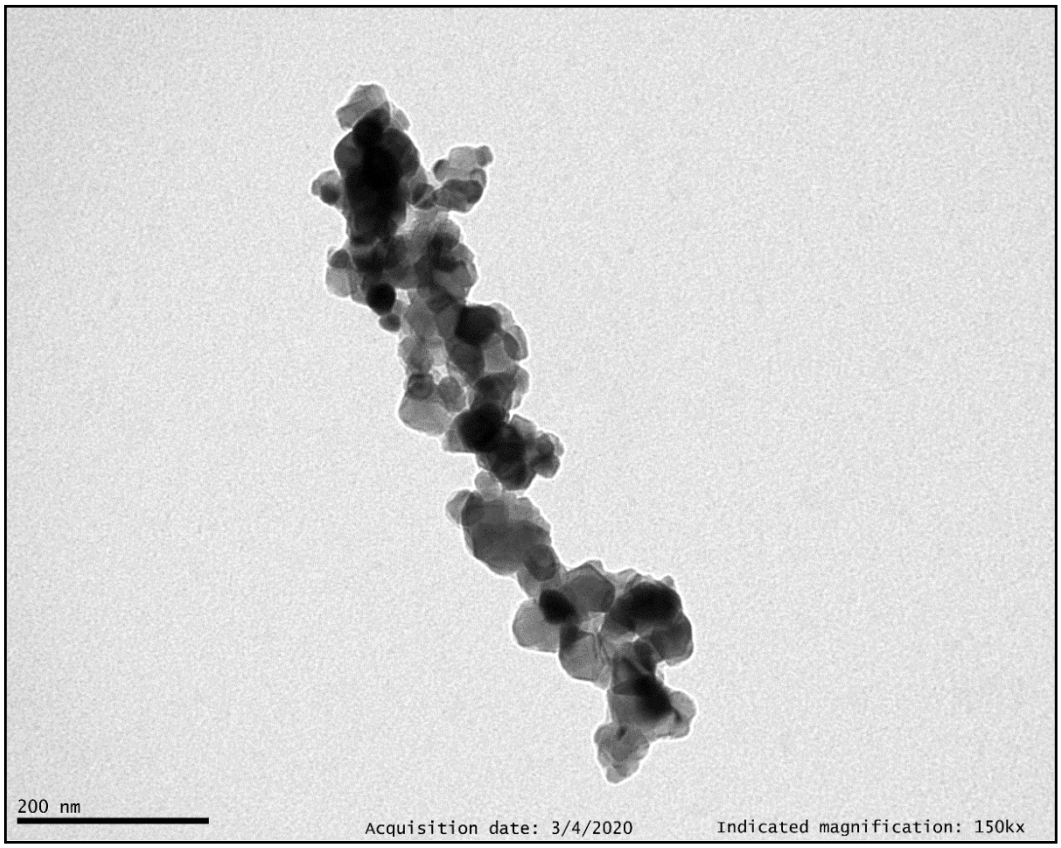

Fig. S4 TEM image of **T5**.

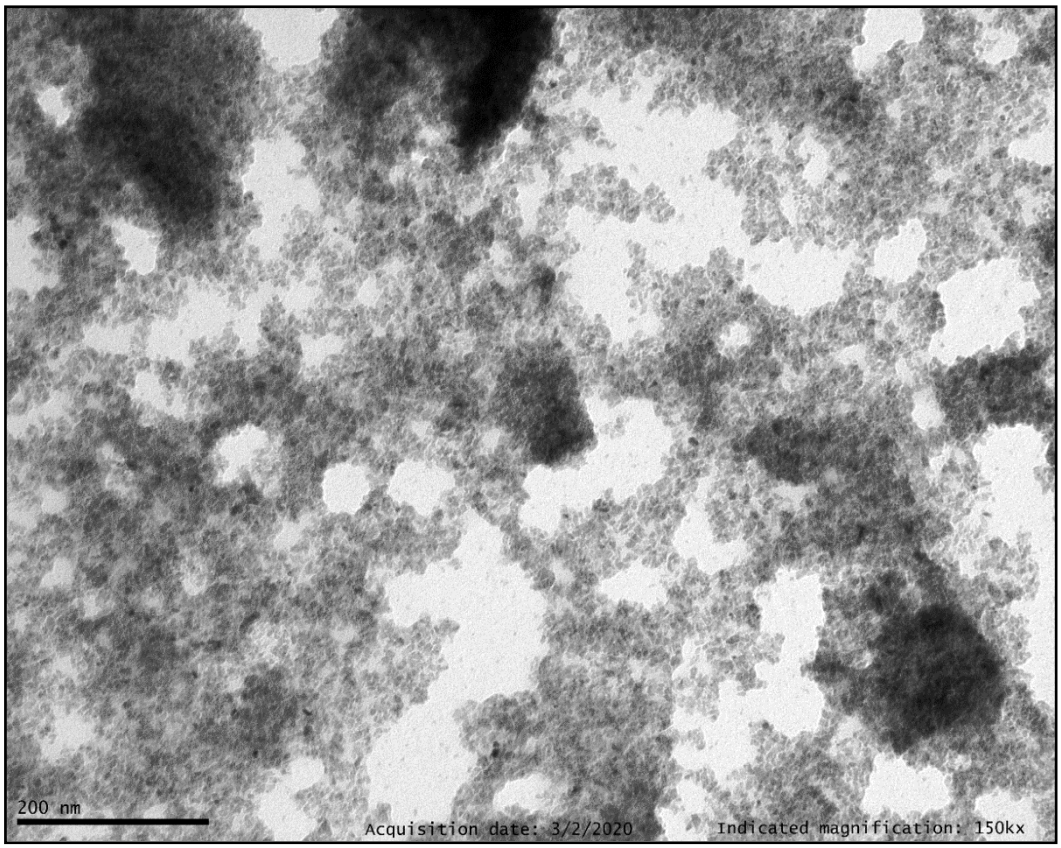

Fig. S5 TEM image of **T6**.

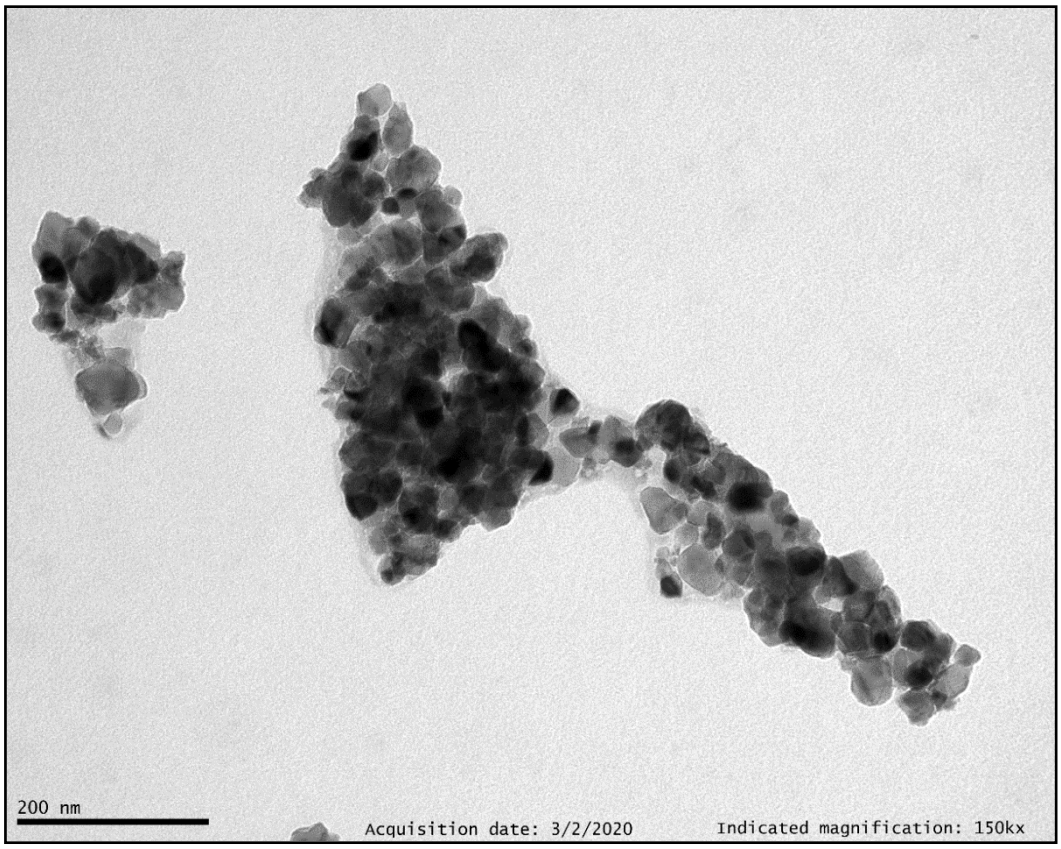

Fig. S6 TEM image of **T7**.

3. Photographs of supported photocatalysts

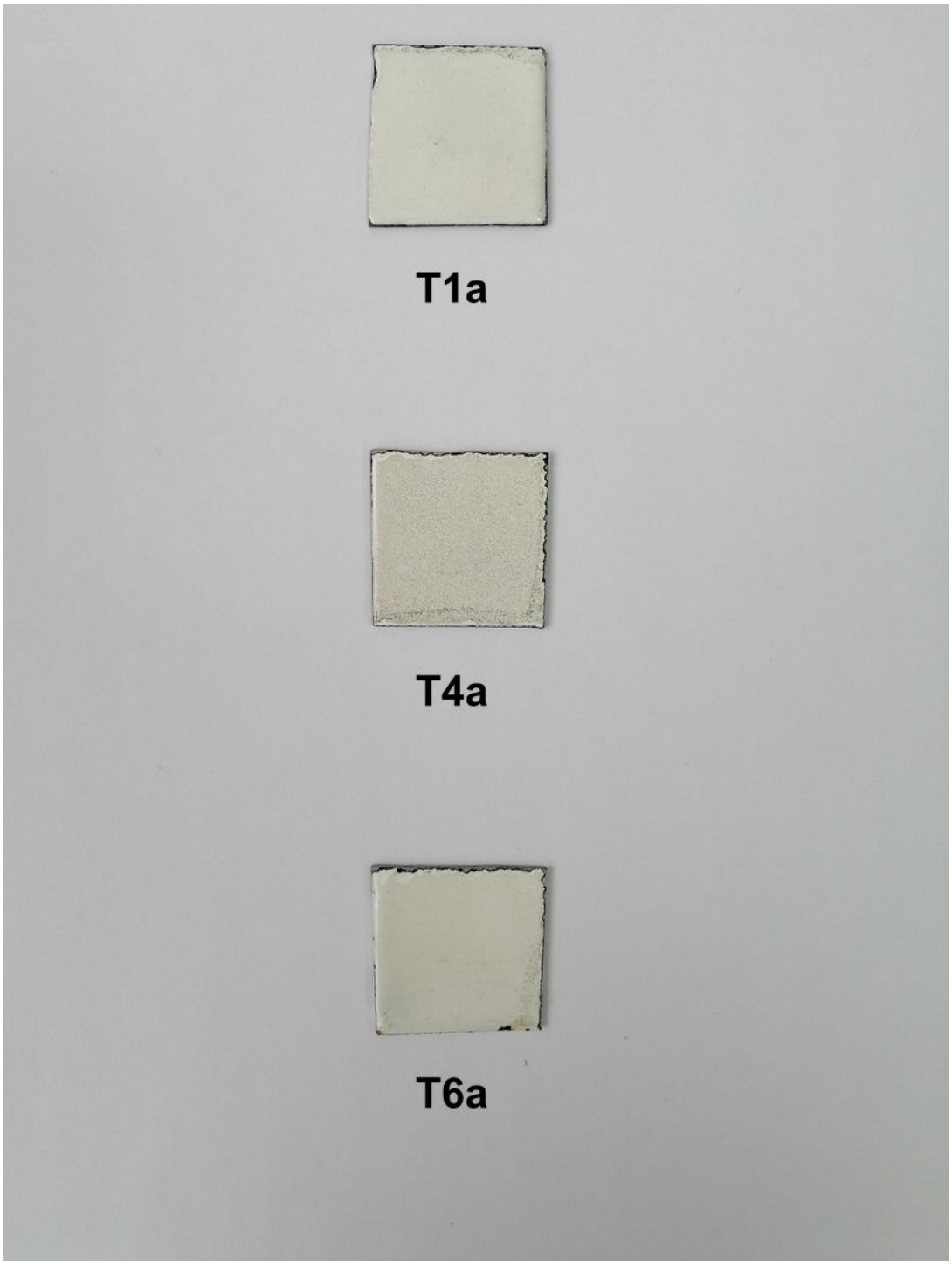

Fig. S7 Photographs of supported photocatalysts containing TiO_2 NCs. T1a: ~~non-doped~~pure TiO_2 NCs; T4a: Mn-doped TiO_2 NCs; T6a: Co-doped TiO_2 NCs.

4. X-ray diffraction analyses of TiO_2 NCs deposited on enamel supported onto steel sheets

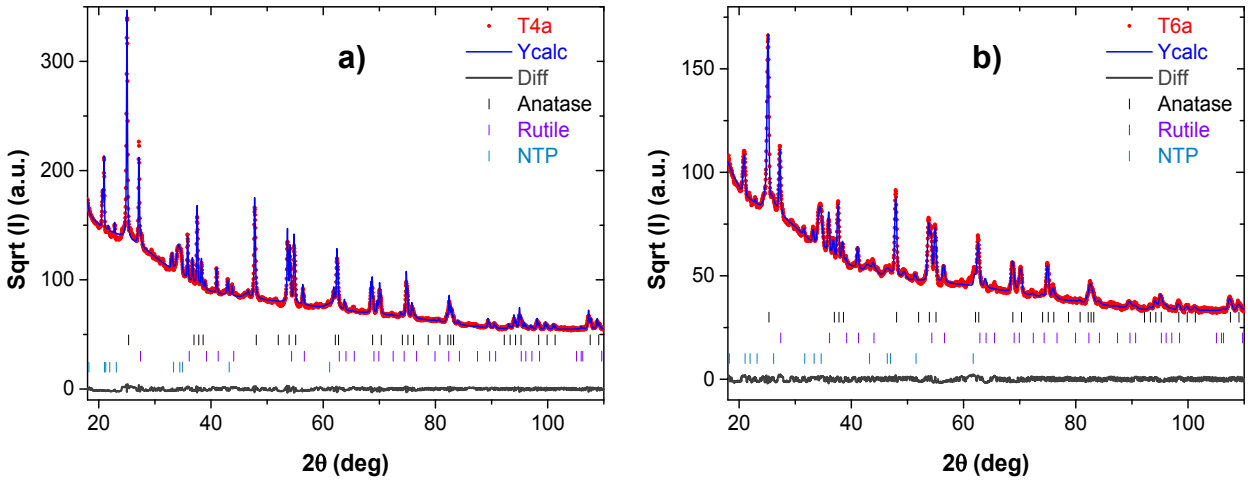

Fig. S8 XRD diffraction patterns of (a) Mn-doped TiO_2 NCs deposited on enamel supported onto steel sheets (T4a). (b) Co-doped TiO_2 NCs deposited on enamel supported onto steel sheets (T6a).

5. Recycling experiments

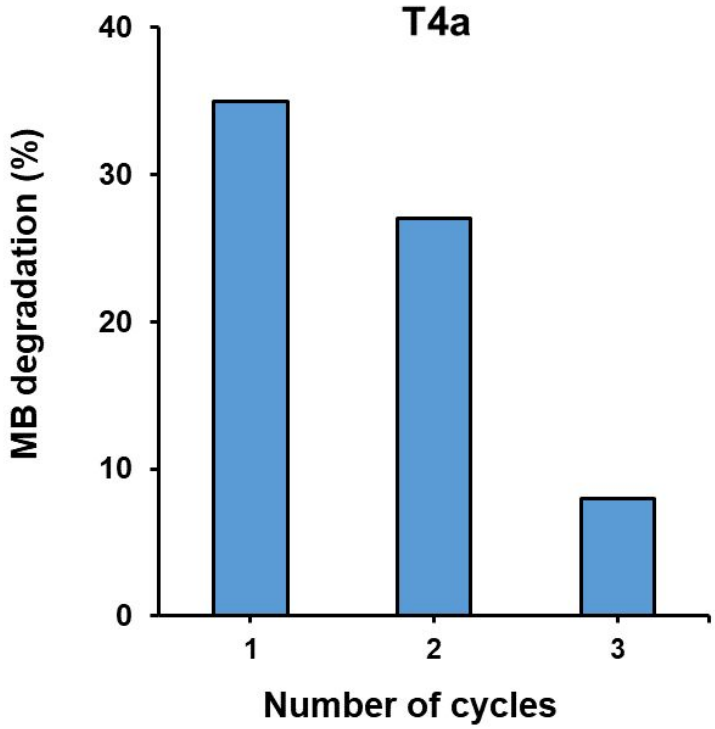

Fig. S9 Reuse of T4a in the degradation of MB. Conditions: MB (150 mL, 10 μM), catalyst (5 x 5 cm^2), 22 W, λ = 395 nm, at RT.

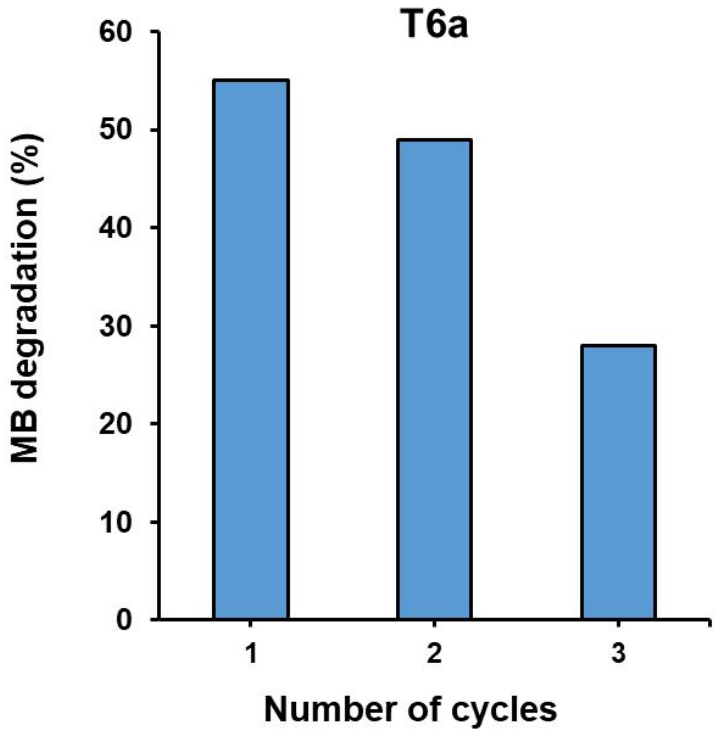

Fig. S10 Reuse of T6a in the degradation of MB. Conditions: MB (150 mL, 10 μM), catalyst (5 x 5 cm^2), 22 W, λ = 395 nm, at RT.